SAPIENZA
UNIVERSITÀ DI ROMA

Faculty of Mathematical, Physical and Natural Sciences

Department of Earth Sciences

Ph.D. in Earth Sciences

XXXII cycle

Rheological effects related to neo-fracturing processes in rock masses

Ph.D. student

Danilo D'Angiò

Advisor

Prof. Salvatore Martino

Co-Advisor

Ph.D. Luca Lenti

December 2019

Table of contents

Abstract

Rockfall hazard is one of the main natural hazards in mountainous areas and along transportation routes. Roads and railways interruptions, as well as damages of buildings, are among the main inconveniences due to the detachment of unstable sectors of highly jointed rock masses. Rockfalls are the result of the combined action of the rock mass creep and of the natural and anthropic solicitations, which lead to the accumulation of inelastic strain within the rock mass and to the formation of new fractures or to the extension and movement of the pre-existing ones (rock mass damaging phenomena). The understanding of rock damaging processes through the microseismic monitoring of rock slopes predisposed for instabilities events can help in defining proper risk mitigation strategies. With the aim of assessing rock mass damaging phenomena, this PhD thesis proposes an analysis of the damping ratio associated with the microseismic emissions recorded in two test sites located in central Italy. Three monitoring campaigns have been conducted: two at the Acuto quarry test site, where the vibrational behaviour of a 12 m^3 rock block partially detached from the back rock wall has been investigated; one at the Terni-Giuncano railway test site, where a rock mass close to a railway was studied to analyse the effects produced by the repeated trains transit. A STA/LTA event detection algorithm has been implemented for the recognition of the microseismic emissions from the seismic datasets acquired in continuous mode and with a sampling frequency of 2400 Hz. The damping ratio of the microseismic emissions, filtered in monofrequential waveforms, was evaluated; in the following, the daily mean damping values for each frequency were compared in respect to the environmental parameters monitored on site. No irreversible trend variations were observed, but significant variations related to transient processes were detected. It is deemed that the proposed approach can be applied on yearly seismic dataset and environments exposed to natural and anthropic forcing actions, to be furtherly tested and validated. Additional analyses were carried out on the train transit recordings. Each train passage was analysed in terms of: a) RMS value of the recording; b) cross-correlation between couples of sensors. The observation of the RMS and cross-correlation time series over time confirmed the unvaried long-term vibrational behaviour of the rock mass, according to the results of the damping analysis. In addition, the seismic noise was investigated by computing the average noise in one-minute intervals filtered at specific frequency bands. The cumulative of the filtered intervals allowed to determine the main energised frequency band, which resulted to be the one comprised between 500 and 1000 Hz.

The derivative of the averaged noise was compared with the environmental parameters recorded in the two test sites. A marked correlation between the variation of air and rock mass temperature and the derivative of the noise in the frequency band comprised between 0.5 and 30 Hz was noted, while the correlation is feeble or lost for the other frequency bands considered. The correlation observed between thermal cycles and ambient noise variations is in agreement with previous bibliographical studies; moreover, a differentiation in the vibrational response for the different frequency bands has been detected.

1 Introduction

Landslides are responsible of damages, casualties, traffic interruptions and economic losses all over the world, especially in mountainous areas (Guzzetti 2000, Nadim *et al.* 2006, Kirschbaum *et al.* 2010, Kirschbaum *et al.* 2015, Froude & Petley 2018), where landslide hazard is one of the major among the natural hazards. In fact, Froude & Petley (2018) report that almost 5000 non-seismically triggered fatal landslides occurred between 2004 and 2016, including several landslide typologies and triggering actions (Figure 1).

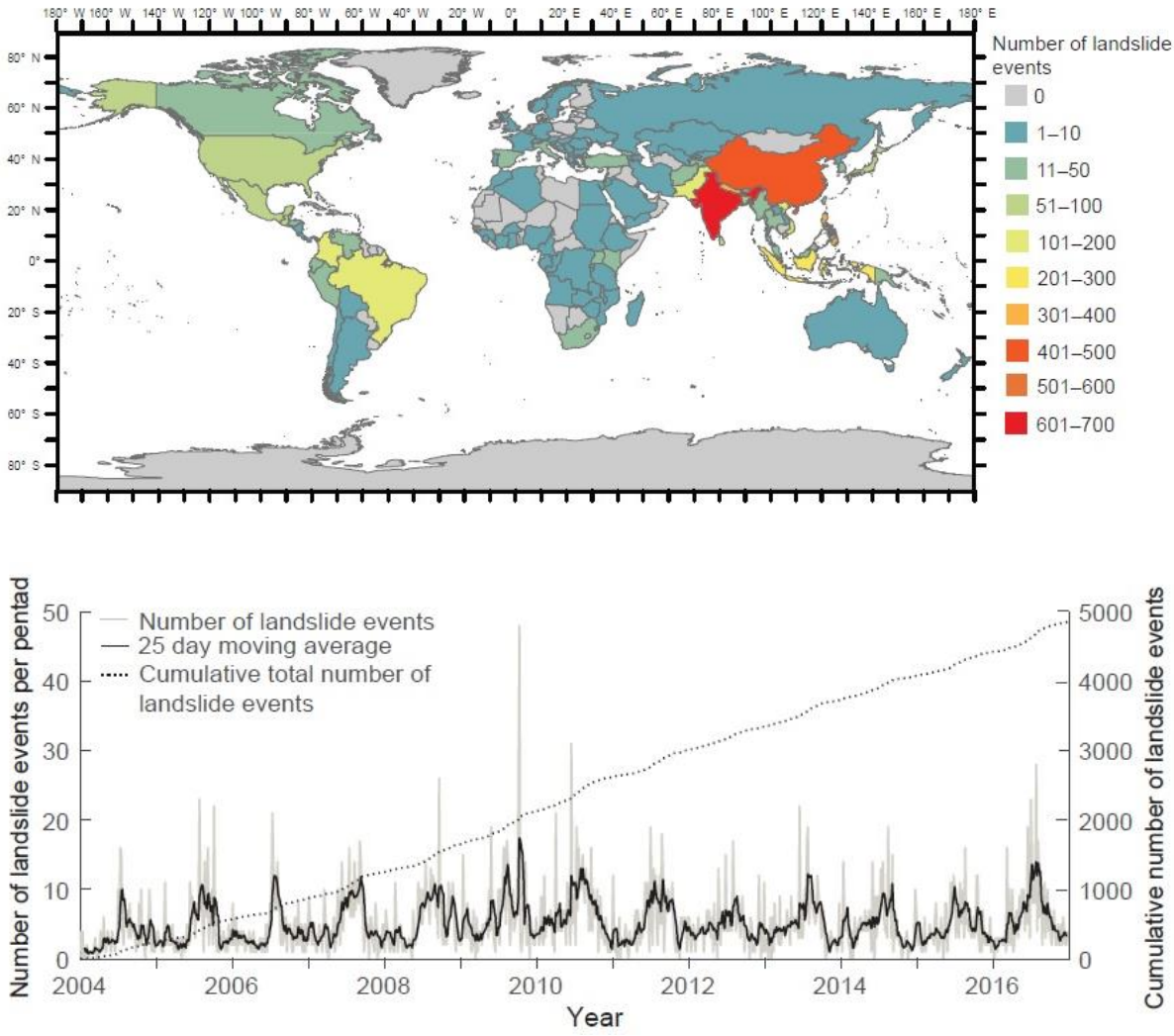

Figure 1: Top: number of non-seismically triggered fatal landslide events from 2004 to 2016 by country (top) and cumulative number of the recorded events (bottom) (Froude & Petley 2018).

In particular, hazard due to rockfalls, is the hardest one to predict among the several landslide typologies, because of the very few precursory phenomena and the short time available to react in respect to these rapid mass movements (Varnes 1978, Sättele *et al.* 2016) that can involve

from huge (slope scale) to very small (less than 1 m^3) volumes of rock. Generally, most of the rockfalls originate from the detachment of small portions of rock by an intensively fractured and jointed rock mass, because of the contribution of environmental (rainfalls, daily and seasonal thermal cycles, earthquakes) and anthropic (impacts, explosions, vehicular traffic) factors to which is added the role played by the long-term creep-driven deformations acting from slope to single joint scale. Considering the probability of small size rockfalls is higher than the one of greater mass movements, proper risk mitigation strategies should be adopted in the environments most sensitive to these kind of phenomena. In fact, especially in mountainous villages and along transportation routes, stabilization of slopes, the employment of retaining nets and protection barriers (Gottardi *et al.* 2011, de Miranda *et al.* 2015) are the most common remedies used to face the occurrence of rockfalls. In addition to these interventions, designed to reduce the vulnerability of infrastructures and of other human activities threatened by rockfalls occurrences, hazard mitigation is the subject currently managed by research activities not only in the field of earth sciences but in more different contexts, as those ones concerning tunnelling, quarrying, drilling and excavation activities.

Indeed, by taking into account the eventuality of injuring or killing people as well as the economic losses deriving from road or railway interruptions, the investigation of the processes leading to rock mass instability can provide useful contributions to the understanding and, subsequently, the prevention of rockfalls. These last, are generally triggered because of the accumulation of inelastic strain within the rock mass structure, which is responsible for the formation of new fractures or to the growth of the pre-existing ones. Such a process, known as rock mass damaging (RMD), leads to the deterioration of the mechanical parameters of the rock mass (as the friction angle and the elastic modulus), thus being at the base of the processes carrying to rockfalls.

A contribution suitable for the understating of RMD effects is given by the analysis of stresses, displacements and passive seismicity characterizing the rock mass, which allow to derive indications on the stability conditions of the monitored object. Especially microseismic monitoring is an affirmed and widespread technique more and more adopted in several ambits, because of the capability of providing information on the modification of the internal structure of a medium before that it becomes evident to other monitoring devices. In fact, as sketched in Figure 2, the phenomenological evolution of the rock mass damaging processes can be

monitored through dedicated microseismic monitoring network, aimed at the understanding of the initial steps of them, which is one of the current topic of slope stability analysis.

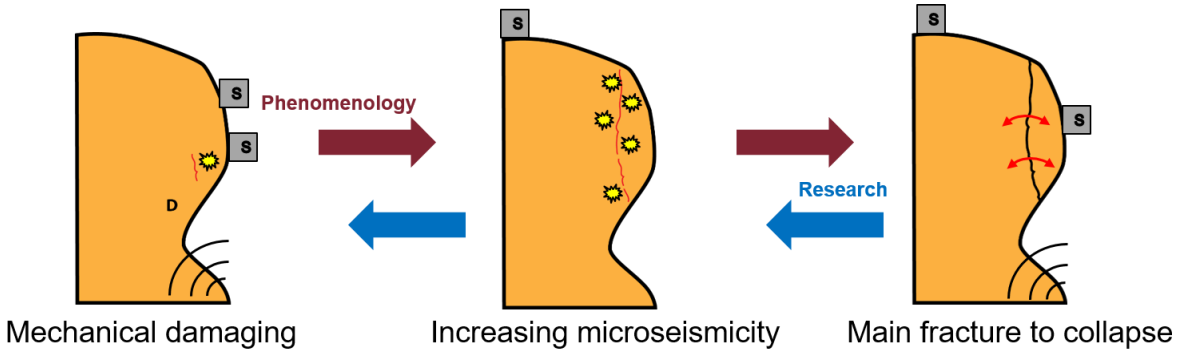

Figure 2: Sketch of the processes of growth, expansion and opening of fractures within a rock mass, which progressively lead to rock blocks separation and detachment. These phases can be investigated with the deployment of a microseismic monitoring network.

In such a research framework, this PhD thesis reports the analysis of three microseismic monitoring datasets acquired in continuous mode on two rock masses, a first one located in an abandoned quarry in the Acuto municipality and a second one along a railway near to Terni, in central Italy. In particular, the focus of this thesis concerns the investigation of how the daily or periodic recurrence of perturbative events, both natural and anthropic, can affect the rock mass stability over time, as a consequence of the progressive accumulation of these solicitations, potentially leading to inelastic strain amassing. Aiming at assessing potential variations in the fractures network (i.e. damaging phenomena), a physical-based approach is presented, dedicated at evaluating the damping ratio associated with the microseismic emissions registered on the rock masses studied, for specific frequency of interest. The trend of the damping ratio over time is analysed and compared with meteorological and seismic data, besides, for the Terni test site the cross-correlation and the root mean square (RMS) values of the train transit records were derived as comparative and alternative tools for the presented methodology. Furthermore, a technique based on the data analysis of the seismic ambient noise recorded in both the test sites is presented and discussed. A comparison of the averaged seismic noise amplitude filtered in specific frequency bands with the environmental parameters registered on-site has been done, and their correlation investigated.

The proposed methodology, based on the analysis of the damping ratio, could be considered and applied on yearly-lasting microseismic dataset in environments subject to rapid

morfoevolutionary changes, as coastal cliffs and high mountain environments, to slopes already involved in landslide processes, as well as to rock masses subjected to recurrent man-induced vibrations, as for quarrying activities or to trenches in proximity of roads and railways.

2 Microseismic monitoring of rock masses: an overview

The investigations of the rock masses aimed at understanding the evolution of their deformational behaviour and the potentiality of generating rockfalls have increased more and more in the last years, also favoured by the development of novel inspections methodologies and by new technologies and devices. In fact, literature widely deals with the topic of rock masses monitoring, both for landslide risk reduction on natural slopes and for the safeness of quarry, mining and tunnelling activities that involve the excavation of rock masses.

In general, rock mass monitoring can be performed through several approaches, taking into account the extent of the area and the processes to be observed. Commonly, the evolution of the stress-strain conditions of the rock masses is investigated by means of a) extensimeters, strain-gauges, inclinometers that are at the base of classical monitoring apparatus (Loew *et al.* 2017); b) laser scanners, photogrammetry, terrestrial and satellite interferometry (Abellán *et al.* 2010, 2014, Barla *et al.* 2010, Strozzi *et al.* 2010, Fanti *et al.* 2013, Salvini *et al.* 2013, Gigli *et al.* 2014); c) accelerometers, geophones and other seismic devices to analyse the passive seismicity of the rock mass as well as the signals related to rockfalls occurring in the monitored area (Lacerda *et al.* 2004, Meric *et al.* 2005, Godio *et al.* 2006, Jongmans & Garambois 2007, Willenberg *et al.* 2008, Travelletti *et al.* 2013, Pazzi *et al.* 2019).

Especially geophysical techniques, being minimally invasive approaches able to characterise the evolution of the stress-strain processes acting within a medium, and thus suitable for providing additional information on it in respect to other approaches, are widely used for field monitoring activities. In fact, geophysical techniques can allow to detect variations in the physical parameters characterising the internal structure of the rock masses, before they become evident to a more classical displacements monitoring system or to laser scanners and other remote sensing ones.

It is clear that geophysical measurements depend on the complex interaction between the seismic waves and the studied medium, which basic principles are reported in paragraph 2.1.

In the large field of geophysical methods, the development of seismic sensors with higher sensitivity, enhanced measurement accuracy and smaller dimensions, permitted the

investigation of the entire frequency spectrum covered by the motion waves, favouring the spreading of microseismic (MS) and acoustic emission (AE) techniques.

These methodologies consist of the detection, location and analysis of low energy seismic signals associated with the generation of new fractures and the movement and propagation of the existing ones that lead to the progressive failure of rock masses. Both the techniques allow to indirectly investigate the internal structure of the studied medium, mainly differing in the frequency range of the seismic motion recordable, which is higher for the AE signals in respect to the MS ones (Cai *et al.* 2007) (Figure 3).

In particular, the microseismic monitoring (MS) technique currently represents an affirmed diagnostic tool to detect vibrational signals in several contexts, as structural monitoring, mining excavation (Sun *et al.* 2012), tunnelling (Tang *et al.* 2010), and slope stability assessment as well (Papini *et al.* 2009, Colombero *et al.* 2018). The field of investigation of this practise is related to the signals characterised by a frequency content from 10^1 to 10^3 Hz, being comprised between the classical ambit of earthquake and seismic noise studies, dealing with lower frequencies, and the acoustic emission domain, characterized by frequencies greater than 10^4 Hz (Figure 3). Since in this thesis is proposed an analysis of seismic signals up to a thousand Hz, the state of the art of the microseismic monitoring technique is presented in paragraph 2.3, focusing on the main works related to the monitoring of rock masses.

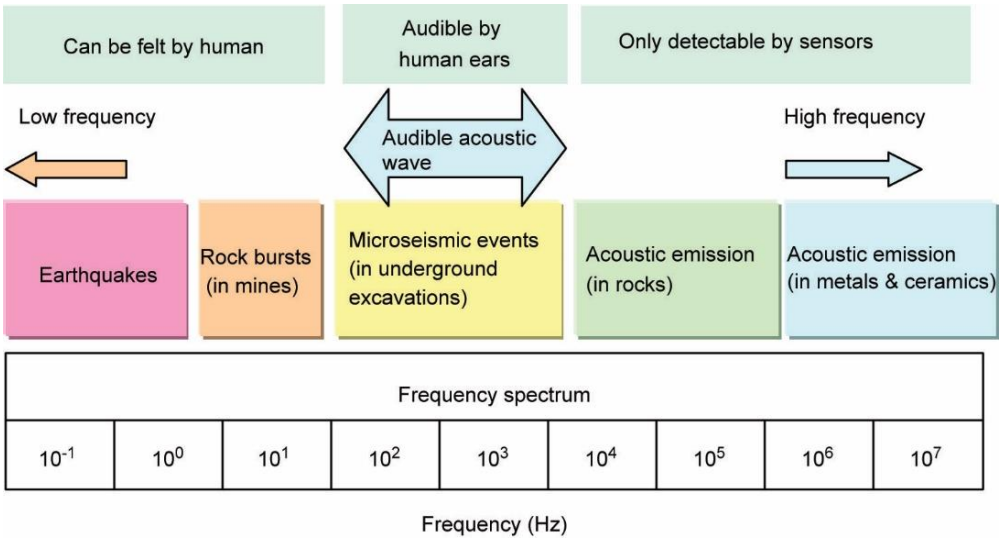

Figure 3: Seismic wave frequency spectrum and field of application of AE/MS techniques (Cai et al. 2007).

In addition to this technique, a recent development in the analysis of the seismic ambient noise measurements has been done. In fact, several studies deal with the information retrievable from the ambient noise and the correlation of its modification associated with changes in the characteristics of the medium, as thermal and hydrological variations (Larose *et al.* 2015) and also with the characterisation of rock slopes (Burjánek *et al.* 2010, Pilz *et al.* 2014, Kleinbrod *et al.* 2019). A summary of the works concerning the analyses of rock masses through ambient noise techniques is presented in paragraph 2.4.

2.1 Seismic wave propagation in rock masses

The propagation of surface waves (Rayleigh and Love) generated by any kind of source of vibrations, both natural (earthquakes, rockfalls) and anthropic (impacts and industrial machinery), strictly depends on the physical and geometrical characteristics of the crossed medium. In particular, the presence of interfaces and interruptions within the medium, as well as the transition among different media, are at the basis of energy dispersion phenomena. By taking into account the rock masses, the main characteristics that influence the wave propagation concern the rock lithology, the presence of several lithotypes characterised by a marked difference in the acoustic impedance and the existence of fractures and joints in the rock mass. Generally, when a seismic wave encounters a discontinuity is subjected to reflection and refraction phenomena. Such effects are responsible for energy dispersion and seismic wave attenuation or amplification. In particular, within a rock mass, because of the plasticity, the seismic wave is attenuated both by the geometric spreading and by the non-linear and viscous damping actions. Wu *et al.* (1998) studied the propagation characteristic of blast-induced shock waves by deploying several accelerometers along specific alignments on a rock surface, finding out that the aperture, the number of joints and the incident angle of seismic waves on them, are among the main factors controlling the wave propagation. Moreover, in agreement with Hao *et al.* (2001), they highlight that the attenuation of the waves is higher in the direction perpendicular to the strike of the joints than in the one parallel to them. Besides these basic principles, on which the approach proposed in this thesis is based, other specific studies have been carried out in the ambit of the mining research and of the wave attenuation for slope stability assessment. A review of the theoretical methods for the analysis of wave propagation

across jointed rock masses was presented by Perino *et al.* (2010). Li *et al.* (2010) performed laboratory testing and numerical modelling on the wave propagation across a filled rock joint observing that also an higher water content results in a lower transmission of the stress waves. A numerical analysis combined with tests conducted with a shaking table on a scaled model of a jointed rock slope was performed by Che *et al.* (2016), which measured the wave propagation at several positions of the reconstructed slope model. The Authors observed a delay in the propagation of the transmitted waves because of the presence of joints, emphasizing the concept that the number and spatial distribution of the joints are responsible for the detected time delay. This key notion has been taken into account in the development of the approach presented in paragraph 3.3.2.

2.2 Rock mass damage

The understanding of the processes that lead to the formation of new fractures and to the extension and movement of the pre-existing ones is fundamental for the assessment of the stability conditions of rock slopes and for the safeness of the engineered projects that insist on rock masses, as transportation routes, mines and dams. In fact, the accumulation of damage over time and its spatial localisation lead to a progressive degradation of the rock mass mechanical parameters, like strength and moduli, consequently causing an amass and redistribution of the stresses that can potentially evolve in failure processes. Within a jointed rock mass, the rock mass damaging processes act at different scales, causing the opening of the already-existing fractures (from millimetric to decametric extent) (Klein *et al.* 2008, Bretschneider *et al.* 2013) or the formation of new cracks (Kranz 1983). Generally, the stress applied on rocks, associated with a temporal factor, is the main parameter responsible for the fracturation phenomena. In addition to these creep-driven deformations, the rock mass damage can be rapidly increased because of natural and anthropic forcing actions that can act in a discontinuous or continuous way.

Among the factors responsible for the genesis of micro-fractures within the rock masses, a main role is played by earthquakes (Gischig *et al.* 2012, Koukouvelas *et al.* 2015, Martino *et al.* 2017, Romeo *et al.* 2017), blasting (Wei *et al.* 2009, Wang *et al.* 2018), tunnelling (Cai *et al.* 2004) and mining activities (Wang *et al.* 2015), rainfalls, daily thermal cycles and freeze-thaw ones (Matsuoka & Sakai 1999, Gunzburger *et al.* 2005, Mateos *et al.* 2012, Collins & Stock 2016, Dietze

et al. 2017) that are combined and superimposed with creep-driven deformations (Brückl & Parotidis 2005, Grøneng *et al.* 2010, Xu *et al.* 2014).

Therefore, it is important to study both the time-dependent behaviour as well as the transient variations occurring within rock masses due to external solicitations (Fiorucci 2018). These factors jointly affect the rock mass from the slope scale (Deep-sited gravitational slope deformations - DSGDS) to the micrometric scale (fractures growth and formation), causing rock mass damage phenomena that cumulate over time, showing deformational effects at different time stints (Figure 4).

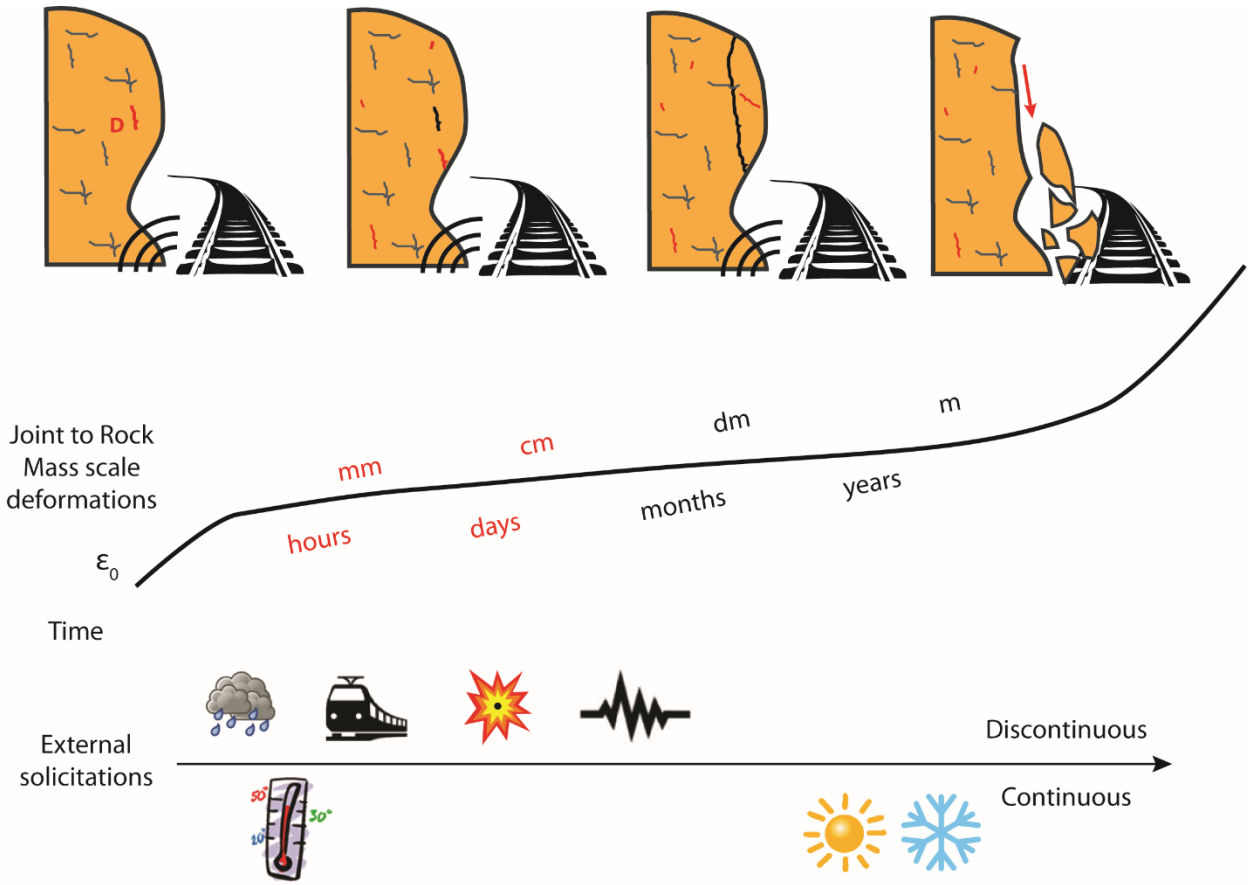

Figure 4: Sketch of the deformational processes acting on a rock mass at different scales and time stints. In addition to the rock mass creep, also external solicitations contribute to rock mass damage.

The stress-strain conditions responsible for the initiation of the fracturation phenomena have been widely investigated, with laboratory testing on rock specimens (Amitrano 2003, Hoek & Martin 2014, Cao *et al.* 2015), numerical modelling (Scholtès & Donzé 2012, Lisjak & Grasselli 2014) and on-site seismic surveys (Walter *et al.* 2012, Colombero *et al.* 2018).

In particular, the effects produced by thermal variations have been deeply investigated (Prick 2003, Yavuz *et al.* 2010, Lan *et al.* 2013, Akdag *et al.* 2018), because of the persistent action on the rock masses. Bakun-Mazor *et al.* (2013) studied the sliding mechanism of rock blocks partially detached from a rock slope, finding that the thermal factors may have been more important than seismic ones in controlling the displacements of the rock blocks.

The damaging phenomena are also studied at the specimens scale to observe and understand the loading conditions leading to the formation of the fractures. In the following, the mechanical properties of the rock are derived, scaled and inputted for numerical simulations.

Amitrano & Helmstetter (2006) realised a damage-based model to simulate the brittle creep of lab specimens by using a finite element model. The damaging of the elements constituting the model was reproduced by progressively decreasing their Young modulus, with the aim of simulating the effect of increasing crack density. Successively, this methodology was applied to simple slope geometries by Lacroix & Amitrano (2013) and to a real slope scale by Riva *et al.* (2016), which also considered the fracturation and varying damage properties of the medium.

Plenty of studies deal with laboratory testing and numerical modelling (Eberhardt *et al.* 2004, Heap *et al.* 2009, Scholtès & Donzé 2012, Brantut *et al.* 2013, Xu *et al.* 2014, Yang *et al.* 2015), moreover an increasing number of works is focused on the direct investigation of damage phenomena at the rock mass scale through on-site microseismic surveys.

2.3 Fields of application of microseismic monitoring

As previously introduced, the microseismic monitoring has several fields of application, especially concerning the study of the rock masses involved in mining and tunnelling activities as well as characterised by slope instabilities. A MS event is a low-energy seismic signal associated with a plastic deformation occurring in a medium, because of the accumulation of elastic energy over a threshold depending on the properties of the material. The rapid release of the accumulated stress is associated with the formation of new fractures or the sliding and propagation of the existing ones. The energy radiated by the microcracks can be detected with proper seismic devices, as accelerometers and geophones, characterised by a wide resolution in frequency and high sensitivity and accuracy. The sensors, mainly three-component ones, are deployed in several

array configurations, in order to enclose (in underground excavations and mines) or to cover (in slope faces and cliffs) the portion of the rock mass to be monitored. Frequently, the environments where the microseismic monitoring is performed are characterised by harsh conditions, and several issues have to be faced: the placement of the sensors, a sufficient data storage capacity and the availability of a stable power supply to guarantee the continuous data recording. These characteristics are progressively harder to find when passing from partly anthropised environments, as mines, to strictly natural environments, as slope faces.

The processing of the recordings is firstly focused on the recognition of the signals referred to the rock mass fracturing, by manual or automatic identification based on the characteristics of the original waveform recorded. Among the automatic identification procedures, STA/LTA based algorithms are extensively used and diffused (Withers *et al.* 1998, Vaezi & Van Der Baan 2015, Li *et al.* 2016) while machine learning techniques (Shang *et al.* 2017, Chen 2018, Dong *et al.* 2019, Lin *et al.* 2019, Peng *et al.* 2019) are rapidly increasing and improving the microseismic events detection.

Once the MS events are recognised, they can be classified, located and the source parameters calculated. The classification of the MS events is mainly based on the shape, duration and energetic characteristic of the signal. The review and the analysis of multiple microseismic events recordings registered on slopes affected by different slope instabilities (slides, falls, topples and flows) led Provost *et al.* (2018) to propose a classification of the various typologies of microseismic signals.

By referring to data analysis and processing techniques, the counting of the MS events and their characterization in terms of energy content, spectral amplitude and other parameters derived from the seismological ambit, as the peak ground acceleration, are the features mainly taken into account. By monitoring the derived parameters over time, it is possible to assess the evolution of the stability conditions of the studied rock mass, permitting the definition of the hazard associated with the collapse of rock portions.

The mechanical properties of the rock mass, derived from the analyses carried out on microseismic data, can be also used as input for numerical simulations in which the parameters of the model are continuously updated with the real damage state of the rock mass. This approach has been recently applied by several Authors (Bozzano *et al.* 2013, Xu *et al.* 2014, Tang

et al. 2015, Zhao *et al.* 2017, 2019, Zhuang *et al.* 2019) in order to obtain a better estimation of the failure time of rock slope portions.

Numerous studies have been carried out in the fields of quarrying and tunnelling activities (Wesseloo & Sweby 2008, Tang *et al.* 2010, Sun *et al.* 2012, Lu *et al.* 2013, Carlà *et al.* 2017, Zhao *et al.* 2018, Peng *et al.* 2019) and for the management of construction projects as dams and powerhouse caverns (Tang *et al.* 2010, Xu *et al.* 2015, Dai *et al.* 2016, Liu *et al.* 2018). In these cases, the microseismic monitoring helps in evaluating the progressive strain effects of rock masses affected by excavation activities as well as by the varying stress conditions exerted by a reservoir basin.

A vast bibliography also concerns the microseismic monitoring of unstable rock slopes (Spillmann *et al.* 2007, Tang *et al.* 2010, Occhiena *et al.* 2014, Ma *et al.* 2017, Yuan-hui *et al.* 2018), which aim is prevalently the investigation of the phenomena and environmental conditions responsible for the microseismicity. Recent studies were also focused on the microseismic monitoring of rock slopes close to railways (Xu *et al.* 2017, Yan *et al.* 2019), as rockfall hazard represent a threaten especially for the transportation routes located along cliffs and in man-excavated trenches (Budetta 2004, Ferlisi *et al.* 2012, Michoud *et al.* 2012, Macciotta *et al.* 2017, Messenzehl *et al.* 2017, Martino *et al.* 2019). In fact, the vibrations induced by trains may act as a repeated solicitation affecting the rock mass stability when long periods are considered.

Helmstetter & Garambois (2010) pointed out a correlation between the occurrence of rainfalls and the seismicity referred to rockfalls, highlighting a rapid response of the rock mass even with tiny amounts of precipitations. A similar correlation was found by Arosio *et al.* (2018), that analysed a three-year microseismic dataset acquired on an unstable rock slope in Northern Italy.

Other studies are focused on the investigation of the dynamic behaviour of unstable rock slopes, by analysing the microseismic emissions as well as the seismic ambient noise recorded prior of the collapse of the investigated sectors (Got *et al.* 2010, Lévy *et al.* 2010, Levy *et al.* 2011, Bottelin, Jongmans, *et al.* 2013, Bottelin, Lévy, *et al.* 2013, Valentin *et al.* 2017). In particular, Got *et al.* (2010) and Levy *et al.* (2011) analysed the pre-failure behaviour of an unstable rock cliff, both recording an increasing microseismicity and observing significant variations of the seismic noise amplitude in the phases prior of the collapse.

Lots of these studies show how the variations detectable in the frequency spectrum, is a distinctive characteristic preceding collapse events of unstable rock blocks. Although the observed frequency shifting is an important feature to be considered for risk management strategies, this characteristic appears only in the final status of the deformation, when a significant mass of material is ready to be released. Moreover, in the perspective of previsional numerical simulation, the frequency data are not directly utilisable.

In order to investigate also minor instabilities phenomena, it is deemed that the analysis over time of the damping ratio associated with the microseismic emissions is suitable for obtaining information related to the modification of the internal structure of the rock mass. An increment of the damping value with time may indicate a tiny change into the micro-fracture network of the rock mass, which can precede instability phenomena.

2.4 Ambient noise measurements

In the last decade, several studies were addressed to the characterisation of the seismic ambient noise, especially for seismic hazard purposes. In fact, the ambient noise is a peculiar attribute that describes the vibrational behaviour of any medium, allowing to retrieve several information on the subsurface in different fields of application, from site seismic response to slope stability.

The seismic ambient noise is the result of the different vibrations produced by several and disparate sources, both natural (sea waves, tides, wind) and anthropic (blasts, traffic, industrial machinery). Each source of vibration contributes to enrich the ground vibration with its own energy, carried by mechanical waves and associated with a specific frequency content.

Several studies deals with the categorisation of the sources constituting the seismic ambient noise (Bonnefoy-Claudet *et al.* 2006 and references therein). In their review, Bonnefoy-Claudet *et al.* (2006) report the general agreement of the specific literature in defining the seismic noise as prevalently constituted by surface waves. In particular, daily and weekly variations at frequencies higher than 1 Hz are related to human activities, while longer period changes associated with lower frequencies (between 0.005 and 0.3 Hz) are due to natural factors (oceanic waves and meteorology).

The composition of the seismic noise and the influences on its modifications were investigated because of the several ambits of application for which is used, among which the seismic microzonation is one of the most important (Nakamura 1989, Bard *et al.* 2010). Ambient noise has been also used for the investigation of landslides (Mainsant *et al.* 2012, Pilz *et al.* 2014, Collins & Stock 2016, Zare *et al.* 2017, Hussain *et al.* 2019) and unstable rock slopes (Burjánek *et al.* 2010, Moore *et al.* 2011, Panzera *et al.* 2012, Galea *et al.* 2014, Kleinbrod *et al.* 2019). The main outcomes consist of the reconstruction of the fracturation pattern of the monitored rock slope and the characterisation of landslide bodies or damaged zones in terms of geometrical and dynamic properties.

In addition to the spatial and dynamic information retrievable from ambient noise analysis, also a relationship with the variations occurring in the environmental parameters has been found. Larose *et al.* (2015) pointed out the correlation among the ambient noise and the thermal variations in the subsoil, buildings and even rock columns. A similar outcome was found by Colombero *et al.* (2018) that observed the correlation between daily and seasonal temperature fluctuations and the resonance frequency values of unstable portions of an highly-jointed rock mass located in Northern Italy.

In this thesis, the variations in seismic noise within specific frequency bands were compared in respect to the environmental parameters recorded in the test sites, to check the existence of a correlation for all the considered frequencies.

3 Materials and methods

This PhD thesis deals with the analysis of continuous microseismic datasets recorded on rock masses, being focused both on the investigation of the physical characteristics of the microseismic events and on long-period ambient noise variations in specific frequency bands, aiming at recognizing rock mass damaging phenomena. In particular, a novel physically-based technique focused on the investigation of the damping ratio associated with the microseismic emissions is proposed (Damping Analysis, paragraph 3.3.2). The study of ambient noise variations deepen an already proposed data analysis technique (Frequency Band Ambient Noise Disaggregation Analysis, paragraph 3.3.4).

To study the RMD processes acting on rock masses, it is needed to collect wide and multi-sensors datasets in natural test sites, lasting from months to years preferably, in order to take in consideration all of the different variables and a sufficient time span necessary to observe potential modification in the monitored deformational/vibrational parameters. Since the processes of fractures formation and propagation can act very slowly, even years-lasting datasets could show no significant results in the monitored parameters, thus the selection of the case study for testing a novel technique has to be accurately done. In fact, contrary to laboratory experiments performed on rock specimens to understand fractures formation conditions (Amitrano 2003), since in natural settings it is not possible to accelerate the physical processes acting within the medium, unless with experimental activities aimed at forcing some boundary conditions (Fiorucci 2018), it is crucial to choose fast-evolving environments. Even if natural settings are less controlled under the point of view of the parameters and boundary conditions that characterise the case studied, in situ microseismic monitoring provides the opportunity, and the challenge, of taking into account the variability of the contribution of environmental and anthropic factors acting at different rock mass scales.

To test the reliability of the proposed technique and in order to obtain a wide collection of microseismic events, specific microseismic monitoring campaigns were performed on the rock masses cropping out in two natural test sites located in central Italy. The first one is the Acuto test site, situated in an abandoned quarry in the municipality of Acuto, about 100 km SE far from Rome; the second one is located along the Terni-Giuncano railway, close to the Terni town, 150 km NE far from Rome. The test sites (paragraph 3.2) were selected to be representative of two

opposite conditions: the Acuto test-site is mainly characterized by natural vibrations, as the abandoned quarry is far from roads and human activities; the Terni test-site was selected because very close to an active railway line, in which the contribution of the repeated train transits in soliciting the rock mass is added to the damaging effect due to natural actions.

For the Terni-Giuncano railway test site, given the presence of trains transiting close to the rock mass, additional analyses have been done on the trains passage recordings (Cross-correlation and RMS analysis, paragraph 3.3.3), in order to investigate even the trend of these parameters over the monitored period.

Furthermore, in both the test sites rock samples were taken and shaped to obtain prismatic test pieces analysed by means of an ultrasonic testing device, to derive the P-waves propagation velocity (ASTM 2005) of the rock masses analysed.

In Table 1 are summarised the type of analysis performed in the two test sites; the microseismic equipment, the test sites and the methodology employed for the analysis of the microseismic dataset are introduced in the following paragraphs.

Table 1: Summary of the analysis performed in the two test sites.

	Acuto test site		**Terni test site**		
Type/Target of the analysis	Ambient noise	MS Events	Ambient noise	MS Events	Train passages
Damping Analysis		X		X	
F-BAND analysis	X		X		
RMS Analysis					X
Cross-correlation analysis					X
PGA, PGV, Arias, FE		X		X	X

3.1 Microseismic monitoring devices

The microseismic monitoring in the two test sites has been carried out through high sensitivity Bruel & Kjaer (BKSV) one-component piezoelectric accelerometers (type 8344) (Figure 5), cable connected with a signal amplifier SomatXR MX1601B-R coupled with a digital acquisition system

SomatXR CX23-R both produced by HBM (Figure 6). The connection between the signal amplifier and the accelerometers was done with twenty-meter long low noise cables. The main features of the sensors are reported in Table 2, while the dimensions and a calibration chart of a sensor are shown in Figure 5. From the latter, it is possible to remark the flat frequency response in the range 5-2000 Hz and the sensitivity of the sensor of 2500 mV/g, characteristics that allow to detect very low signals emitted by the monitored object. Besides, the very small dimensions of the accelerometers and the sealed structure made them proper to be used even in harsh environments.

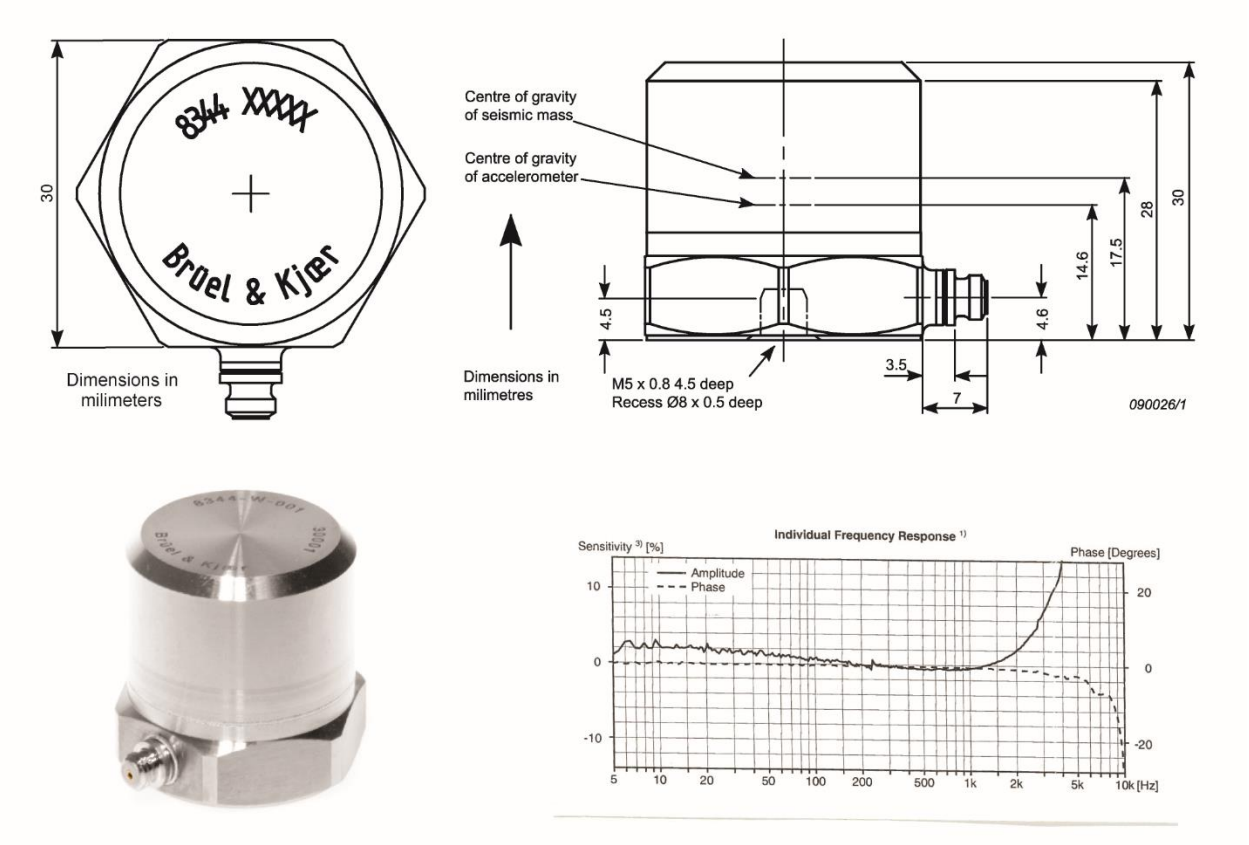

Figure 5: Dimensions, characteristics and calibration chart of the BKSV 8344 accelerometer.

Even the digital acquisition system (Figure 6) has a robust and watertight design and it can record up until 16 different channel contemporaneously, with a sampling frequency up to 20 kHz and an internal storage capacity of 64 GB. Data are saved in a compressed SIE file format: an automatic saving is done every 5 seconds, avoiding to lose the recorded data in the case of power supply interruptions, furthermore, the data logger has the capability of automatically restart the acquisition with the set parameters when the electricity supply is restored. Moreover, in the

occasion of continuous monitoring and of very high sample rates, to avoid troubles in managing just one huge data file, it is possible to set the creation of several files according to a desired duration or to a specified time of the day. The system is also predisposed for the automatic sending of data packages through LAN connectivity, but both the test-sites are not reached by the internet, thus data download was manually done. In fact, as for all the microseismic monitoring campaigns conducted in natural environments, it was required to face some technical issues related to the absence of electricity and internet connection as well as the installation and maintenance of the microseismic equipment. For both the test sites, the time recurrence of the maintenance of the equipment and the data download was established in about two interventions per month.

Figure 6: Digital acquisition system SomatXR CX23-R (left) and signal amplifier SomatXR MX1601B-R (right).

In both the test sites, as detailed described in paragraphs 3.2.1 and 3.2.2, the sensors were deployed on the rock mass surface. Once that the spots to be monitored were individuated, 7 mm diameter holes were drilled perpendicular to the rock surface to host metallic 5 mm diameter studs, subsequently fixed by using epoxy resin. In the following, the accelerometers were tightened to the metallic studs, which guaranteed the coupling between the sensors and the rock surface.

Since both the localities are not reached by electricity, the power supply was guaranteed by means of a 105 W solar panel connected to an automatic voltage regulator and to a 40 Ah lead backup battery. Unfortunately, for reasons related to the exposition of the solar panel, the season, and the alternation of sunny, cloudy and rainy phases, some interruptions during the monitoring periods were unavoidable. The data logger, the signal amplifier, the backup battery

and the automatic voltage regulator were placed into a watertight box placed in proximity of the monitored rock masses.

In addition to the microseismic monitoring devices, also environmental data were collected by means of on-site installed weather stations, providing information about the external conditions affecting the monitored slopes.

Before introducing the methodology used for the analysis of the microseismic datasets, the two test sites will be presented in the next paragraph, to better specify differences and similarities of the two case studied and to show the configurations adopted with the sensors.

Table 2: Main dynamic, environmental and physical characteristics of the employed accelerometers.

Dynamic Characteristics	Voltage Sensitivity (@ 159.2 Hz and 4 mA supply current)	*mV/ms^{-2} (mV/g)*	250 ± 20% (2500± 20%)
	Measuring Range	*ms^{-2} peak (g peak)*	±26 (2.6)
	Frequency Range (±10% limit) Amplitude Response	*Hz*	0.2– 3000
	Frequency Response		Individual Frequency Response on calibration chart
	Mounted Resonance Frequency	*kHz*	>10
	Transverse Sensitivity (@ 30 Hz, 100 ms^{-2})	*%*	< 5 of the sensitivity of the axis in question
	Transverse Resonance Frequency	*kHz*	3.5
Environmental Characteristics	Operating Temperature Range	*°C (°F)*	– 50 to + 100 (– 58 to + 212)
	Temperature Coefficient of Sensitivity	*%/°C*	+ 0.05
	Temperature Transient Sensitivity (3 Hz LLF, 20 dB/decade)	*ms^{-2}/°C*	0.001
	Base Strain Sensitivity (at 250 με in base plane)	*Equiv. ms^{-2}/με (g/με)*	0.002 (0.0002)
	Magnetic Sensitivity (50 Hz, 0.038 T)	*ms^{-2}/T (g/T)*	0.5 (0.05)
	Max. Non-destructive Shock	*ms^{-2} peak (g peak)*	3500 (350)
	Humidity		100% RH non-condensing
Physical Characteristics	Case Material		Stainless steel AISI 316– L
	Sensing Element		Piezoelectric, Type PZ 27
	Sealing		Hermetically sealed
	Weight (excluding cable)	*gram (oz.)*	176 (6.2)

3.2 Case studies

The case studies are both located in the central sector of the Apennine chain (Figure 7) and were chosen in order to be representative of two opposite conditions: the first one implies a rock mass

and a prone-to-failure rock block mainly solicited by natural actions (Acuto quarry test site, also abbreviated as “Acuto” in the text); the second one is mainly devoted to the understanding of the contribution of anthropic vibrations given to a rock mass close to a railway line (Terni-Giuncano railway test site, also abbreviated as “Terni” in the text). For both the sites, the Research Centre for Geological Risks (CERI) of Sapienza University of Rome carried out different research activities devoted to the definition of rockfall hazard prevention strategies. In particular, the Acuto test site is directly managed by the CERI since 2015, while the Terni-Giuncano railway site has been individuated in agreement with the Italian National rail infrastructure manager (RFI), which allowed the access to the rail network for performing the experimentation planned for this PhD thesis. In both the test sites, preliminary investigations were carried out in order to choose and then predispose the sectors to be monitored.

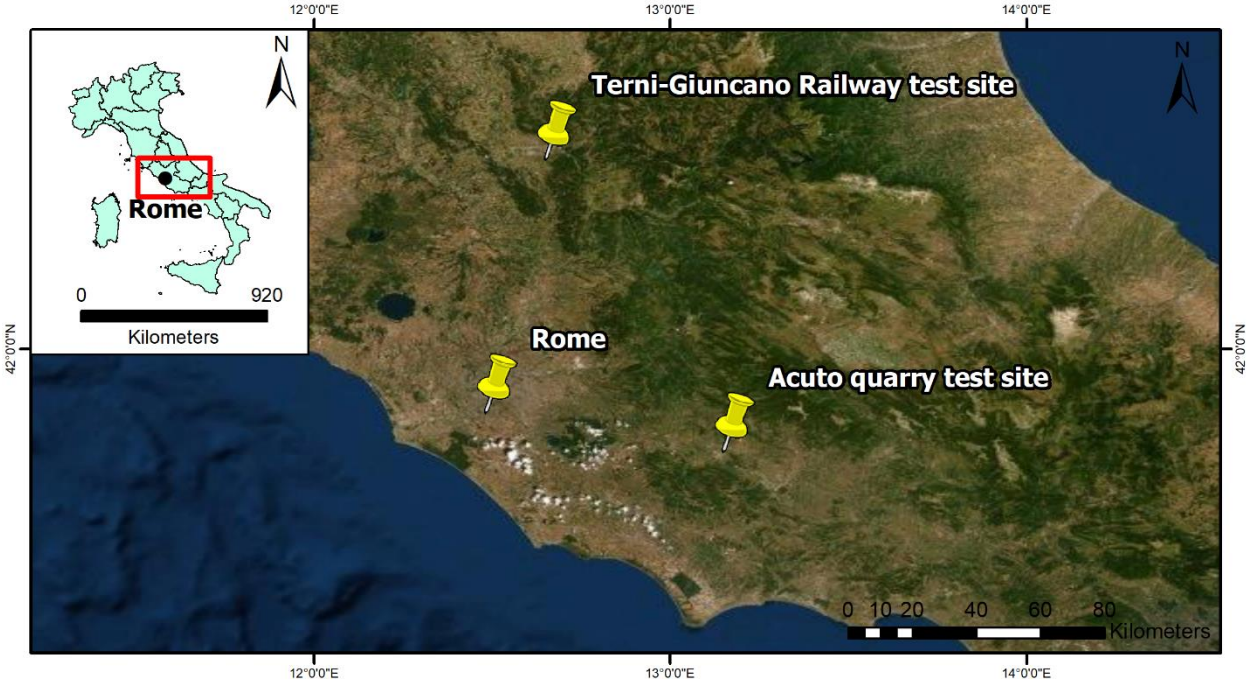

Figure 7: Satellite view and location of the two test sites in central Italy.

A total of three microseismic monitoring campaigns, resumed in Table 3 and Figure 8 and extensively presented in the following paragraphs, have been carried out in the two test sites. In all the cases, the data acquisition was set in continuous mode, with a sampling frequency of 2400 Hz and for saving files every three hours; vibrational data were saved in g (m/s^2) unit and in Coordinated Universal Time (UTC or GMT, Greenwich Mean Time).

Table 3: Resume of the microseismic monitoring campaigns and of their main features. For the Acuto 2019 campaign, the duration of 145 days is referred to the dataset analysed until April 22nd 2019.

Campaign	Beginning	End	Duration (days)	Deployed sensors	Measured component	Sampling Frequency (Hz)	Location of the sensors	On-site weather monitoring
Acuto 2018	23/02/2018	31/05/2018	97	6	NS	2400	Rock block Rock mass	All the period
Terni 2018	04/06/2018	14/11/2018	163	3 - 6	EW	2400	Rock mass	From 08/08/2018
Acuto 2019	28/11/2018	ongoing	145*	6 - 7	NS - EW - UP	2400	Rock block Rock mass	All the period

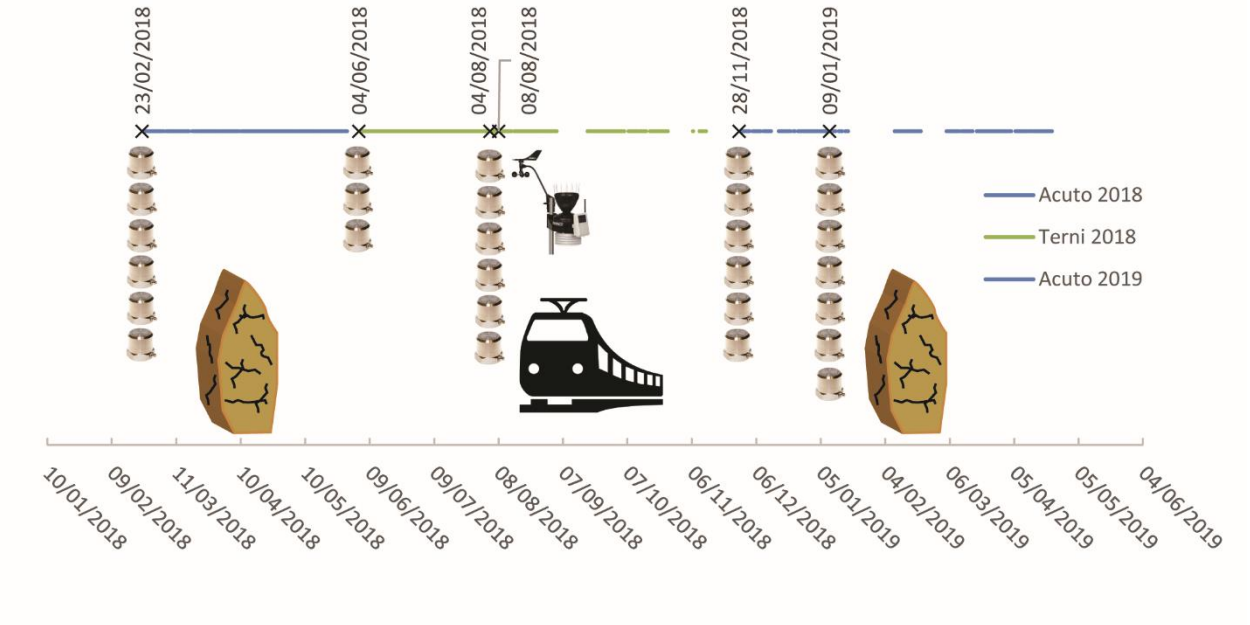

Figure 8: Time spans of the microseismic monitoring campaigns and sensors deployed.

3.2.1 The Acuto quarry test site

In the ambit of the research activities conducted by the CERI, the abandoned quarry of Acuto (Frosinone, central Italy) was selected since Summer 2015 as test site for the installation of a permanent multi-sensor monitoring system on a prone to failure rock block, aiming at investigating the long-term rock mass deformations due to temperature, wind and rainfalls (Fantini *et al.* 2016, Fantini *et al.* 2017). The quarry is located in the municipality of Acuto (Figure

9), 100 km SE far from Rome, on a carbonatic hill at an altitude of about 750 m a.s.l. The site location corresponds to the carbonatic Ernici Mounts ridge, which is part of the Latium-Abruzzi platform sedimentary domain, mainly constituted by thick Meso-Cenozoic carbonatic successions. In particular, Mesozoic wackestones with rudists outcrop on the sub-vertical quarry front (Accordi *et al.* 1986), which is extended about 500 m with a height ranging from 15 up to 50 m.

The quarry wall is aligned along the E-W direction, while the northwestern sector of it is oriented at N 10. The geomechanical characterisation of the rock mass led to the identification of four joint sets (Fantini *et al.* 2016), here indicated according to dip direction/dip convention: S0 (130/13) corresponding to the limestone strata, S1 (270/74), S2 (355/62) and S3 (190/64). In the NW portion of the quarry, a 12 m^3 intensely jointed protruding block exposed to SE has been individuated as target for the installation of the permanent multi-sensor monitoring system in 2015 and as focus of the temporary microseismic monitoring performed in the ambit of this PhD thesis. The rock block is separated on its western portion (also named block side) by a main open fracture (oriented 115/90) from the quarry wall, while on the eastern part, even if limited by a secondary fault line, the block is more contiguous with the rock mass wall. For this reason, the front and the lateral side of the rock block resulted to be the more interesting sections to be monitored, first under the deformational point of view, then under the vibrational one.

The permanent multi-sensor monitoring system consists in:

- 1 thermometer for the rock mass temperature, installed on the frontal face of the rock block;
- 6 strain-gauges installed on micro-fractures of the rock mass;
- 4 extensimeters installed on open fractures;
- 2 weather stations, installed at the foot and the top of the slope wall, equipped with an air thermometer, a hygrometer, a pluviometer and an anemometer for wind speed and direction.

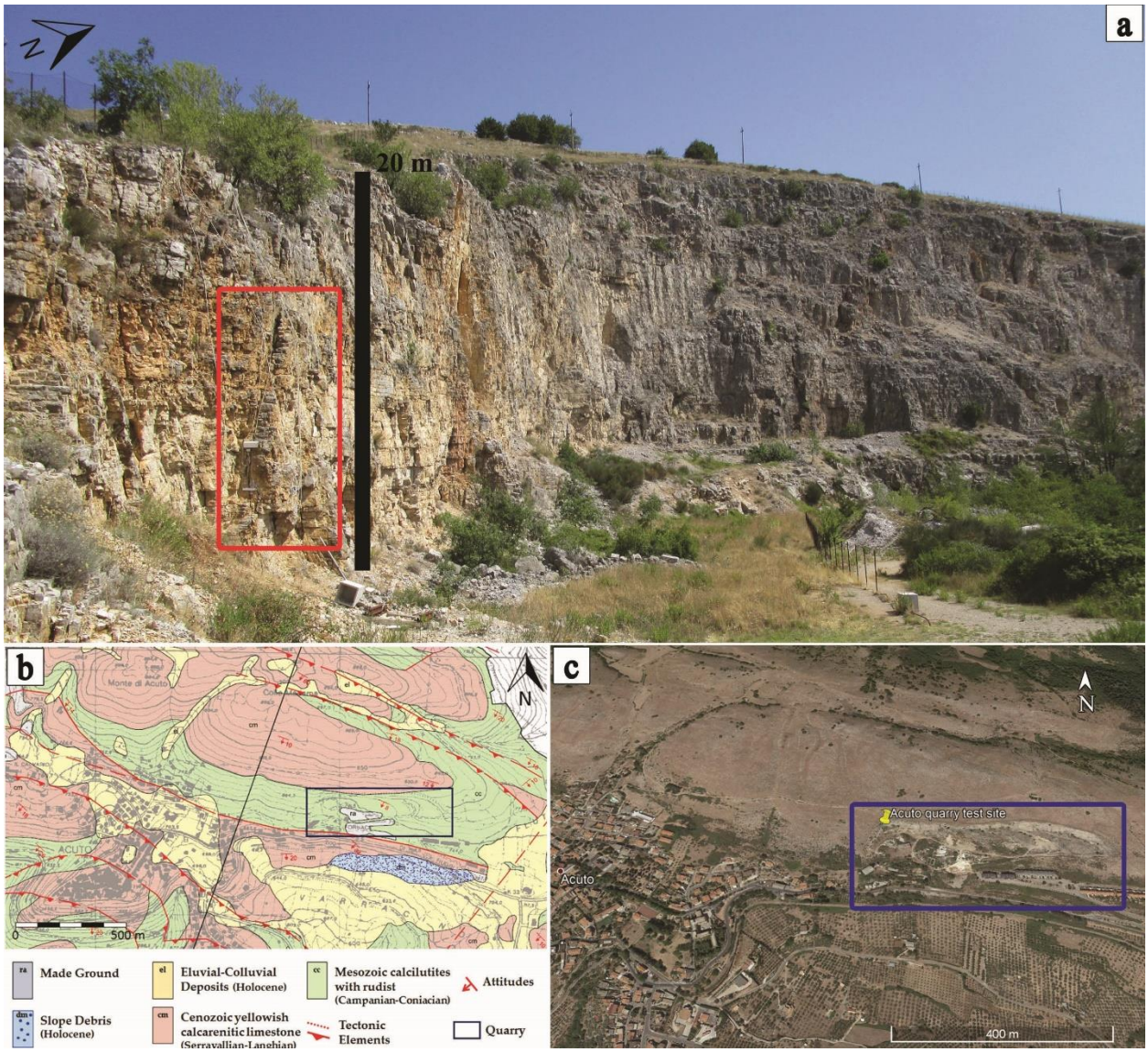

Figure 9: View of the Acuto quarry wall (a) with the rock block selected as the focus of the multi-sensor monitoring system (red rectangle). Geological sketch (b) and satellite view (c) of the Acuto municipality and of the quarry area (blue rectangles).

All these sensors are connected to a data logger CR1000 Campbell Scientific, equipped with 24 acquisition channels and set to sample data every minute in the local time unit. Besides, a GPRS wireless connection system allows the automatic transmission of data packages to a local server every 4 hours and enables the remote control of the datasets. The deformational and meteorological datasets are acquired in continuous mode since Autumn 2015.

Several studies and investigations have been carried out so far, both focused on the predisposing conditions for rockfall release and the testing of new technologies and methodologies. Among them, the thermal response of the rock mass was investigated via a monthly infrared

thermographic survey (Fiorucci *et al.* 2018), in order to understand the potentiality of thermal cycles in releasing rock portions. Furthermore, aiming at recreating real rockfall hazard scenarios impacting on infrastructures, also a railway track was posed to test a prototypal optical device for the detection of rockfalls, based on a change detection algorithm working in a selected region of interest (i.e. the railway track and its surroundings) (Fantini *et al.* 2017). Besides, the reliability of the nanoseismic monitoring technique (Joswig 2008) in detecting rockfalls was also investigated (Hakes *et al.* 2018).

To carry on the investigations on rockfalls predisposing phenomena at the Acuto quarry, the 12 m^3 rock block was chosen as the focus of the microseismic monitoring for this PhD thesis. Moreover, considering that the rock block is partially separated by the rock mass, it was deemed potentially subject to greater mobility in respect to the rock mass, and thus worthy to be investigated. Furthermore, the location of the quarry, far from anthropic disturbances and with the main quarry front exposed to south direction, makes this site ideal to study the evolution of deformation and fracturation processes mainly attributable to thermal cycles and natural actions.

To characterise the P-waves velocity of the rock mass, some rock blocks were sampled and shaped in 6 parallelepipedal test pieces. The ultrasonic testing executed following ASTM (2005) resulted in P-waves velocity ranging from 3923 to 4460 m/s resulting in an average of 4193 m/s.

Two microseismic monitoring campaigns have been carried out: the first one took place from February 23th 2018 to May 31st 2018 (Acuto 2018), lasting a little more than three months; the second one started on November 28th 2018 and is currently ongoing (Acuto 2019). A summary of the placement adopted for the accelerometers for both the monitoring campaigns is reported in Table 4.

Table 4: Summary of the accelerometer deployments for the two monitoring campaigns conducted at Acuto test site. Full period is intended with the exception of the interruptions due to no power supply.

Campaign	# Sensors on rock block	# Sensors on rock mass	Measured component	Monitored period	# Sensors in same position
Acuto 2018	1, 2, 3, 4	5, 6	NS	Full period	6, 2
Acuto 2019	4	1	NS	Full period	1, 4
	5	2	EW	Full period	
	6	3	UP	Full period	
	7	-	NS	Starting 09/01/2019 Several interruptions	

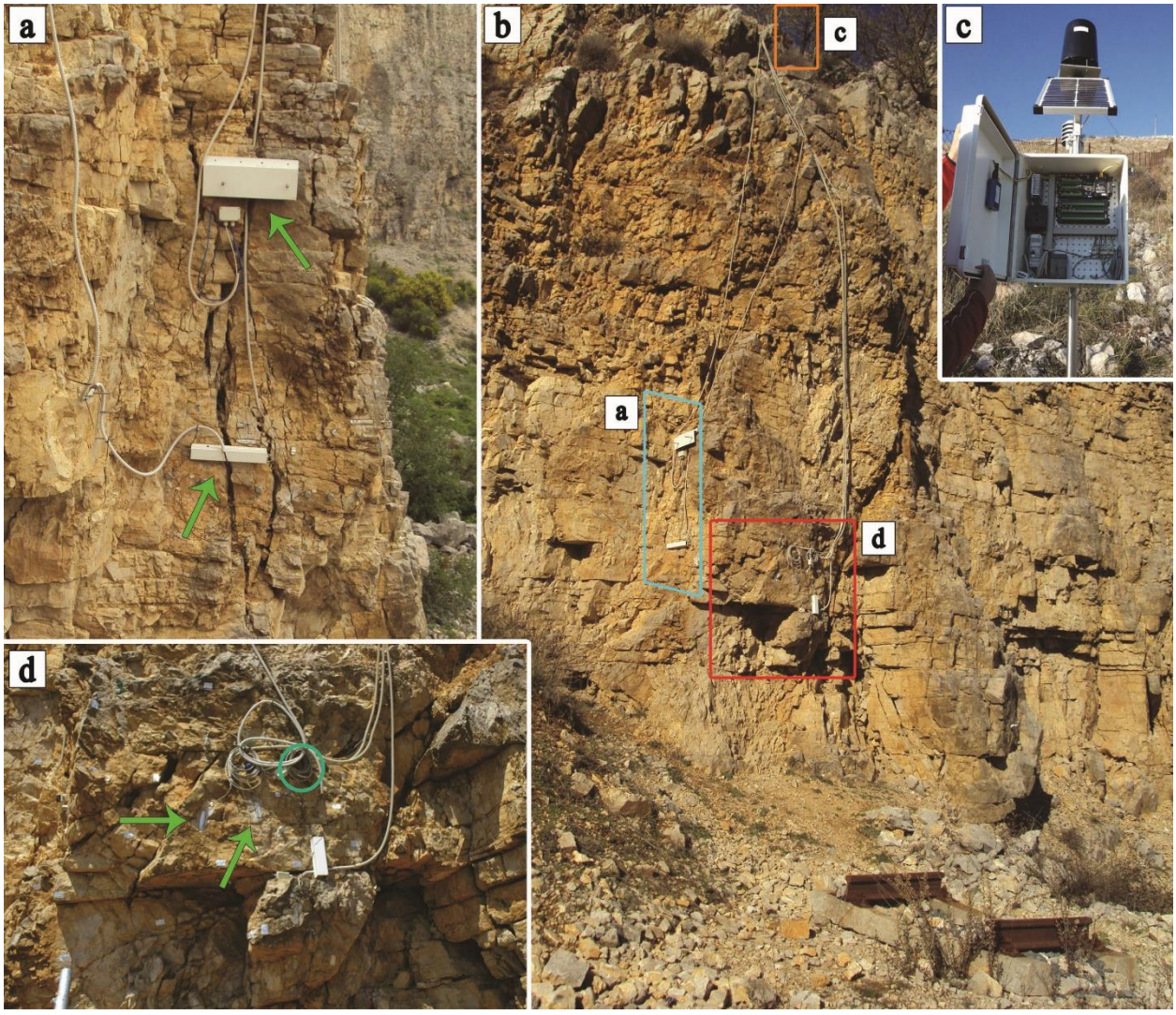

Figure 10: In b) is shown the rock block with the railway track posed at its base. The squared areas zoomed in a), c) and d) show respectively: the block side with a main open fracture on which are installed two extensimeters (pointed by the arrows); the data logger and the weather station located at the top of the slope; the block front on which is circled the position of the thermometer for the rock mass temperature, while the green arrows point to two strain gauges.

For the first monitoring campaign (Acuto 2018), six BKSV one-component accelerometers were deployed along an horizontal alignment with a spacing of about 15 cm: in this configuration 3 sensors were placed on the rock block (ID: 1, 2, 3), 2 were located on the rock mass wall (ID: 5, 6) and the last one was positioned at the passage between the rock block and the rock mass wall (ID: 4). In the adopted configuration, all the sensors were measuring the N-S direction (Figure 11). During the three-month monitoring period, it was recorded also an intense and unconventional meteorological event in the last days of February, in which a strong decrease of the temperatures was recorded.

Figure 11: Positioning and ID of the accelerometers for the first microseismic monitoring campaign (Acuto 2018) (a). The location of the sensors on the rock block side is also shown in the circled area in b). The digital acquisition system and the backup battery were put into a watertight box placed on the top of the slope wall (c).

For the second monitoring campaign (Acuto 2019) a different configuration of the accelerometers has been adopted, keeping only two sensors in the same position of the previous monitoring period (in particular sensors with ID: 6 and 2, that in this new campaign are respectively ID: 1 and 4) (Figure 12). This new configuration was chosen to point out the 3D vibrational behaviour of both the rock mass and the rock wall, by measuring along three

orthogonal components. The microseismic monitoring started by deploying six accelerometers following the scheme shown in Figure 12, in particular sensors with ID 4, 5, 6 were placed on the rock block, measuring respectively the N-S, E-W, and vertical components of the motion; the same components were measured by the sensors positioned on the rock mass wall (ID: 1, 2, 3). A new sensor (ID: 7) has been added on the eastern side of the rock bock aligned along the N-S direction. Due to technical issues, the new sensor was not available for all the duration of the monitoring period. For both the monitoring campaigns, the acquisition was set in continuous mode and with a sampling frequency of 2400 Hz. The maintenance of the equipment and the download of the data took place about twice per month.

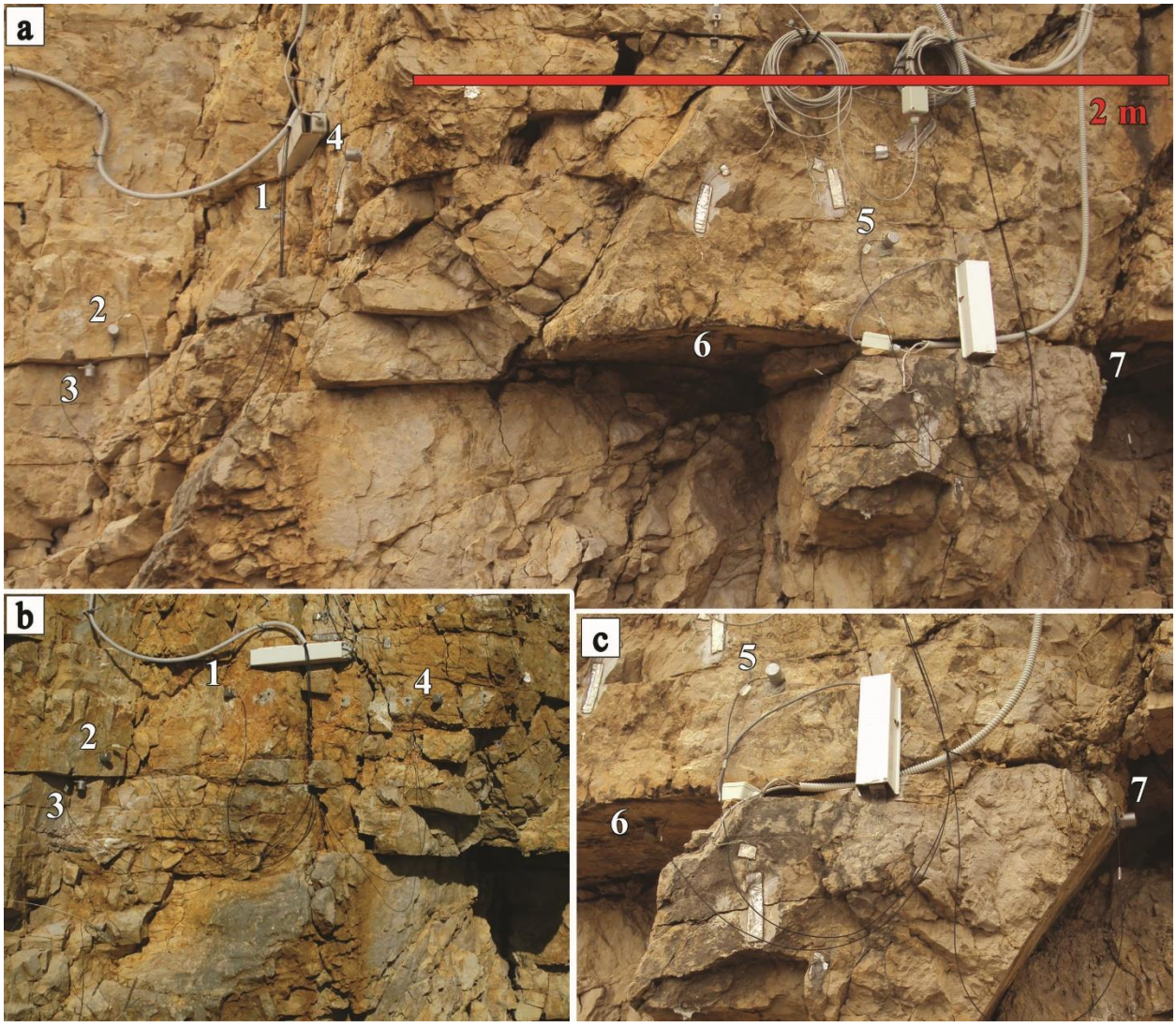

Figure 12: Positioning and ID of the accelerometers for the second microseismic monitoring campaign (Acuto 2019) (a). The position of sensors 1 and 4 coincides with that one of accelerometers 6 and 2 in the previous monitoring campaign. A zoom of the block side and of the rock mass is shown in b), while the block front is reported in c).

3.2.2 The Terni-Giuncano railway test site

The national railway line, which connects Terni to Giuncano, is characterised by a single-track line passing through a narrow and deep-incised valley in a hilly area of Umbria region, in central Italy. This section of the railway is part of the Rome-Ancona railway, an important and historical route crossing the Apennines and linking the Tyrrhenian Sea to the Adriatic Sea. In fact, this railway is classified as “fundamental railway line”, because it allows to connect central Italy from east to west, both in terms of passengers and of goods. In particular, the railway comprised between the cities of Terni and Giuncano is affected by a number of transits per day of about 42 trains on weekdays and 25 trains on bank holidays, with a maximum velocity limited at 80-100 km/h. As usual, the majority of the transits is clustered during rush hours in the morning and in the afternoon, while the traffic is interrupted during nights. Because of the importance of this transportation corridor and considering that of the total length of 292 km, 121 km are on a single track, several parts of the line have been doubled in recent years, others are currently in progress and others are planned for the future. Among the latter, the development of the track comprised between the cities of Terni and Spoleto is intended with the realization of a 22.4 km long tunnel that would allow in speeding up the circulation, increment the railway traffic and avoid the path crossing along the flanks of the slopes. In fact, this sector of the Apennines is constantly affected by slope instabilities threatening the infrastructures (Cardinali *et al.* 2002, Guzzetti *et al.* 2003, Guzzetti *et al.* 2004, Guzzetti *et al.* 2004, Galli & Guzzetti 2007), because of the presence of highly jointed rock masses outcropping along the man-cut trenches.

Under a geological point of view, the considered area is characterised by folded and jointed rock masses involved in thrusting and faulting events originated by the Apennine chain genesis. In particular, the Terni-Giuncano railway runs along the Serra River valley in correspondence to a canyon cut by the homonymous river in the southern sector of the Martani Mounts, NE of the Terni geological basin. In this area, main tectonic elements as the Monte Torricella thrust and the Battiferro fault (Calamita & Pierantoni 1994, Bruni *et al.* 1995) constantly modified the stress-strain status of the rock formations that constitute the current slopes. The Scaglia Rossa formation, a Mesozoic limestone, outcrops along extensive sections of the railway trench, and even in the location individuated as test-site (Figure 13).

Field inspections and geomechanical surveys were carried out along the railway line between January and March 2017, to select the rock mass wall more suitable for installing seismic devices (Figure 14). Finally, the test-site was selected close to a tunnel, where no retaining nets were deployed to equip the rock walls and a visible block-size slope debris testified previous small-size rockfalls. The test-site is located at about 280 m a.s.l., where the railway line, running approximately along the N-S direction, passes 4.5 m far from a rock mass partially excavated to allow the realization of the northern entrance of the tunnel.

The highly weathered conditions of the outcropping rock mass resulted by the concurrence of the main joint patterns, also related to the outcropping parasitic folds, hydraulic conditions of joints and the presence of vegetation on the rock wall favoured by its north-facing. Despite the very complex fractures network and the alteration conditions, a geomechanical characterisation, performed following ISRM (1978), provided a number of joint per cubic meter (J_v) of 7-10 and I_b: 0.3-0.5, indicating the small to medium size of the blocks potentially releasable from the rock mass. Two main joint sets were individuated, which are respectively indicated according to the dip direction/dip convention: J1 (170/80) and J2 (350/78), both presenting an opening of 2-3 mm and with a terrain filling. For both the joint sets, a mean Joint Roughness Coefficient (JRC) of 8 was evaluated, while the Joint Coefficient Strength (JCS), resulted in an average interval of 44-46 MPa, according to Barton & Choubey (1977).

Furthermore, in order to derive the physical and mechanical properties of the outcropping limestone some of the rock block at the base of the slope wall were sampled to perform laboratory tests on them. In particular, some rock blocks were shaped in parallelepipedal 3x3x5 cm test pieces then used to derive the P-wave velocity; some others were employed for the assessment of the uniaxial compressive strength by means of the point load test. According to the hydrostatic weighing method (ISRM 1979), the test pieces were used for deriving the average density (ρ) of the rock, that resulted to be of 2630 kg/m^3, corresponding to a natural specific gravity (γ_n) of 25.79 kN/m^3. The specific gravity of soil solids, determined following ASTM (2006), resulted to be of 26.62 kN/m^3 .

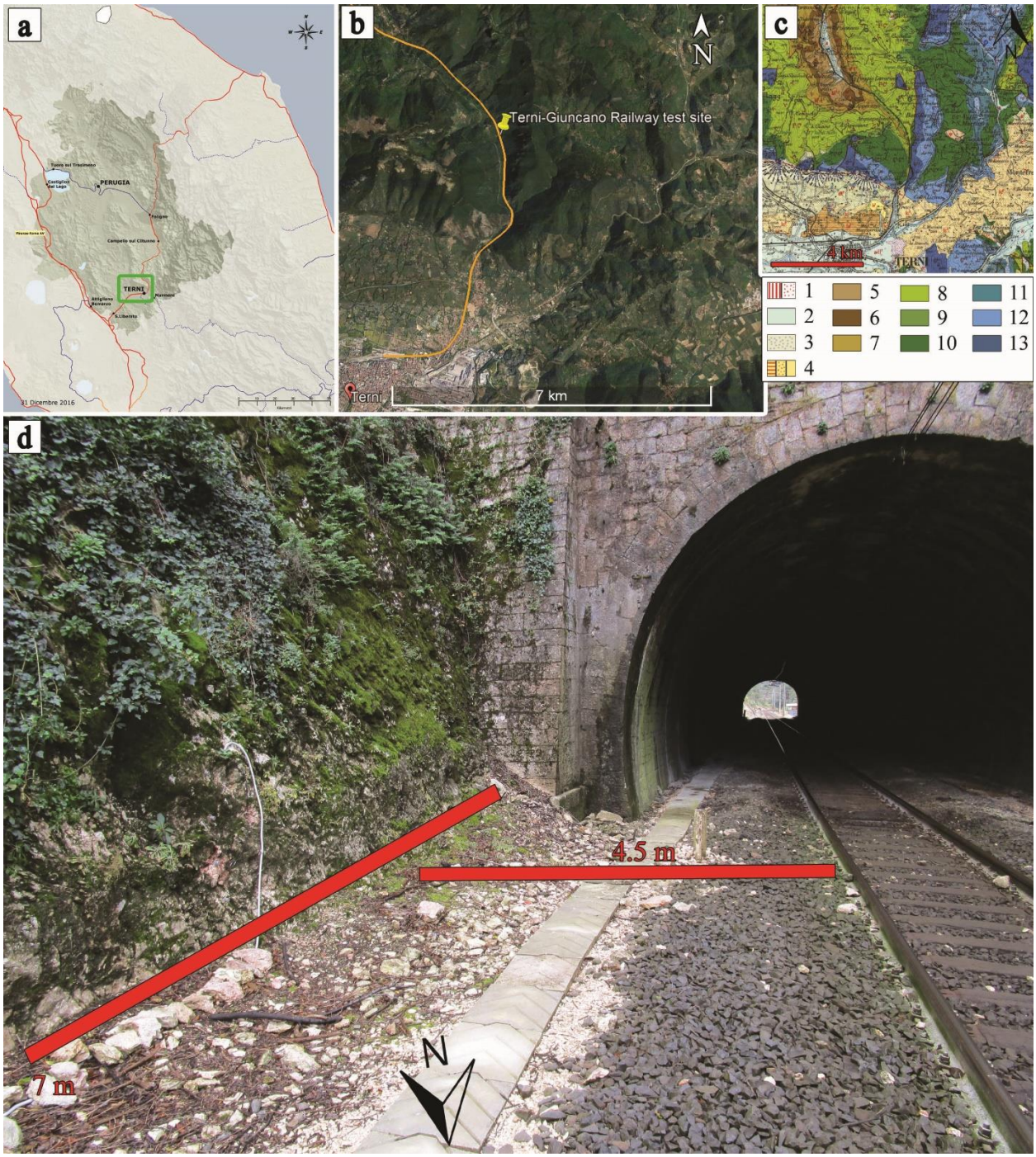

Figure 13: National Railway infrastructure in the Umbria region (a). A satellite view of the study area (green rectangle) is zoomed in b), where the railway line is highlighted in orange and also the location of the test site is marked. In c) the geological map of the area reported in b) is represented; the legend corresponds to: 1) Red earth and debris (Holocene); 2) River floods (Holocene); 3) Debris and alluvial fan (Pleistocene); 4) Sands and clayey sands (Plio-Pleistocene); 5) Clays and arenaceous clays (Marnoso-Arenacea Formation, Miocene); 6) Marly limestones (Bisciaro Formation, Miocene); 7) Marls and marly limestones (Scaglia Cinerea Formation, Miocene); 8) Marly limestones (Scaglia Rossa Formation, Eocene); 9) Marls (Marne a Fucoidi Formation, Cretaceous); 10) Limestones (Maiolica Formation, Cretaceous); 11) Limestones and marly limestones (Jurassic); 12) Limestones (Corniola Formation, Jurassic); 13) Limestones (Calcare Massiccio Formation, Jurassic). In d) the rock mass selected for the microseismic monitoring is shown.

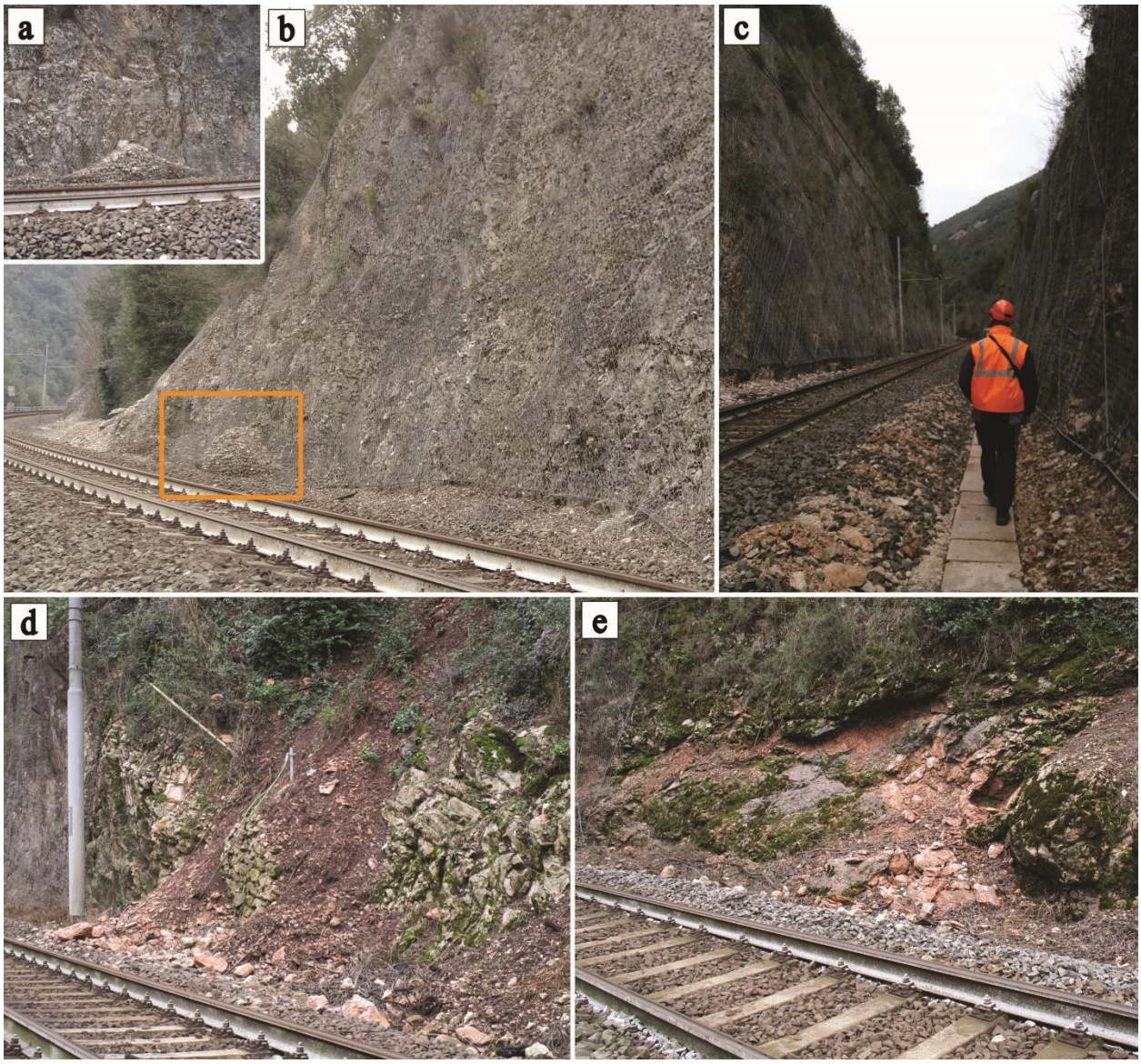

Figure 14: Views of the inspected section of the Terni-Giuncano railway line. Many sectors of the railway pass close to rock masses equipped with retaining nets (b) or in deep excavated trenches (c). In a) a zoom of the material accumulated in the retaining net reported in b) is shown. During the maintenance interventions, small instability events occurred in the proximity of the railway line were also detected (d and e).

The ultrasonic test performed on 5 test pieces according to ASTM (2005), provided P-waves velocity ranging from 3580 to 4763 m/s resulting in an average of 4222 m/s. Moreover, the results obtained from the ultrasonic test were used for the determination of the porosities of the test pieces following the empirical relation by Fourmaintraux (1975), resulting in a total porosity comprised between 2.1 and 3.8%, with an average of 2.8%. The point load test performed on 8 rock samples following ASTM (2008) resulted in an average Uniaxial Compressive Strength (UCS)

of 65.32 MPa. All the parameters derived from laboratory and on-site testing are resumed in Figure 15.

Rock mass matrix				
Natural specific gravity γ_n	**Specific gravity of soil solids γ_s**	**Uniaxial Compressive Strength σ_c**	**Average porosity n**	**Average Vp**
kN/m^3	*kN/m^3*	*MPa*	*%*	*m/s*
25.79	26.62	65.32	2.8	4222

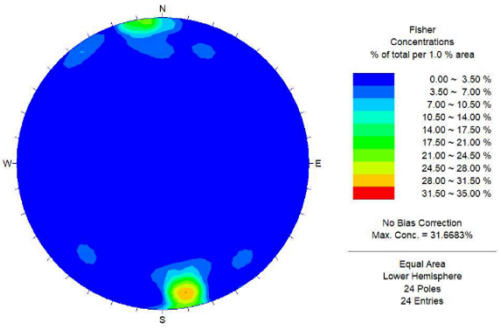

Rock mass joints							
Joint set	**Dip direction and dip**	**Alteration status**	**Hydraulic conditions**	**Opening**	**Joint Filling**	**JCS**	**JRC**
-	°	-	-	*cm*	-	*MPa*	-
J1	170/80	High	Yes	0.3	terrain	46	8
J2	350/78	High	Yes	0.2	terrain	44	8

Figure 15: Main geomechanical parameters derived from on-site and laboratory testing of the outcropping rock mass at the Terni test site and stereographic equal-angle projection (lower hemisphere) of the joint sets surveyed.

Following the obtainment of the authorisation for access to the railway line from the RFI and the predisposition of the rock wall, the microseismic monitoring started on June 4th 2018. Initially, it was planned the deployment of six BKSV accelerometers with a spacing of about 15 cm along a vertical alignment covering about 2 m, with the aim of studying the wave propagation through the rock mass (Figure 16). Unfortunately, during the installation phase, three sensors were not working properly, that is why the configuration was modified keeping only the accelerometers with IDs 1, 5 and 6, respectively the closer one to the ground and the uppermost ones along the alignment. In this way, the possibility of studying the delays in the wavepaths through the entire section of the rock mass monitored was maintained before the original six devices configuration was restored on August 3rd 2018. All the accelerometers were measuring the vibrational component oriented about E-W, which is the direction perpendicular to the slope face orientation.

In addition, on August 8th 2018, a Davis Vantage Pro 2 weather station equipped with pluviometer, air thermometer, and anemometer for wind speed and direction, was installed on-site to better characterize the local environmental conditions. The acquisition was set with a

sampling rate every 15 minutes, which allowed to do not saturate the internal storage memory before the scheduled maintenance and data download operations. A general interruption in the acquisition of the equipment was planned between September 4th 2018 and September 18th 2018, for the maintenance of the installed devices. A summary of the data collected during the monitoring period is reported in Table 5.

The microseismic monitoring system recorded until November 14th 2018, when all the installed devices were removed to be furtherly employed in the Acuto test site. Also in this campaign was adopted a sampling frequency of 2400 Hz and a power supply guaranteed by a solar panel connected to a backup battery. Unfortunately, this led to several interruptions in the last period of the monitoring, coinciding with the shortening of the days in the autumnal season jointed with the beginning of the most rainy period and the unfavourable northern exposition of the solar panel.

Table 5: Summary of the data collected during the monitoring campaigns.

Period	*From*	04/06/2018	04/08/2018	08/08/2018	04/09/2018	18/09/2019
	To	03/08/2018	08/08/2018	03/09/2018	17/09/2019	14/11/2018
Data	*Microseismic*	3 sensors: ID 1, 5, 6	6 sensors	6 sensors	Acquisition interruption	6 sensors
	Weather	Terni weather station	Terni weather station	On-site weather station	Acquisition interruption	On-site weather station

Air temperature and rainfalls intensity (cumulative mm) data related to the period previous of the installation of the on-site weather station and during the acquisition interruption were recovered by the hydrographical service of the Umbria region, which manages a weather station located in the Terni town, about 7 km far from the test site. Just one data per day was available but it permitted to fill the uncomplete weather dataset for the first two months of the monitoring.

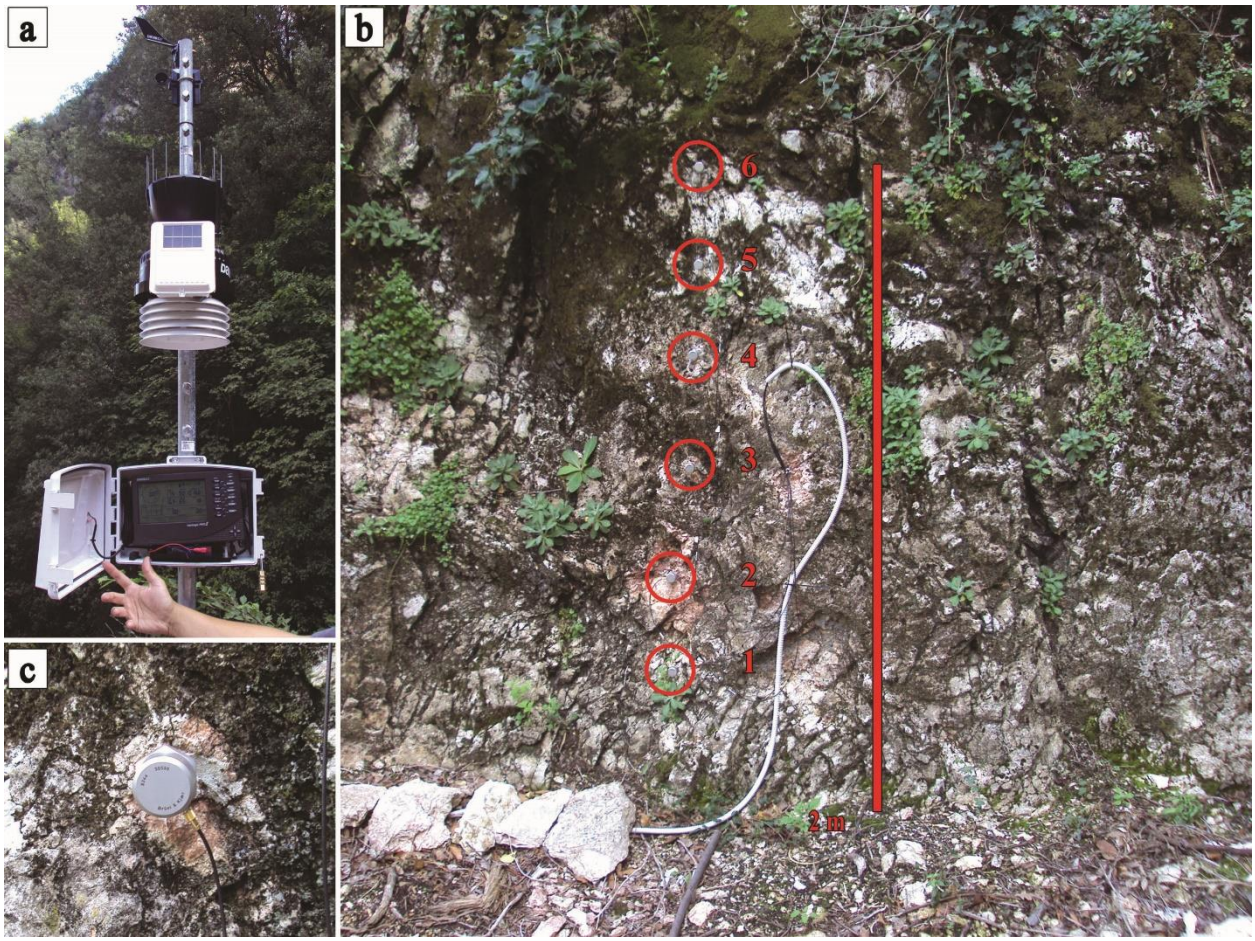

Figure 16: Positioning and ID of the accelerometers employed for the microseismic monitoring campaign (b). A zoom on an accelerometer is shown in c) and the on-site weather station is presented in a).

In order to support the following data analyses, the timetables of the trains effectively transited on the railway line in the monitored period were requested to the RFI. Such documents were provided at the end of the monitoring period, reporting all the trains transited, their typology (passenger, freight, single locomotive), their identification number, and the time of effective transit at the Terni or Giuncano railway stations, between which is comprised the monitored rock mass. By joining all of the provided information, a database of all the transits was created, including not only the already-listed features of the trains, but also by assigning an identification number related to the train type and two progressive numbers referred to the total count of trains transited for each day and from the beginning of the monitoring. Furthermore, knowing the distance of the test site from the two stations, it has been possible to evaluate for each train the approximate time of transit near to the rock mass monitored, which helped in the identification of the trains in the seismic records. A few number of trains (37) has been removed from the database because of the incompleteness of the information in the provided timetables,

reporting only the departure time from a railway station but not the time of arrival in the other one. Given that most of these trains were of the single locomotive type, frequently used during the circulation interruption time by the railway maintenance personnel, they have been removed even because probably not actually passed in the monitored sector and also considering the remnant high number of trains available for the analyses.

By taking into account the entire monitored period, thus excluding the interruption of the first two weeks of September, a total of 5994 trains transited on the railway line. Unfortunately, this is not the actual maximum number of train detectable, because of the power supply interruptions occurred during the monitoring period, typically in the late and early hours of the day. In any case, considering the time spans in which the acquisition was on, 2811 trains transited on the railway, thus still a considerable sample for the following analyses.

3.3 Seismic data processing

As already introduced, the seismic data analysis regarded both the entire ambient noise records and the single microseismic emissions happened during the monitored period. The procedure employed to analyse the ambient noise records is presented in paragraph 3.3.4, while the following ones (paragraphs 3.3.1, 3.3.2, 3.3.3) describe the process designed and utilised to detect and treat the microseismic events. In this thesis, the classification of the microseismic events based on their waveforms or energy contents (Provost *et al.* 2018) is not relevant for the following analysis focused on the damping ratio and to the final scope of the thesis. For this reason, all the detections have been considered proper for the analysis and in this thesis are generally named as “events” or “microseismic events” (also found as “MS events”).

Concerning the analysis of the microseismic events, given the amount of the data to be treated and in order to perform an objective analysis on different kinds of parameters, a specific procedure has been implemented by means of the SAC software (Seismic Analysis Code) (Goldstein *et al.* 2003, Goldstein & Snoke 2005), integrated with bash and Matlab scripting. The entire process, starting with reading the raw data and ending with the results presented in graphs, is reported in the simplified flow chart of Figure 17, and the main steps are presented in the following paragraphs.

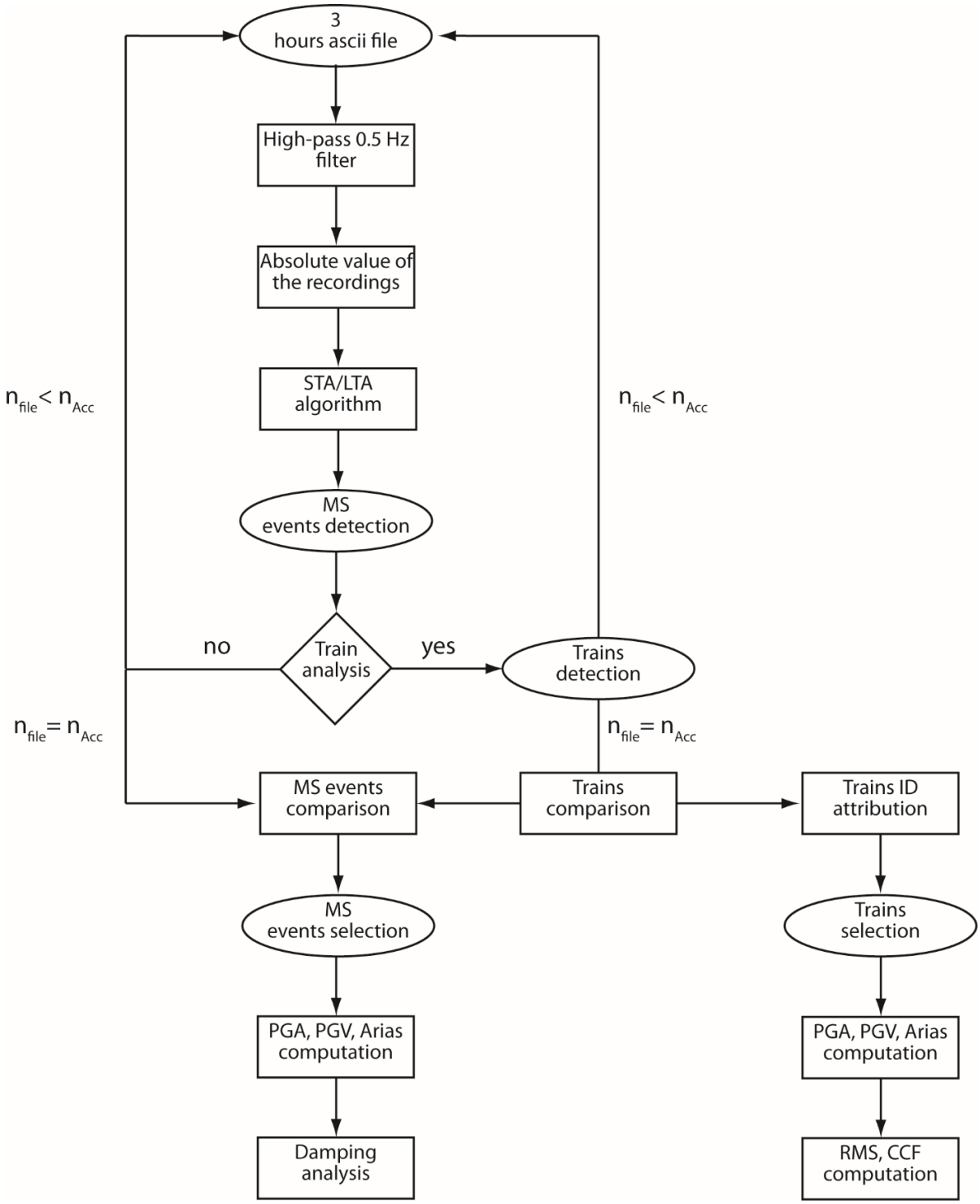

Figure 17: Simplified flow chart of the data processing procedure defined for the analysis of the microseismic datasets (n_{file}: number of the Ascii file in analysis; n_{Acc}: number of accelerometers employed).

In particular, the procedure aims at analysing the damping ratio of the microseismic emissions registered on the rock mass, while other determinations have been done for the train transit records.

A pre-processing step consisted of exporting all the compressed SIE files in the ASCII file format, thus obtaining one three-hours long file containing data related to all the sensors in use: these ASCII files are the input of the entire workflow. In the following, the mean and the trend of the seismic tracks were removed by applying an high-pass filter above 0.5 Hz, which allowed also to remove disturbances due to very low frequencies, like those carried by the wind.

3.3.1 STA - LTA event detection algorithm

Once the data were high-pass filtered, the following step concerned the selection of the microseismic events hidden in the three-hour recording for each accelerometer employed. To objectively analyse all of the seismic records, avoiding the manual picking of the events, which is affected by the sensibility and the experience of the seismic analyst dealing with data, an automatic detection procedure has been implemented in Matlab. Since the most diffused and affirmed techniques for events detection in seismology are threshold-exceeding based algorithm and STA/LTA ones (Vaezi & Van Der Baan 2015, Lee *et al.* 2017, Kinali *et al.* 2018), both the methods were evaluated to process the seismic datasets. These algorithms are generally already implemented in digital acquisition systems for real-time events detection and selected according to the method that is expected to provide the best result for the scope of the monitoring, allowing to register only the slices of the ambient noise containing the most energetic events. Such an attitude, not only permits to save storage memory, but it is also at the base of the workflow of the early warning systems. In the case of continuous monitoring, as those performed in the ambit of this thesis, the two algorithms had to be applied to the entire ambient noise records available.

The threshold-exceeding based algorithm is widely used for accelerometric networks devoted to earthquake recording, as generally an earthquake as a greater intensity in respect to the ambient noise level. On the contrary, when the signals to be found are characterized by a lower energy level in terms of signal over noise ratio, it is difficult to set proper thresholds. In fact, by applying a threshold-exceeding algorithm on a data sample and varying the thresholds in the range comprised from $5x10^{-4}$ to $1x10^{-3}$ g, the results obtained were not satisfactory, even taking into account the moderate-to-high risk of recording spike signals rather than truly microseismic

events. That is why a STA/LTA algorithm has been preferred for the detection of the microseismic events.

The short time amplitude (STA) versus long time amplitude (LTA) algorithm is widely used for seismic data acquisition systems (Withers *et al.* 1998, Li *et al.* 2016), allowing the detection of signals over ambient noise variations. In fact, this technique permits the individuation of events balancing the effect of noise variations, thus being more refined in events detection than a threshold-exceeding based algorithm.

Considering the absolute value of the records, the mean of the amplitude in a short time window (STA) is divided by the mean of the amplitude calculated over a longer time (LTA). If the ratio STA/LTA exceeds a user-defined triggering threshold, the event is registered until the ratio decreases to a detriggering threshold value, usually chosen lower than the first one. The selection of the length of the two time windows, as well as of the two threshold values has to be done by taking into account the typology of event looked for, and it is crucial for obtaining acceptable results that should be neither too much noisy nor too much restrictive for the detection of the events (i.e. too many or too few events). After several attempts and tests aimed at properly define these values and to find a good compromise in their selection, the STA has been set to 0.01 seconds, the LTA to 30 seconds and the STA/LTA to 4, both for triggering and detriggering thresholds. A pre and a post event time was set to 0.5 seconds: this operation allows to ensure the recording of the pre and post phase of event occurrence. Moreover, in the case of repeated exceeding of the established STA/LTA ratio, in a time span set to 2 seconds, the multiple events are recorded as a single longer event.

Instead of running the event detection algorithm on just one recording per time, this procedure was planned to comparatively analyse the recordings of all the accelerometers used, with the aim of individuating events common to more accelerometers at the same time. This operation not only allows to detect contemporaneous events but also permits to be even more conservative in the determination of them, cutting out spikes and localised transient ambient noise variations.

The seismic records referring to the same three-hour interval (6 or 7 depending on the number of accelerometers deployed) are primarily analysed one by one, the starting time of the events is saved for each track and then is compared among all the available recordings. If the starting

time of each event of whichever track is found in any other track comprised in a time span of 1 second and identified on a minimum number of accelerometers chosen by the user, the event is considered coherent and thus its starting time is saved for the following steps of the workflow. The time span interval set to 1 second is introduced for obvious reasons of impossibility of exactly-synchronous event occurrences, considering the travelling time of the waves in the medium and the high sample rate adopted. The number of accelerometers selected for comparing the starting time of seismic records can vary from 1 to the maximum number of accelerometers employed: the higher the number of the accelerometers selected, the higher the coherence looked for and thus the reliability in characterising truly microseismic events. On the other hand, when dealing with microseismic events or generally with low signal-to-noise ratio signals, because of the distance among sensors, as well as the presence of fractures or the variation in the physical properties of the medium and the possible malfunctioning of one or more sensors, it is not unusual to miss the detection of an event. That is why choosing to find events common to a high number of accelerometers can prevent the recognition of some of them. For this study, the minimum number of accelerometers has been set to two, which is the minimum from a theoretical point of view. Once the events and the starting time common to two accelerometers are selected, an output file is exported, allowing to furtherly subgroup them according to a greater number of accelerometers or to specific ones (for instance by taking in account their disposition on the rock surface).

Once the events are detected, their initial and final time, both expressed as relative seconds from the beginning of the track and as absolute local time, is registered and exported to an output file that will be used as input for the damping analysis discussed in the following paragraph.

Given the algorithm settings previously introduced and resumed in Table 6, some typical detected events are shown in Figure 18, in which also the spectrograms computed using the short-time Fourier transform are shown. According to Arosio *et al.* (2018) and to Provost *et al.*, (2018), these detections can be classified as signals related to MS events, slopequakes and rockfalls. Generally, all the MS events are characterized by a very short duration in time, quantifiable in hundredths of seconds, and by a wide-varying frequency content, while the signals related to slopequakes and rockfalls cover longer time spans (more than 1 second), and are mainly associated with a frequency content lower than 150 Hz.

Table 6: Selected parameters for the STA/LTA algorithm.

STA	LTA	STA/LTA (triggering - detriggering)	Pre-Post event	Event separation	Number of accelerometers with synchronous event
s	*s*	-	*s*	*s*	*at least*
0.01	30	4	0.5	2	2

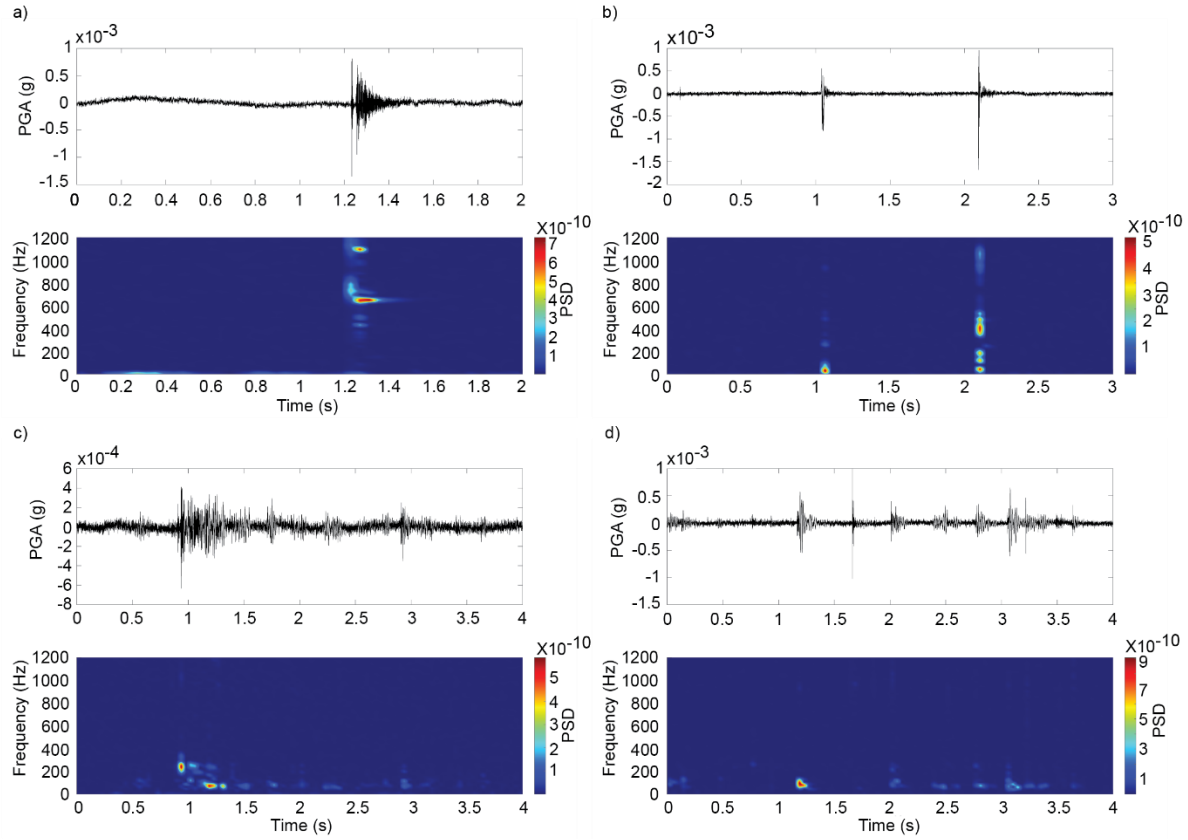

Figure 18: Typologies of detected events and associated spectrograms computed using the short-time Fourier transform: a) single MS event; b) double MS event; c) slopequake; d) multiple events/rockfall.

In the case of the Terni-Giuncano railway test site, the train transits had to be recognized by the detection algorithm, in addition to the microseismic events. For this reason, it has been implemented a section for choosing if performing or not the recognition of the train transits (i.e. if the data analysed are referred to the Terni or to the Acuto test site). Starting from the seismic records already analysed for the detection of the microseismic events, with the same procedure and parameters explained above, some additional evaluations are done for the data acquired at the Terni test site. Given that a train generates a signal much more energetic than a microseismic

event, and that its signal certainly exceeds the STA/LTA threshold set, the train passage is already recognized by the algorithm but mixed among all the microseismic events.

A conditional loop begins to check if a detected signal truly represents a train transit, starting with the evaluation of its duration. If the duration is comprised in an interval from 4 to 18 seconds, which allows to take into account both single locomotives and freight trains, respectively associated with a shorter and longer transit time, then the signal is converted in acceleration expressed in m/s^2, detrended and finally its Arias intensity is evaluated.

The Arias intensity is a cumulative ground motion measure intensity, used for determining the energy associated with earthquakes as well as with other sources of vibrations, obtained by the time integral of the squared acceleration, as reported in Equation [1]:

$$AI = \frac{\pi}{2g} \int_0^{t_{max}} a(t)^2 \, dt \qquad [1]$$

where *a(t)* is the ground motion acceleration at time *t*, t_{max} is the total duration of the ground motion, and *g* is the gravitational acceleration.

Given that this parameter is directly proportional to the duration and to the ground acceleration of a signal, it is obvious that the Arias intensity related to a train transit is much higher than that referred to a microseismic signal. That is why it has been chosen to mark a signal as a train transit by setting an Arias intensity threshold fixed to 0.1 m/s. This value was chosen after evaluating it on several waveforms certainly referred to trains passage and in order to be reliable for the detection of all the train typologies.

Moreover, in order to be even more conservative in the identification of a train transit, with a procedure similar to the already described one for the comparative analysis of the seismic records focalised to the detection of microseismic events, the above-described conditions have to be verified on at least two accelerometers. This allowed to exclude wrong attributions due to malfunctioning sensors.

If all the conditions are verified, the starting and final time of the train passage, even in this case expressed both as relative seconds form the beginning of the track and as absolute local time, is saved and exported to an output file. This last one is then inputted to another Matlab routine written to perform the attribution of the detected train transits to their typology (passenger,

freight, single locomotive). The routine looks for a match between the detected transit time and the estimated transit time of the trains close to the rock mass, which is based on the timetables of the effective train transits on the railway line, provided by the RFI.

If the detected time is comprised in a time span of ± 10 minutes of an estimated transit, the detection is confirmed and the information inherent to the train typology are added to the relative and absolute time of the passage. If there is no matching with an effective transit, the event is discarded and not considered for the following analyses.

Figure 19 shows a typical recording of a train passage, with its associated spectrogram: the example is referred to the passenger train REG 2324. The averaged Fourier spectrum referred to all the REG 2324 trains transited in the monitored period is also shown.

From the time history, it is possible to note the presence of peaks associated with the passage of the axes of the train bogies, while the spectrogram and the averaged Fourier spectrum show a main frequency contribution in the band between 50 to 250 Hz.

Once the initial and final times of the microseismic events, as well as those of the trains, are exported, by means of the software SAC each signal is cut from the seismic record and Peak Ground Acceleration, Peak Ground Velocity, Arias Intensity are computed and exported to a text file.

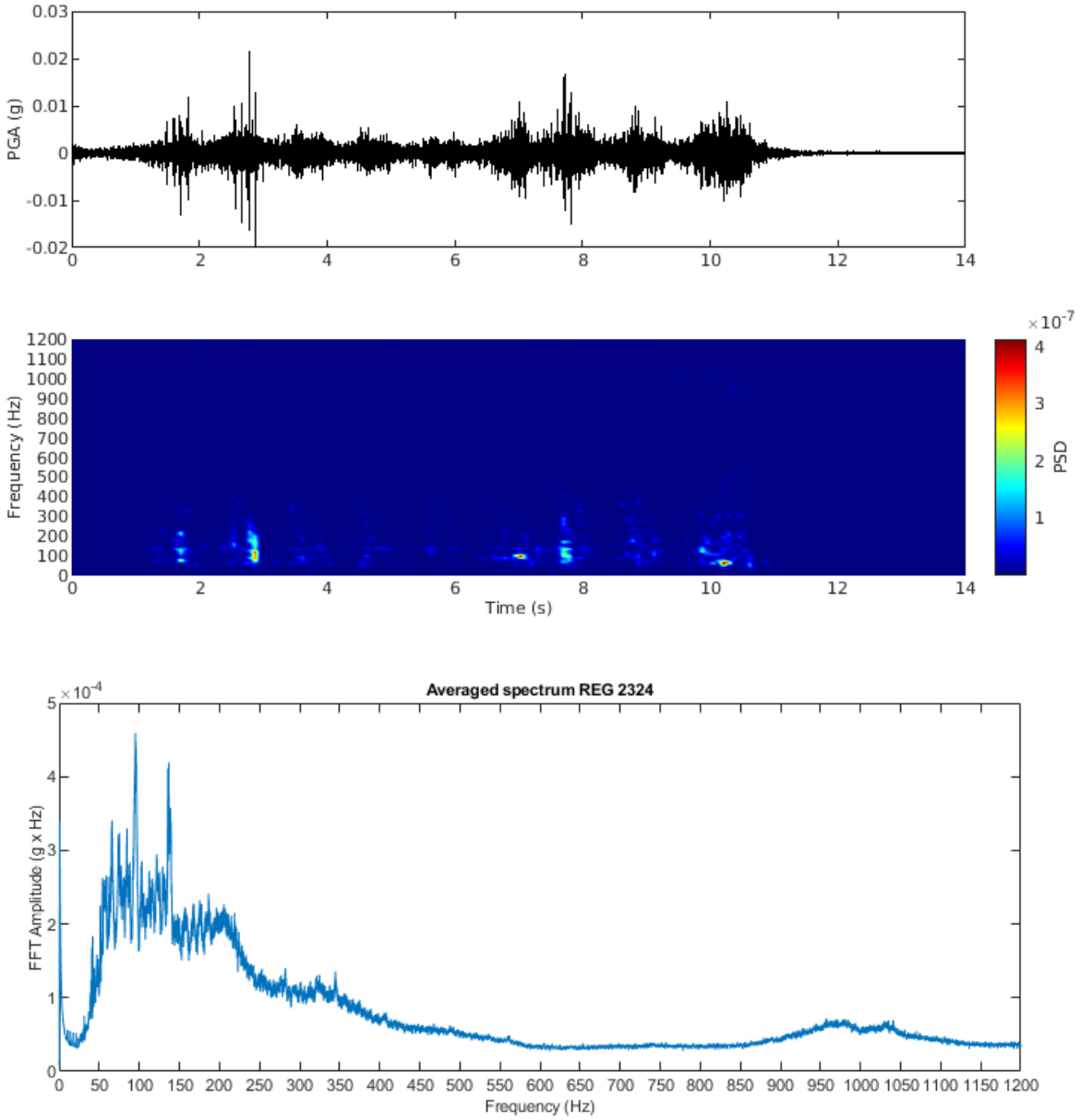

Figure 19: Time history (up) and spectrogram (middle) of a train passage (REG 2324). The averaged spectrum of all the recorded transits of REG 2324 trains is also shown (bottom).

3.3.2 Damping analysis of microseismic events

The focus of this PhD thesis is the evaluation of the damping coefficient associated with the detected microseismic emissions. The definition of the damping can be found in the more general theory of the one degree of freedom linear oscillator (1 DOF) (Pecker 2010). In fact, each object interested by an external stress, a building as well as a rock mass or a rock block can be transposed into the model sketched in Figure 20, in which the medium is considered as an

oscillator with mass *m* that is fixed to a rigid support and can move only along the horizontal direction.

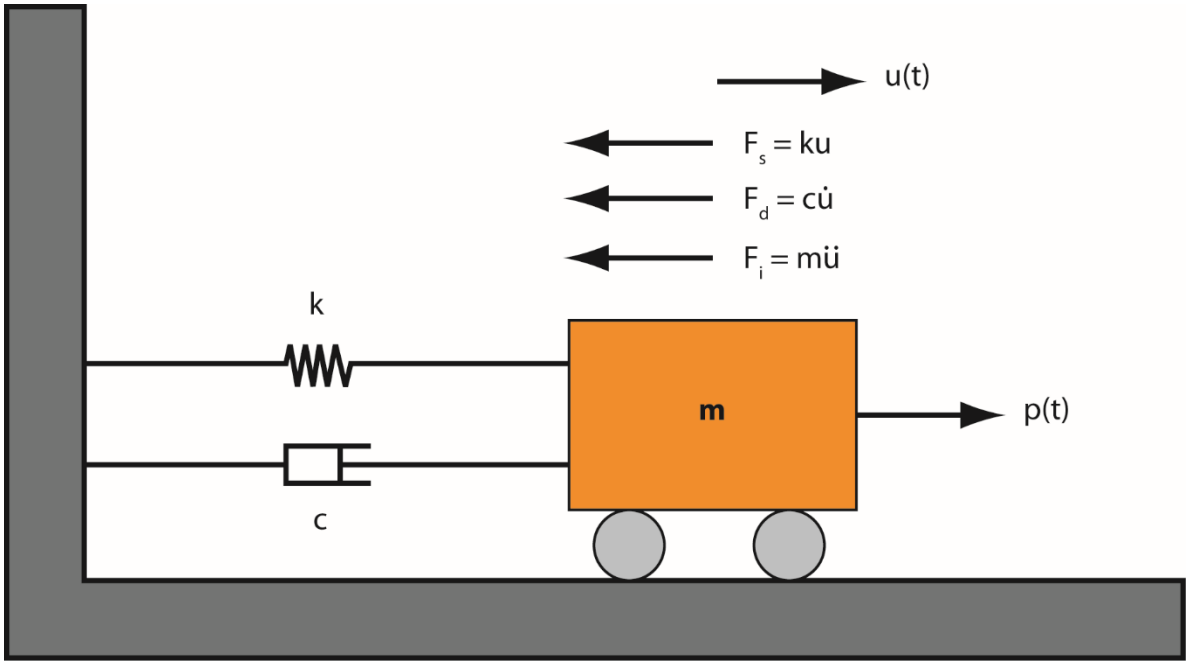

Figure 20: Sketch of a linear visco-elastic oscillator with one degree of freedom.

When an external force *p(t)* acts on the oscillator it causes a displacement *u(t)* of the mass *m*. The forces that resist to this displacement are the restoring force (F_s), the damping force (F_d), and the inertial force (F_i), respectively depending on the displacement (u), velocity ($\dot{u}$) and acceleration ($\ddot{u}$), related to the application of the external force *p(t)*.

The restoring force F_s directly depends on the induced displacement, and if the proportionality between the force and the displacement is constant, the oscillator has a linear elastic behaviour, that is the case representable with the behaviour of a spring:

$$F_s = ku \qquad [2]$$

The elastic energy of the spring is fully restored, while part of the energy stored in the dashpot is dissipated through time, which is the damping phenomenon. The damping is the result of different ways of dissipating the energy, depending on the physical properties of the medium and its possible modification, as the fracturation phenomena. All the factors controlling the energy dissipation are simplified by considering a linear viscous damper. The latter is characterized by a linear relationship between the force produced by the damper and the relative velocity of its end-member values:

$$F_d = c\dot{u} \quad [3]$$

The constant *c* is characteristic of the oscillator and can be determined when an harmonic force *P* of pulsation $\bar{\omega}$ is applied to the linear damper:

$$P = P_0 \sin(\bar{\omega} t) \quad [4]$$

$$c = \frac{F_{d\,max}}{\dot{u}_{max}} = \frac{P_0}{\bar{\omega} u_{max}} \quad [5]$$

To obtain the relation of the dynamic equilibrium, the resultant of all the forces must be null:

$$F_s + F_d = p(t) - F_i \quad [6]$$

For a linear visco-elastic system, considering Equations [2] and [3], the [6] can be written as:

$$m\ddot{u} + c\dot{u} + ku = p(t) \quad [7]$$

By dividing all the members by the mass *m*, the equation of the dynamic equilibrium can be written as follows:

$$\ddot{u} + 2\xi\omega\dot{u} + \omega^2 u = \frac{p(t)}{m} \quad [8]$$

From this equation, it is possible to derive the fundamental physical quantities that characterize the oscillator, the radial frequency ω and the damping ratio ξ:

$$\omega = \sqrt{\frac{k}{m}} \quad [9]$$

$$\xi = \frac{c}{2\sqrt{km}} \quad [10]$$

The solution of Equation [8] provides the vibrational behaviour of the 1 DOF oscillator. The general solution is obtained considering both the solution of the homogenous equation that allows to study the free vibrations of the system and the particular solution related to the forced vibrations.

To solve the homogenous equation, the right term of Equation [8] is nulled, obtaining Equation [11]:

$$\ddot{u} + 2\xi\omega\dot{u} + \omega^2 u = 0 \quad [11]$$

that has a general solution in the form of Equation [12]:

$$u(t) = \lambda e^{st} \quad [12]$$

By substituting the solution [12] in the Equation [11], the variable *s* can be determined from Equation [13]:

$$s^2 + 2\xi\omega s + \omega^2 u = 0 \quad [13]$$

whose solution depends on the sign of the determinant:

$$\Delta = \omega^2(\xi^2 - 1) \quad [14]$$

The determinant depends on the value assumed by ξ that can be referred to three possible conditions:

- undamped system: $\xi = 0$ or with subcritical damping $\xi < 1$
- critically damped system: $\xi = 1$
- supercritically damped system: $\xi > 1$

Since all the natural media are generally characterised by subcritical damping and even the cases treated in this thesis fall in this condition, only this circumstance will be examined.

When $\xi < 1$, the solution of the Equation [13] is given by two terms:

$$s = -\xi\omega \pm i\omega\sqrt{1 - \xi^2} \quad [15]$$

Introducing the damped pulsation ω_d:

$$\omega_d = \omega\sqrt{1 - \xi^2} \quad [16]$$

and by using the amplitude ρ and the phase ϑ, the response of the system can be written in the form of Equation [17], which is represented in Figure 21 as a function of time.

$$u(t) = \rho e^{-\xi\omega t}\sin(\omega_D t - \theta) \quad [17]$$

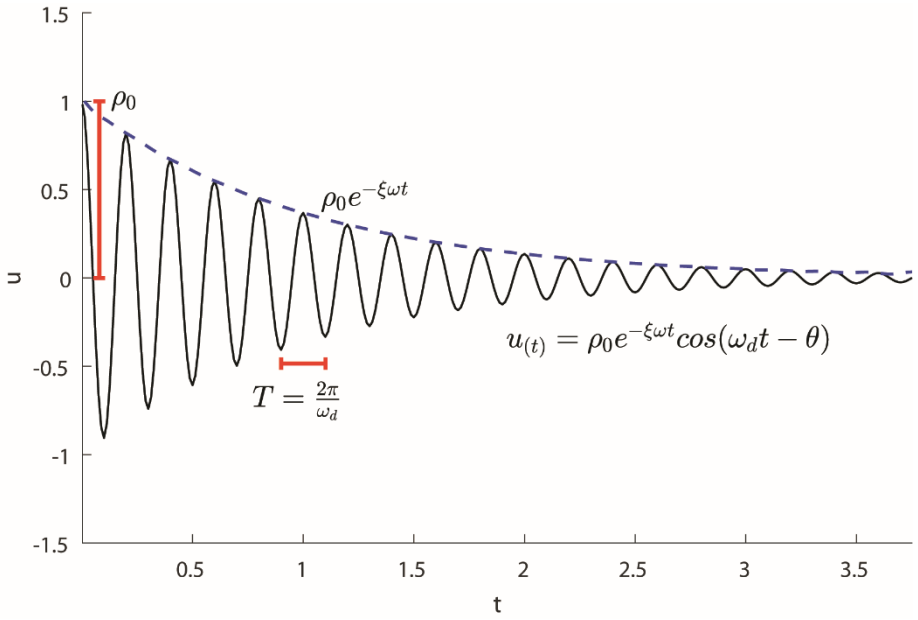

Figure 21: Vibrations of a system with subcritical damping.

From Figure 21 it is possible to observe that the amplitude of the oscillation decreases as a function of time, tending to 0 at an infinite time. The return to the initial equilibrium position is much faster and with fewer oscillations when the damping ξ is high (Figure 22).

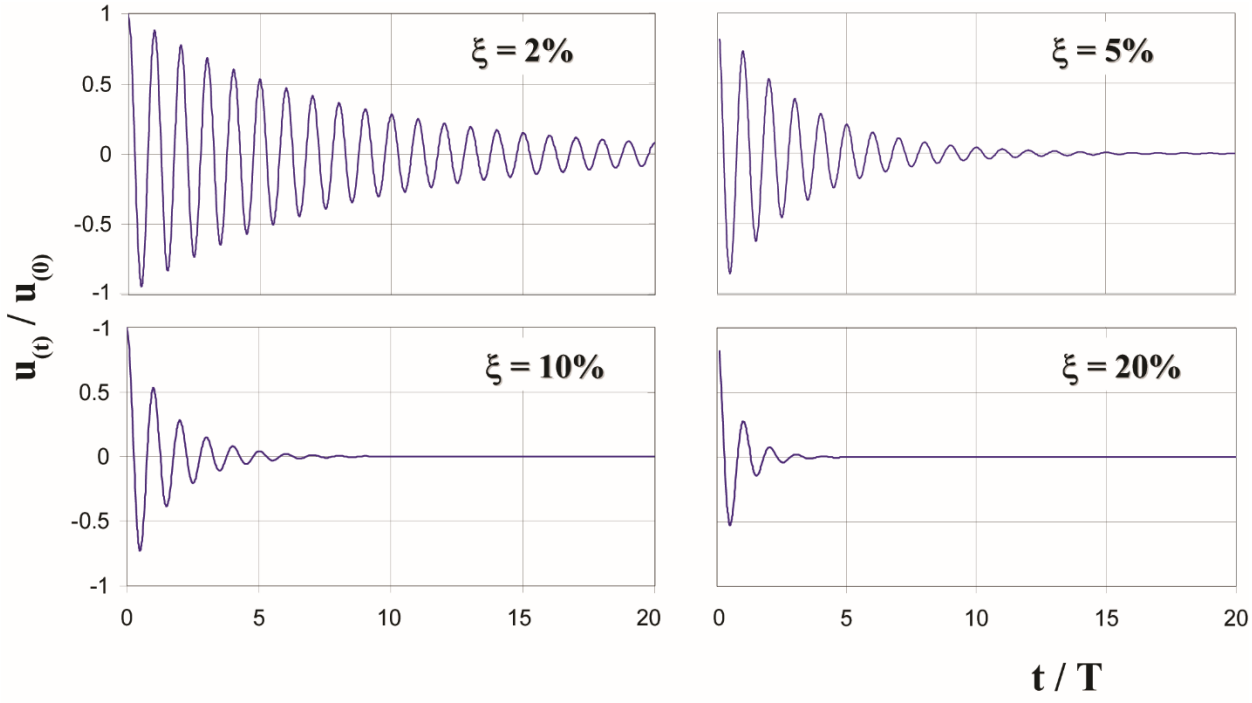

Figure 22: Influence of the damping on the vibrations of an underdamped system (Pecker, 2010).

Considering two successive extrema of the vibratory response, having the same sign, the ratio of the amplitudes is equal to:

$$\frac{u_n}{u_{n+1}} = e^{2\pi\xi\frac{\omega}{\omega_D}} \quad [18]$$

The logarithmic decay is thus equal to:

$$\delta = ln\frac{u_n}{u_{n+1}} = \frac{2\pi\xi}{\sqrt{1-\xi^2}} \quad [19]$$

that for tiny values of ξ is reduced to:

$$\delta = 2\pi\xi \quad [20]$$

where δ represents the logarithmic decrement of the vibratory response.

In general, this parameter is experimentally measured in order to derive the damping ratio of the studied system.

In this thesis, the damping ratio ξ is determined by means of a linear interpolation of the logarithmic decrement δ of the considered waveforms. It is thus possible to derive the damping ratio ξ from the [21]:

$$\xi = \frac{\delta}{2\pi} \quad [21]$$

The damping ratio controls the rapidity with which the vibrations are attenuated after that an impulsive signal perturbs the stationary condition of a medium. Given that the intensity of the damping depends on the physical characteristics of the medium as its density, stiffness (i.e. Young Modulus), and cohesion (i.e. absence of discontinuities within the medium), a change in these properties can be directly revealed by modifications of the damping ratio. In fact, theoretically speaking, the higher the damping the higher the jointing of the medium, because of the modification in its microstructure, assuming the other properties remaining equal. Based on this principle, the damping ratio associated with the microseismic emissions recorded on the rock masses was evaluated in order to observe potential variation attributable to modification of its fracturing network, thus indicating rock mass damaging process phenomena.

The procedure described below is sketched in Figure 23. As first step, the microseismic signals were filtered within a narrow frequency range, in order to obtain a monofrequential waveform, on which is possible to observe the attenuation of the signal over time (i.e. the damping). The

bandpass filter was applied for obtaining the monofrequential waveforms referred to 5, 10, 30, 50, 100, 200, 500 and 1000 Hz, in order to be representative of the entire Fourier spectrum analysable. The disaggregation in monofrequential waveforms allows also to assess the dimension of the physical elements associated with the energisation of the considered frequencies. Given that the retrieved P-waves velocity for both the test sites was comparable (4193 m/s for Acuto and 4222 m/s for Terni), a mean value of 4207 m/s has been considered for the estimation of the characteristic dimensions of the physical elements reported in Table 7.

Table 7: Estimation of the characteristic dimension of the physical elements associated with the frequencies investigated and considering a P-waves velocity of 4207 m/s.

Frequency	*Hz*	5	10	30	50	100	200	500	1000
Estimated characteristic dimension	*m*	842	421	140	84	42	21	8	4

By obtaining the absolute value of the filtered signals, it is possible to double the points describing the decreasing curve that represents the logarithmic decrement. In a second step, each selected signal is analysed with a routine conceived for recognizing the peak values of a function, aiming at detecting the maximum peak that, in this case, coincides with the Peak Ground Acceleration (PGA) for the considered frequency.

Once the maximum peak is recognized, all the following values (i.e. the values describing the logarithmic decrement) are normalized in respect to it. To derive the angular coefficient of the points describing the decay of the signal, a linear interpolation is performed to obtain the best curve fitting of the data points. Only the data points referred to the logarithmic decrement are considered, while the values following the decay of the signal (i.e. the points referred to the restored stationary vibrational condition, the seismic ambient noise) are removed by using of a filter value. In this way, the slope of the interpolated curve is truly referred only to the decreasing part of the signal, and the damping is accurately evaluated. Moreover, in order to obtain a better interpolation, only the signals characterized by more than 10 data points were considered for deriving the angular coefficient and thus studying the damping ratio. The R^2 coefficient associated with the curve fitting has been also evaluated, consequently, the damping calculated only for the interpolations characterised by a R^2 major than 0.8. For each three-hour-long seismic

record, the angular coefficient of the curve fitting, its associated R^2 coefficient, the value of the damping and the time of the detected microseismic events are exported to a text file. The procedure is repeated for all the monofrequential waveforms considered and for all the seismic records referred to the entire monitored period.

Finally, the derived damping values have been averaged in a daily time interval, obtaining a damping value with its standard deviation for each day monitored. Performing the average of the data allows to obtain a better estimation of the real value of the variable, rather than the single measurements, as stated in the measurements error theory. The averaged measures were compared along all the monitored period according to the frequency and the sensor for which they have been determined. Given that a measure can be considered different from another one if they differ even when their standard deviation is taken into account, to analyse damping variation in the time series, a superimposition index between the daily averaged damping ± its standard deviation and the first averaged value of the series, taken as reference, has been evaluated. When the index is equal to 0, the two compared measures can be considered different among them, thus potentially indicating a variation in the monitored parameter. The obtained damping time series were compared with the ones referred to the temperature and to the rainfalls, in order to observe if the variations occurred in the damping series were linkable to particular weather conditions.

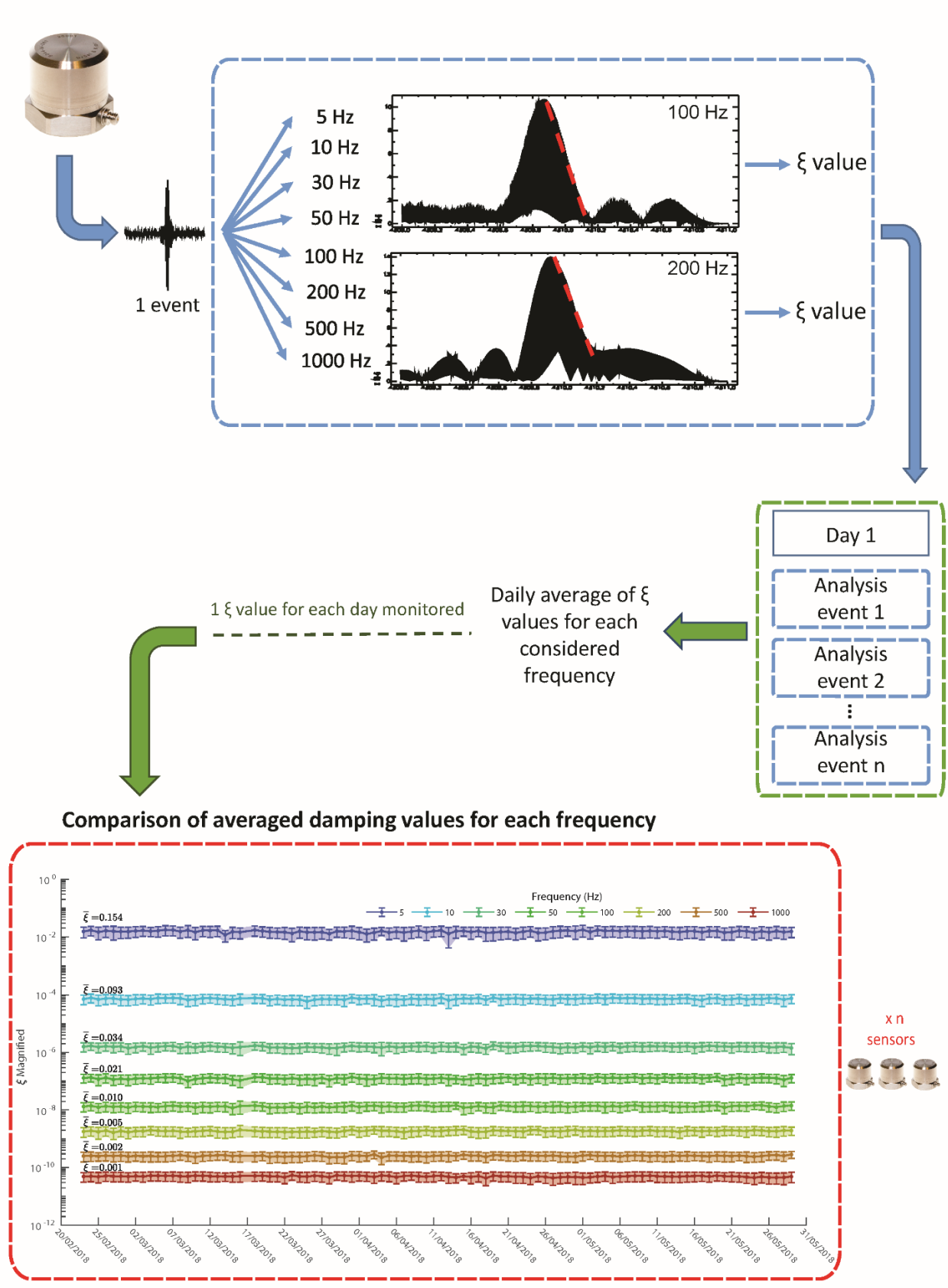

Figure 23: Scheme illustrating the steps of the here-proposed damping analysis (details in the text).

3.3.3 Cross-Correlation and Root Mean Square analysis

Additional analyses have been carried out on the trains passage records acquired at the Terni test site. In fact, the damping analysis could not be applied with the signals related to train transits, due to the complex coda waves generated as discussed in Chapter 5. In particular, the Root Mean Square (RMS) value associated with each train transit is evaluated to quantify the energy associated with each recording, with the aim of evaluating potential variations of it due to rock mass damaging phenomena. Besides, the evaluation of this parameter allowed to make a comparison with the introduced methodology. The RMS of the acceleration (Equation [22]) provides an approximation to the standard deviation for stationary random processes, which include the usual treatment of earthquakes and other sources of vibrations, as trains.

$$a_{rms} = \sqrt{\frac{1}{T_2 - T_1}\int_{T_1}^{T_2}[f(t)]^2 dt} \qquad [22]$$

For each train passage and each accelerometer, the RMS defined in Equation [22] was computed and then exported to a text file keeping the information about the train typology. This allowed to successively compare the RMS obtained for each train typology, as theoretically passenger, freight and single locomotive trains have different weights and loadings, thus generating different energies. The RMS was determined on the unfiltered recording and for specific monofrequential waveforms. In particular, the recordings were filtered in narrow frequency intervals in order to obtain the waveforms related to 30, 50, 80, 100, 120, 200, 500, 1000 Hz on which the RMS was determined. This analysis was intended to observe if at particular frequencies was observable a marked change in the RMS through time. All the obtained RMS data series were successively compared with the meteorological ones.

The Cross-Correlation Function (CCF) allows to measure the similarities between two functions and to determine with how much delay there is the best superimposition between them. In this thesis, the CCF function has been applied to analyse the recordings of the train transits registered by the deployed accelerometers. The basic idea is to compare the records in order to observe if the delay among the registrations remains the same or if it is subject to a variation. If a persistent variation is detected, i.e. an increased delay between two sensors, a modification in the internal structure of the rock mass may have occurred, given that the wavepath has been delayed.

In this sense, the accelerometer closer to the ground (ID: 1, Figure 16) has been taken as a reference point, and the cross-correlation between it and the other accelerometers was evaluated. Given that in the first period of the monitoring three sensors were not working, the CCF was evaluated only between the couples of sensors 1-5 and 1-6, successively was determined also for the remnant accelerometers. The CCF lag was exported to a text file keeping the train typologies separated and then compared with the meteorological dataset collected.

3.3.4 Frequency Band Ambient Noise Disaggregation (F-BAND) Analysis

In addition to the analyses carried out on the microseismic events and on the train passages, also the entire ambient noise records acquired in both the test sites were analysed. In fact, given the recent studies dealing with the correlation of the seismic ambient noise with the environmental actions (Larose *et al.* 2015), also in context of prone-to-failure rock blocks (Bottelin *et al.* 2013, Bottelin *et al.* 2013), a comparative analysis of the seismic ambient noise and the on-site recorded environmental parameters was performed.

In a first step, the seismic records were filtered in frequency intervals of interest, which were: 0.5 – 30, 30 – 50, 50 – 100, 100 – 250, 250 – 500, 500 – 1000 Hz. This operation was done in order to distinguish the prevalent component of the seismic ambient noise and to roughly characterise its main source, i.e. a natural one in the case of low frequencies and an anthropic one for high frequencies.

In a second step, the average and the standard deviation of the records were computed in time intervals of 1 minute and the obtained values were exported to a text file. Eventually, all the exported text files were joined for the different frequencies and the considered accelerometers.

The one-minute averaged seismic noise dataset can be thus analysed with two approaches: by cumulating it and by calculating its derivative. By cumulating the dataset it is possible to note which is the most energised frequency band, and also understand if the vibrations are mainly attributable to natural factors (low frequencies) or to anthropic ones (high frequencies).

The alternative approach consisted in evaluating the derivative of the dataset to better observe the incoming of an external stress in the rock mass. A comparison with the environmental data has been done, in particular with the air and rock mass temperature and the rainfalls for the

Acuto test site and air temperature and rainfalls for the Terni test site. The weather datasets, collected with two different sample rates, were filtered in order to select only the values having a temporal correspondence with the ones of the ambient noise dataset. In this way, the vibrational and environmental datasets were equalized also in term of length. Successively, also the derivative of the filtered weather datasets were computed and then cross-correlated with the derivative of the ambient noise dataset. The cross-correlation of the derivative of the two time series was intended to objectively look for a potential relationship between the ambient noise variation and one or more of the environmental ones.

4 Results

The results of the analyses performed on the microseismic datasets are presented in the following paragraphs. In Table 1 are summarised the type of analysis performed in the two test sites. Before presenting the results of the analysis specifically carried out for this thesis, some other general results of the monitoring campaigns will be introduced in section 4.1.

4.1 Preliminary analyses of the microseismic monitoring campaigns

For each microseismic monitoring campaign, the total amount of events detected adopting the STA/LTA algorithm described in paragraph 3.3.1 is shown, presenting the total number of events detected per each accelerometer employed, as well as the events common at least to two accelerometers. Moreover, the rainfalls occurred in the monitored periods are shown, as they resulted to have a relation with the detected events.

In Figure 24, Figure 25 and Figure 26 are reported the data respectively referred to the first and second microseismic monitoring campaign carried out at the Acuto quarry test site (Acuto 2018 and 2019) and the one performed at the Terni-Giuncano railway test site (Terni 2018).

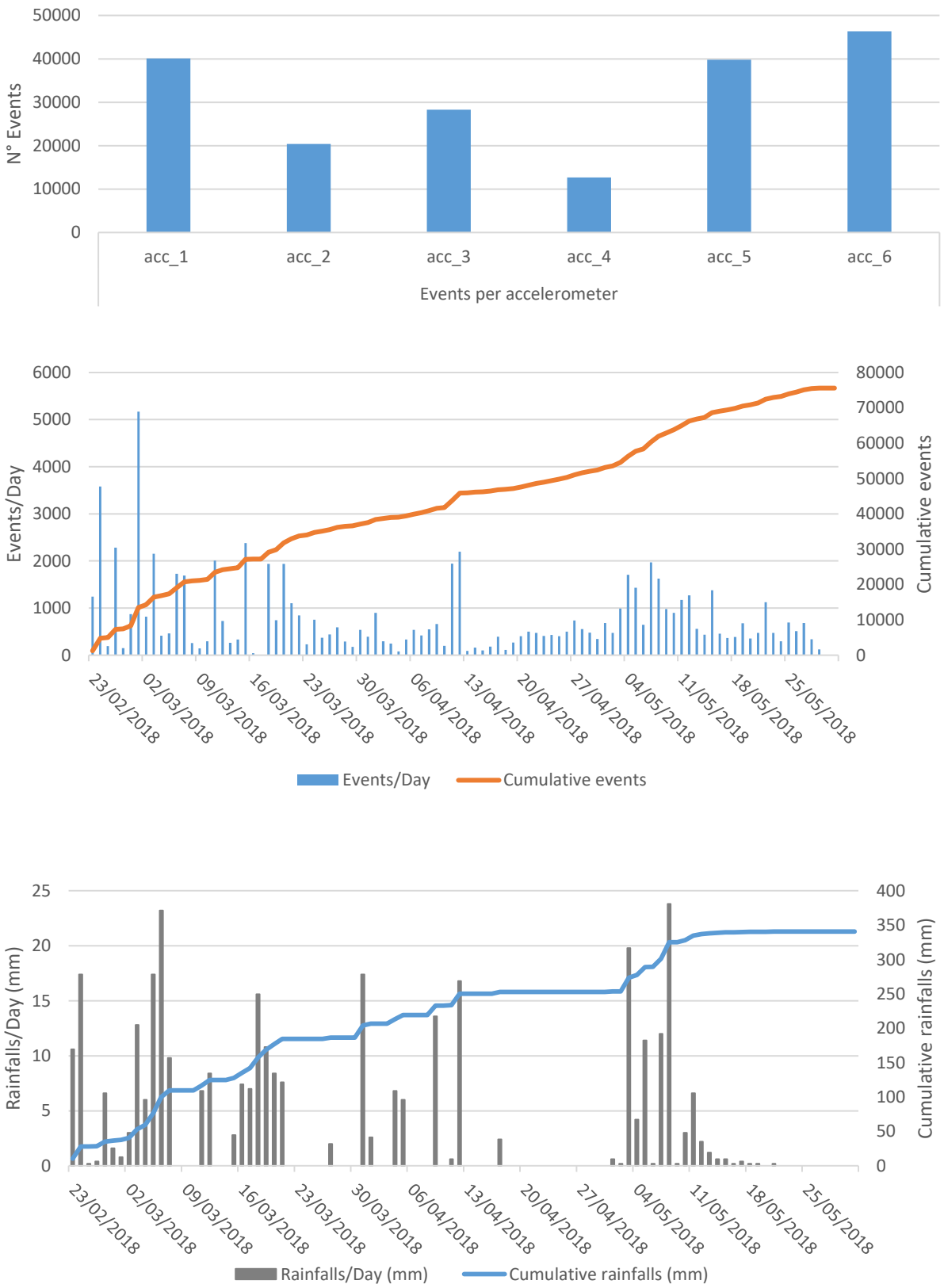

Figure 24: Events detected in the first microseismic monitoring campaign conducted at the Acuto test site (Acuto 2018). Up: number of events per accelerometer. Middle: distribution of the events common to at least two accelerometers expressed as events per day and as cumulative value. Bottom: rainfalls occurred shown as cumulated mm per day and total cumulative.

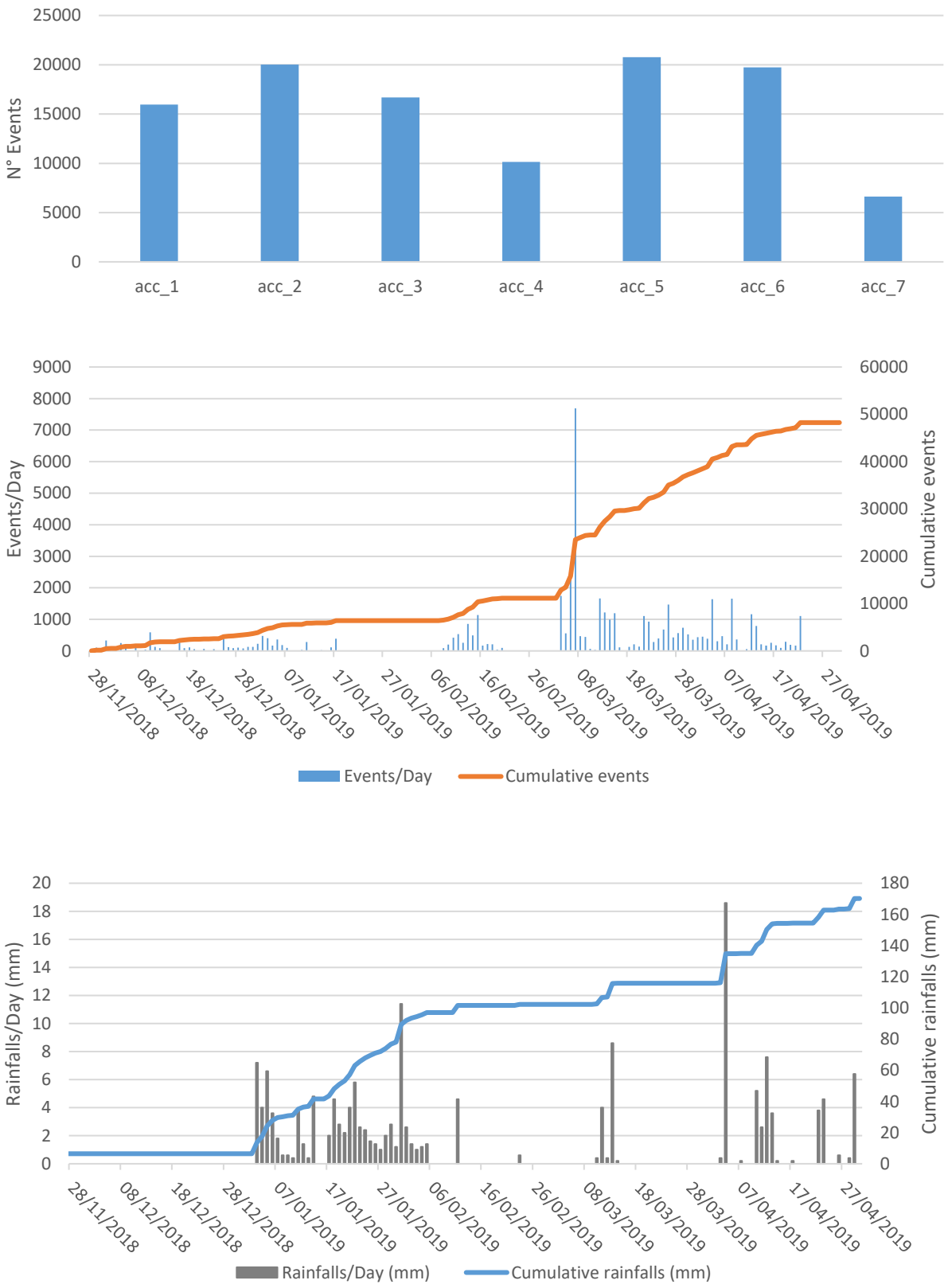

Figure 25: Events detected in the second microseismic monitoring campaign conducted at the Acuto test site (Acuto 2019). Up: number of events per accelerometer. Middle: distribution of the events common to at least two accelerometers expressed as events per day and as cumulative value. Bottom: rainfalls occurred shown as cumulated mm per day and total cumulative.

From the detected events of the first microseismic monitoring campaign carried out at Acuto (Figure 24), it is possible to note a number of detected events partially in agreement with the disposition adopted for the accelerometers. In fact, sensors 5 and 6 registered approximately the same number of events (respectively 39824 and 46343 counts) and were both installed on the rock mass. A reduced number of events (12688) is recorded by sensor 4, which for its particular position, enclosed between two main fractures may have been interested by attenuation phenomena of the seismic waves, thus resulting in registering only the strongest solicitations. By referring to the sensors deployed on the rock block, accelerometers 2 and 3 show a comparable number of events (respectively 20399 and 28294), while the accelerometer 1 shows a higher counting (40098), probably because of its more external and exposed position in respect to the other sensors. It is worth to note a major clustering of events in the first period of the monitoring, which is the coldest and rainiest one, and even freezing and thawing of the fractures surely contributed in increasing the microseismic emission of that period. Another observation is the increasing number of the microseismic events recorded in correspondence of rainfalls, as also found by Helmstetter & Garambois (2010) and Arosio et al. (2018).

The considerations made for the first monitoring campaign carried out at Acuto can be extended also for the second monitoring period (Figure 25). Except for sensor 7, which was installed later and experienced more acquisition interruptions, and sensor 4 that registered a little bit more than 10000 events, all the other accelerometers registered a number of events comprised between 15000 and 20000. In this case, the comparison between the sensors installed on the rock mass and the ones on the rock block has less sense in respect to the previous campaign, because of the increased distance between sensors and the different direction measured. The significant increasing number of events detected in the first tens of March 2019 is related to a not balanced restart of the system following an acquisition interruption.

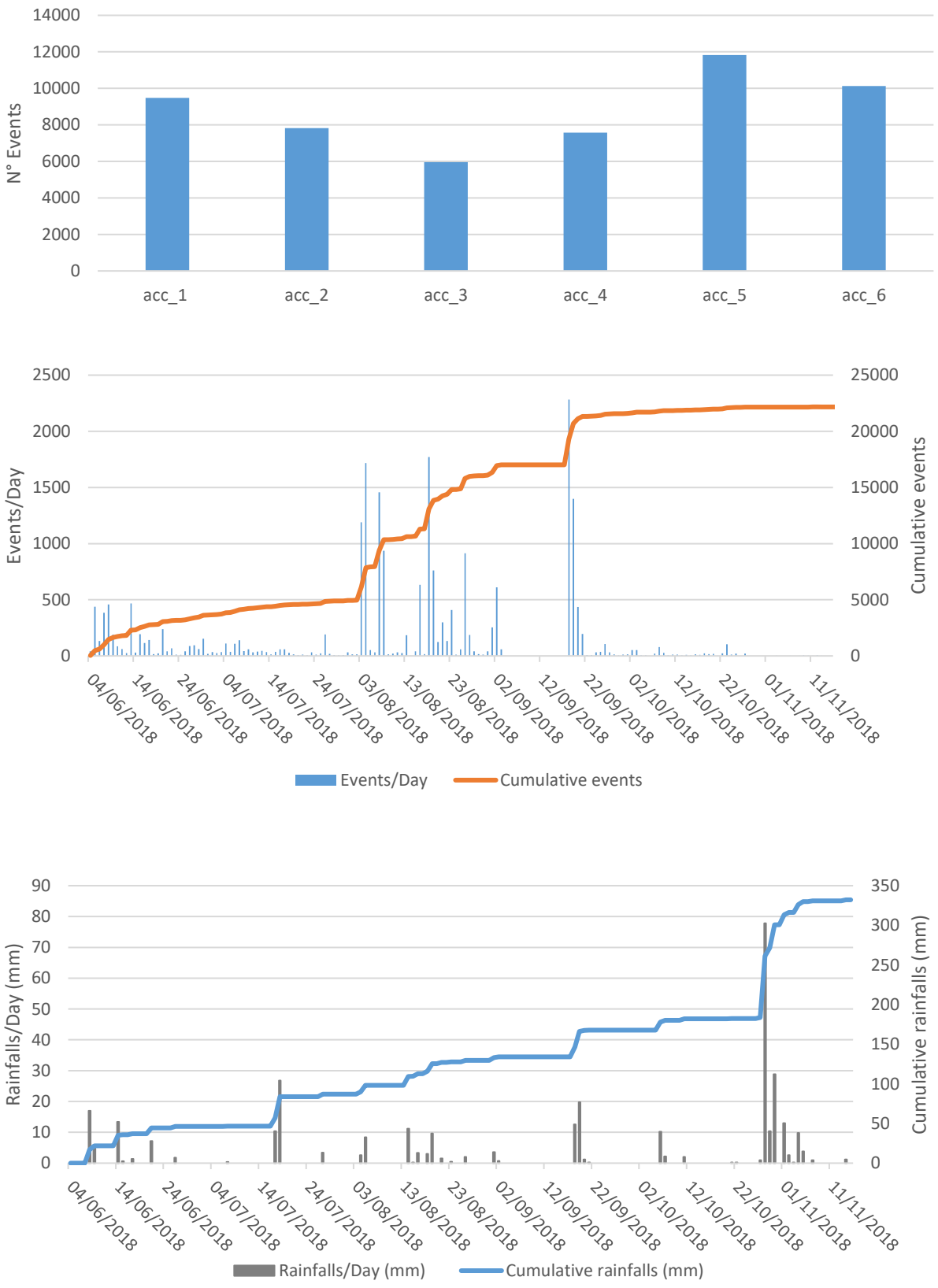

Figure 26: Events detected in the microseismic monitoring campaign conducted at the Terni-Giuncano railway test site (Terni 2018). Up: number of events per accelerometer. Middle: distribution of the events common to at least two accelerometers expressed as events per day and as cumulative value. Bottom: rainfalls occurred shown as cumulated mm per day and total cumulative.

As it regards the Terni-Giuncano railway test site, the same issue affected the registration in the first week of August 2018 and the third week of September 2018 (Figure 26), when in both the occasion the monitoring had to be restarted after maintenance interventions. Even in this test site, a correlation between the rainfalls events and the microseismicity was found, but less important than in the Acuto test site. This is also because the monitoring campaign took place during the summer season, while during the rainy autumnal phase the actual period of acquisition was very limited, just 77 hours during the last month. Moreover, even if the weather dataset was integrated with the data of the closest weather station available, the rainfalls referred to the first period (before the installation of the on-site weather station) may be not truly happened in the test site, and conversely, some precipitations actually occurred might have been missed. In fact, the different geographical settings where the weather stations were installed, a deeply incised valley in a hilly area and an intermontane plain, could introduce slight-to-moderate variations in the distribution of the precipitations. However, the total amount of detected events is less than the ones recorded in both the monitoring campaign conducted at the Acuto test site. This is confirmed also after comparing the total hours of actual acquisition, which were computed and resulted to be of 1581 and 1431 hours for the first and second campaign carried out at Acuto respectively, and 1589 hours at Terni, thus similar in terms of entity of the monitored period.

Regarding the railway traffic, 2763 trains have been detected and assigned to their identification code (i.e. REG, IC, ES for passenger train; MRV, MRI for freight trains; LIS, INV for single locomotives). When the acquisition was on, 2811 trains transited on the railway: 98% of the transited trains has been detected following the procedure described in paragraph 3.3.1. In Figure 27 are reported the most transited trains according to their typology, and the percentage of detection in respect to the trains actually transited with the acquisition system on. Generally, almost all the transited trains were recognised and correctly assigned to their identification code, but also some wrong attributions were done, as the percentages over 100% testify. In those cases, the wrong ascriptions were probably linked to the temporally close transit of two or more trains, or to external disturbances that triggered the algorithm. Given the few number of erroneous assignations, the trains dataset was maintained as outputted from the STA/LTA algorithm, even because it has a very limited influence on the following analysis carried out. In fact, from the analysis of the RMS associated with each recording (paragraph 4.3), the non-train

registrations are easily recognisable from the lower RMS with respect to the real train transits. The 2763 events resulted to be mostly passenger trains (2565) with a subordinated number of single locomotives (144) and freight trains (54).

Train	Actually transited	Detected with STA/LTA algorithm	Missing trains	% of detection
Total	2811	2763	48	98%
REG 2324	131	131	0	100%
REG 2325	121	130	-9	107%
REG 2484	124	123	1	99%
IC 540	120	120	0	100%
REG 2483	119	118	1	99%
REG 2326	115	117	-2	102%
INV 27755	48	45	3	94%
INV 27756	29	25	4	86%
MRV 56662	22	22	0	100%
MRV 56653	13	9	4	69%

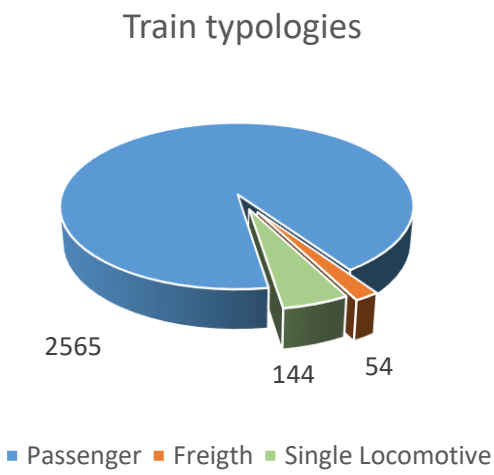

Figure 27: Types of the detected trains during the monitoring campaign performed at the Terni-Giuncano railway test site and percentage of detection of the most transited trains when the acquisition system was recording.

4.2 Results of damping analysis

In this paragraph, the results of the damping analysis performed on the recorded microseismic events are presented. For each accelerometer employed is shown the trend of the averaged value of the damping with its standard deviation for the entire monitored period and for each monofrequential waveform considered for the analysis (5, 10, 30, 50, 100, 200, 500, 1000 Hz). In order to graphically display all the analysed waveforms for each accelerometer, the ξ values of each waveform were magnified, while the real average damping coefficient $\bar{\xi}$ is reported at the beginning of each time series. A general consideration regards the average damping coefficient $\bar{\xi}$, which decreases when the frequency increases. A red dot marks the values in the damping time series that, considered with their standard deviation, are not comprised in the standard deviation interval of the first value of the respective series, which is taken as reference. As previously explained (paragraph 3.3.2), these values represent measurements truly different from the initial value of the time series, thus being considered as variation or anomalies in the

series. Moreover, the meteorological datasets referred to the air and rock mass temperature, the cumulated rainfalls and the earthquakes with local magnitude major than 2 occurred within a 50 km radius from the test sites are also shown for a comparative analysis with the damping time series.

Figure 28, Figure 29, Figure 30, Figure 31, Figure 32, Figure 33 are referred to the first microseismic monitoring campaign carried out at the Acuto test site (Acuto 2018). From the graphs it is possible to note that there is no remarkable variation in the derived damping values through all the monitored period and that no significant differences exist among the accelerometers deployed on the rock block (1, 2, 3, 4) and the ones fixed on the rock wall (5, 6). Moreover, there are no measurements that can be considered as anomalies, as proved by the absence of red dots in all the reported series.

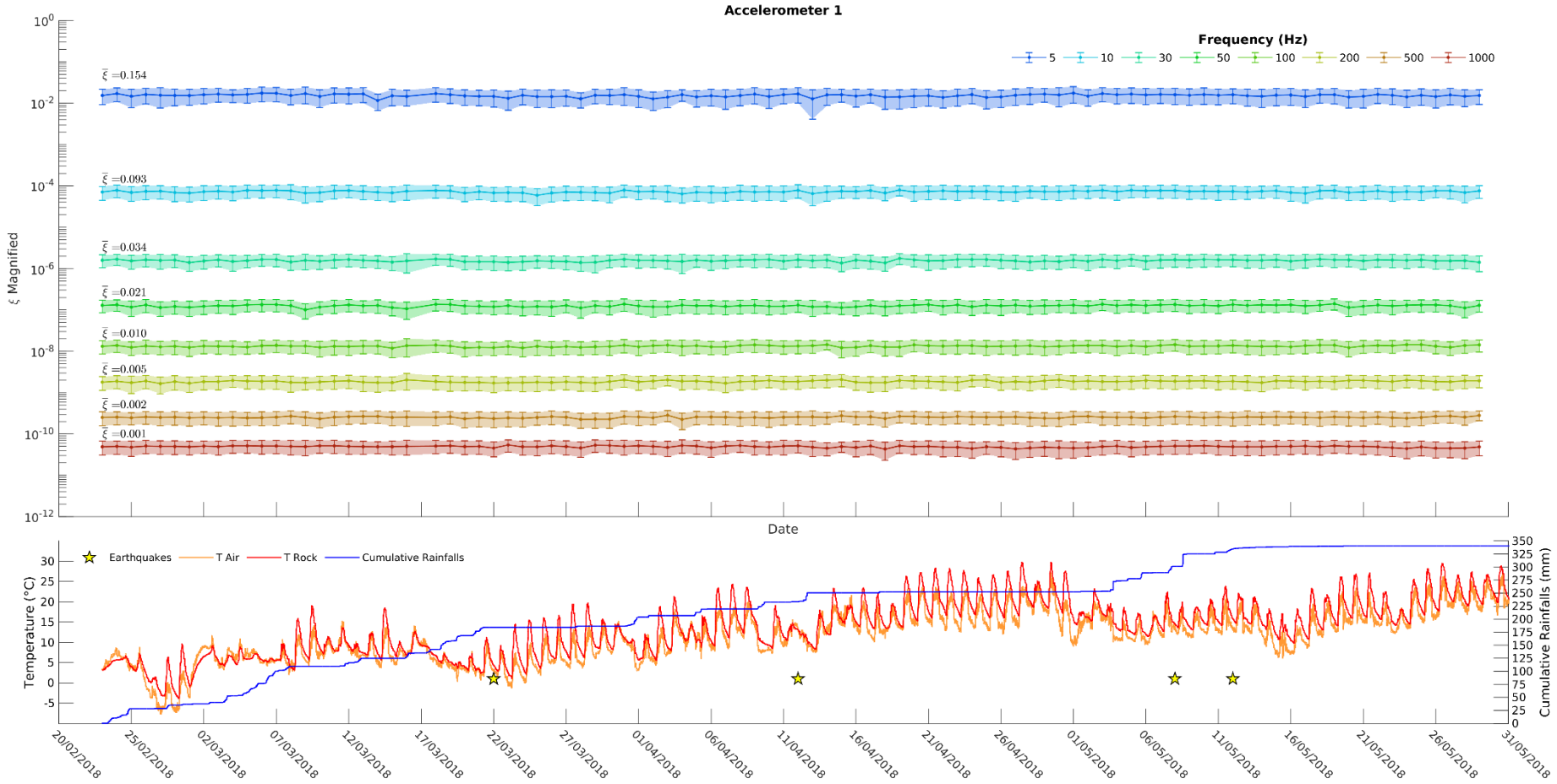

Figure 28: Damping analysis of the microseismic events detected for the first monitoring campaign conducted at the Acuto test site (Acuto 2018), relative to accelerometer 1 (Figure 11). The panel below shows the environmental parameters recorded on site and the earthquakes occurred within a radius of 50 km (details in the text).

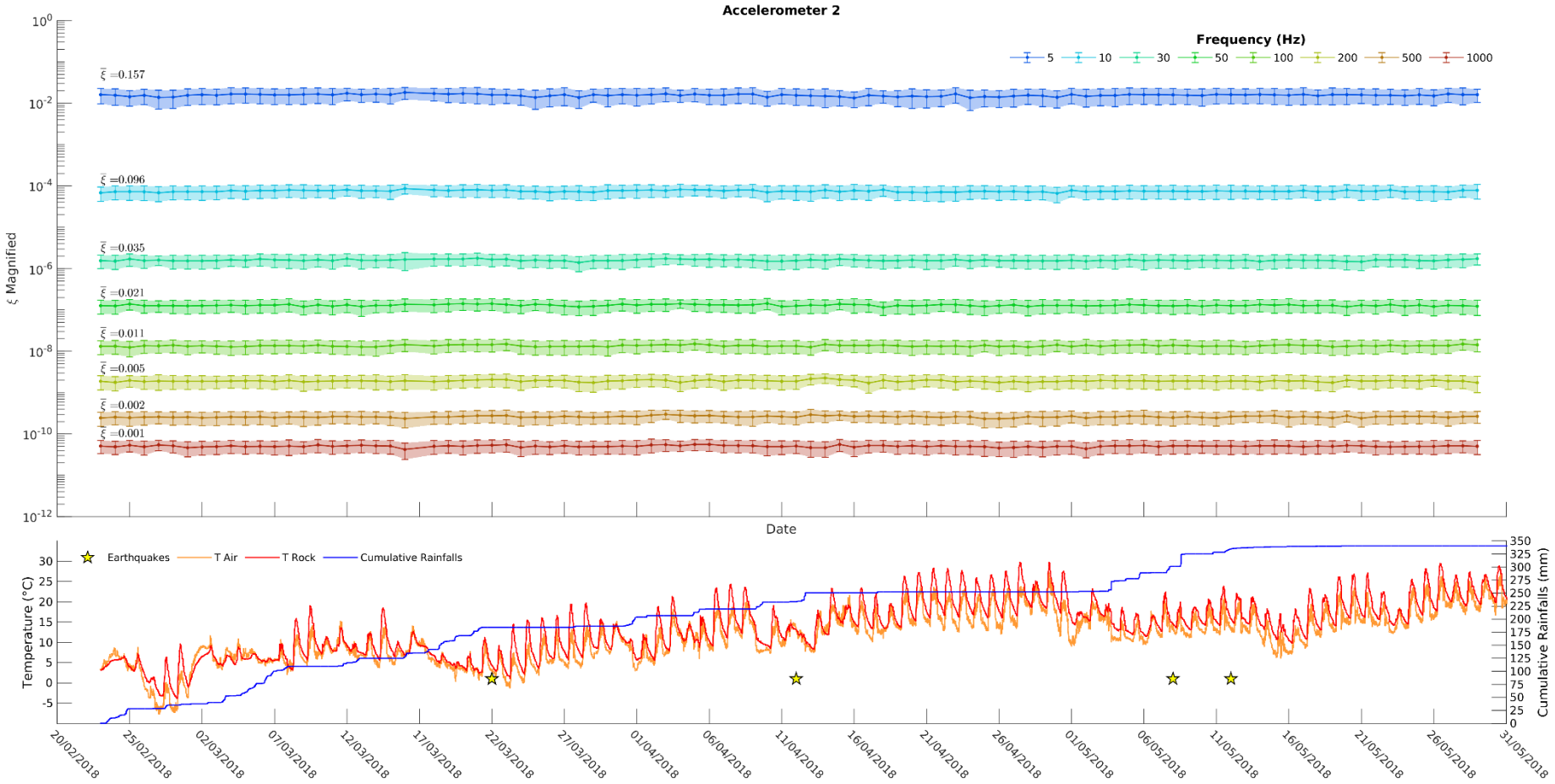

Figure 29: Damping analysis of the microseismic events detected for the first monitoring campaign conducted at the Acuto test site (Acuto 2018), relative to accelerometer 2 (Figure 11). The panel below shows the environmental parameters recorded on site and the earthquakes occurred within a radius of 50 km (details in the text).

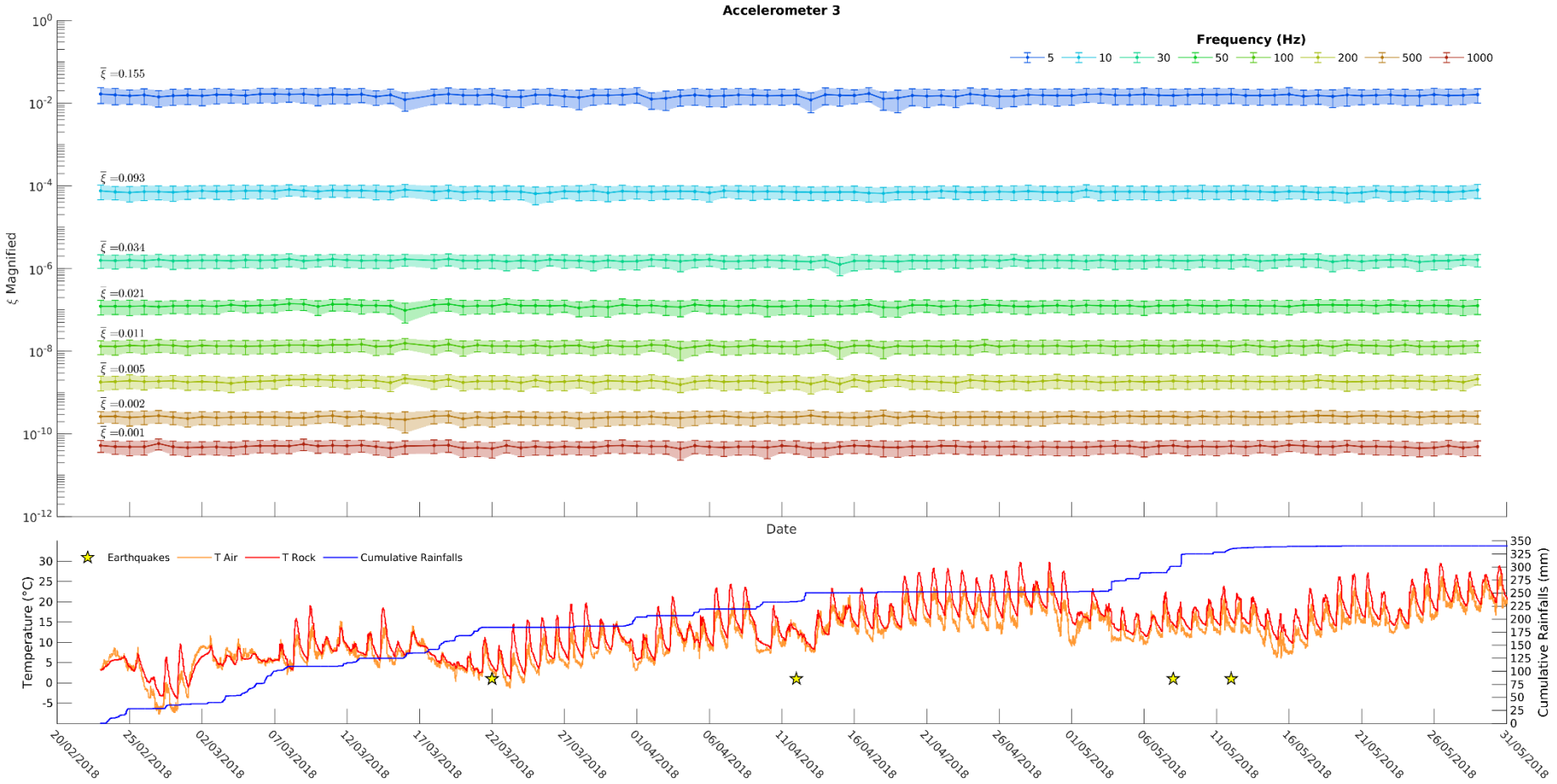

Figure 30: Damping analysis of the microseismic events detected for the first monitoring campaign conducted at the Acuto test site (Acuto 2018), relative to accelerometer 3 (Figure 11). The panel below shows the environmental parameters recorded on site and the earthquakes occurred within a radius of 50 km (details in the text).

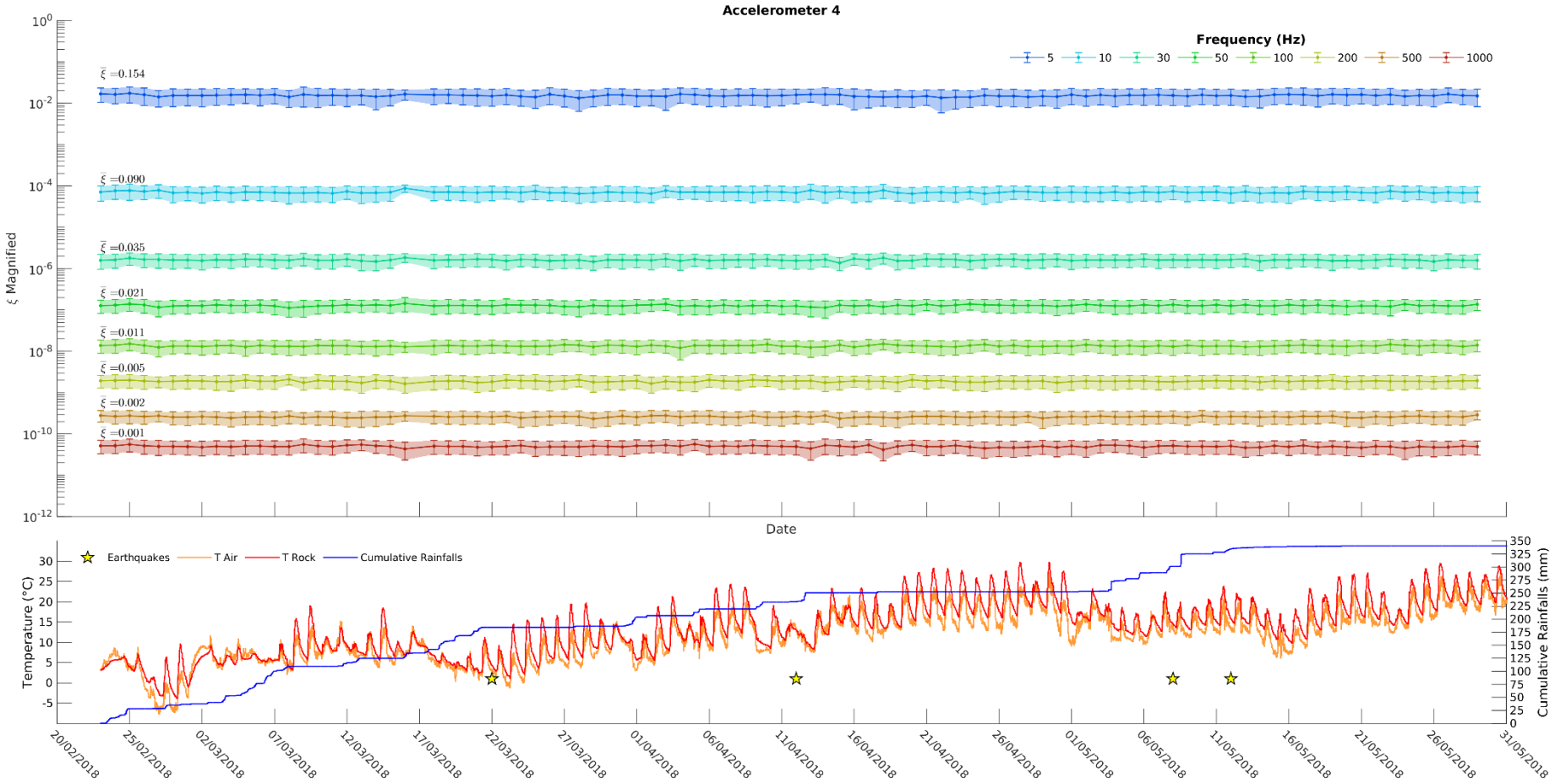

Figure 31: Damping analysis of the microseismic events detected for the first monitoring campaign conducted at the Acuto test site (Acuto 2018), relative to accelerometer 4 (Figure 11). The panel below shows the environmental parameters recorded on site and the earthquakes occurred within a radius of 50 km (details in the text).

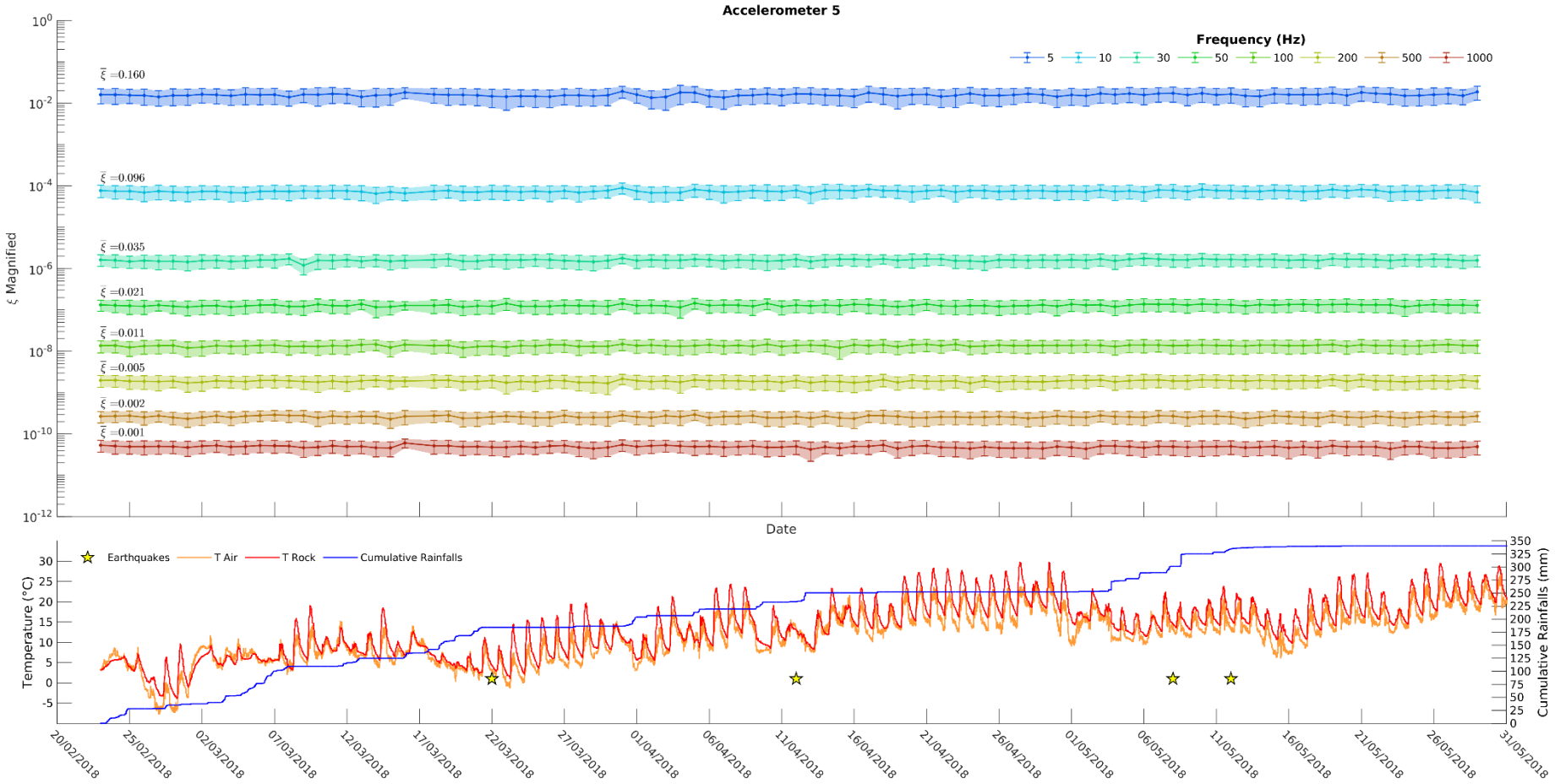

Figure 32: Damping analysis of the microseismic events detected for the first monitoring campaign conducted at the Acuto test site (Acuto 2018), relative to accelerometer 5 (Figure 11). The panel below shows the environmental parameters recorded on site and the earthquakes occurred within a radius of 50 km (details in the text).

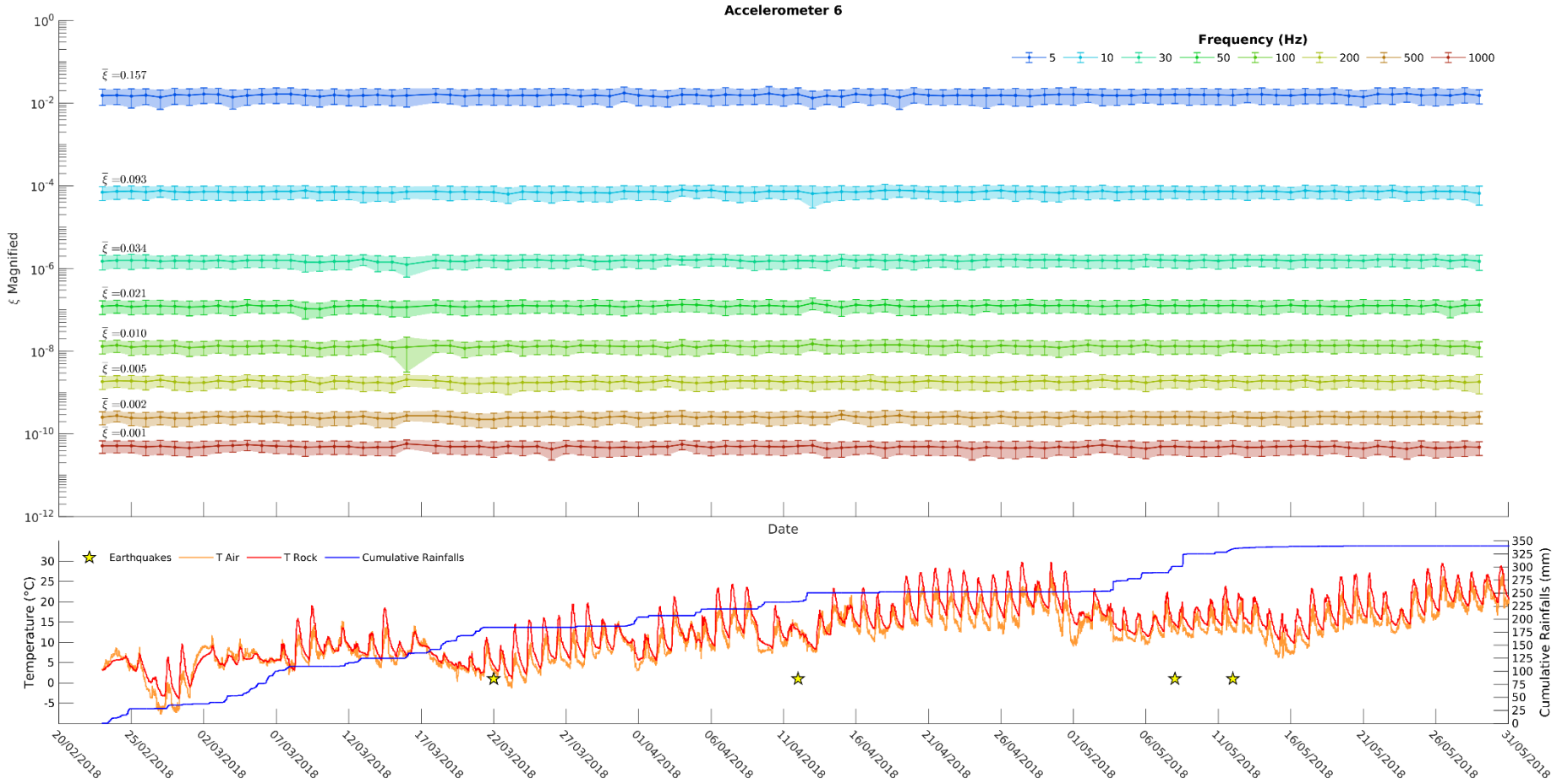

Figure 33: Damping analysis of the microseismic events detected for the first monitoring campaign conducted at the Acuto test site (Acuto 2018), relative to accelerometer 6 (Figure 11). The panel below shows the environmental parameters recorded on site and the earthquakes occurred within a radius of 50 km (details in the text).

The results referred to the second monitoring campaign performed at the Acuto test site (Acuto 2019) are shown in Figure 35, Figure 36, Figure 37, Figure 38, Figure 39, Figure 40 and Figure 41. During this campaign, only the position of the accelerometers 1 and 4 was the same of the accelerometers 6 and 2 used in the previous monitoring campaign. The acquisition started simultaneously for six accelerometers, while the seventh sensor was successively installed. The blank sections in the graphs correspond to periods in which the acquisition was off, due to power supply issues or to the maintenance of the microseismic network.

In respect to the previous monitoring campaign, it is possible to note several points marked with red dots: it is worth to notice that these anomalies are prevalently clustered in the first part of the monitored period, coinciding with the winter season. To properly assess the distribution of the anomalies, the time series were divided into two parts: a first period, from the beginning of the monitoring to January 17th 2019; a second period with the remnant data. The percentage of anomalies for each period was obtained by comparing the number of anomalies with the total available data in the two time intervals. The results presented in Figure 34, show that the anomalies are prevalently localised in the first monitored period, involving with different extent all the monofrequential waveforms considered. The seventh sensor was not considered because of its unavailability in the first part of the monitored period.

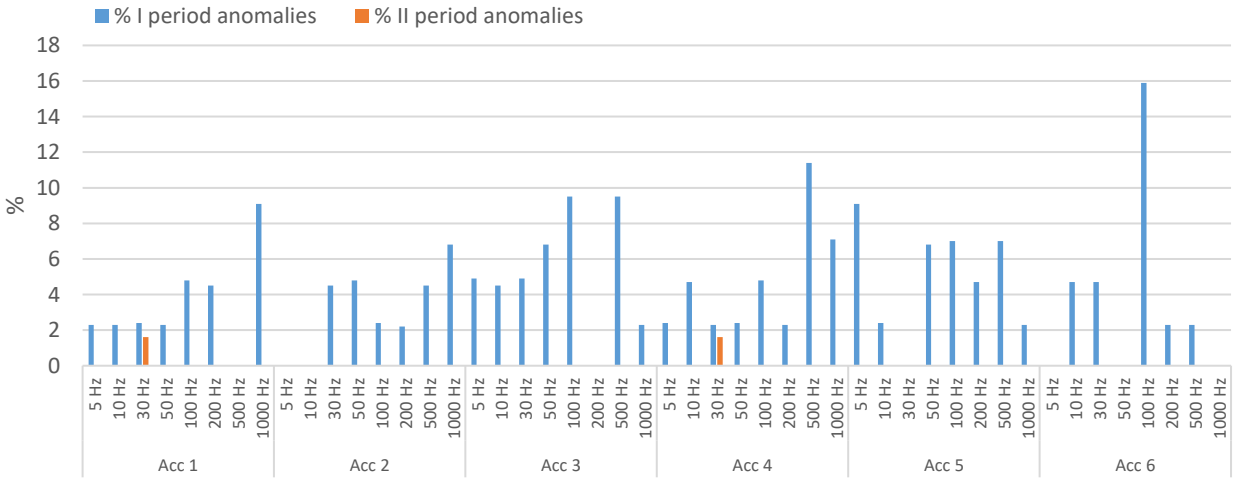

Figure 34: Percentage of anomalies in respect to the available data for the damping time series subdivided into two time intervals, before (I period) and after (II period) January 17th 2019.

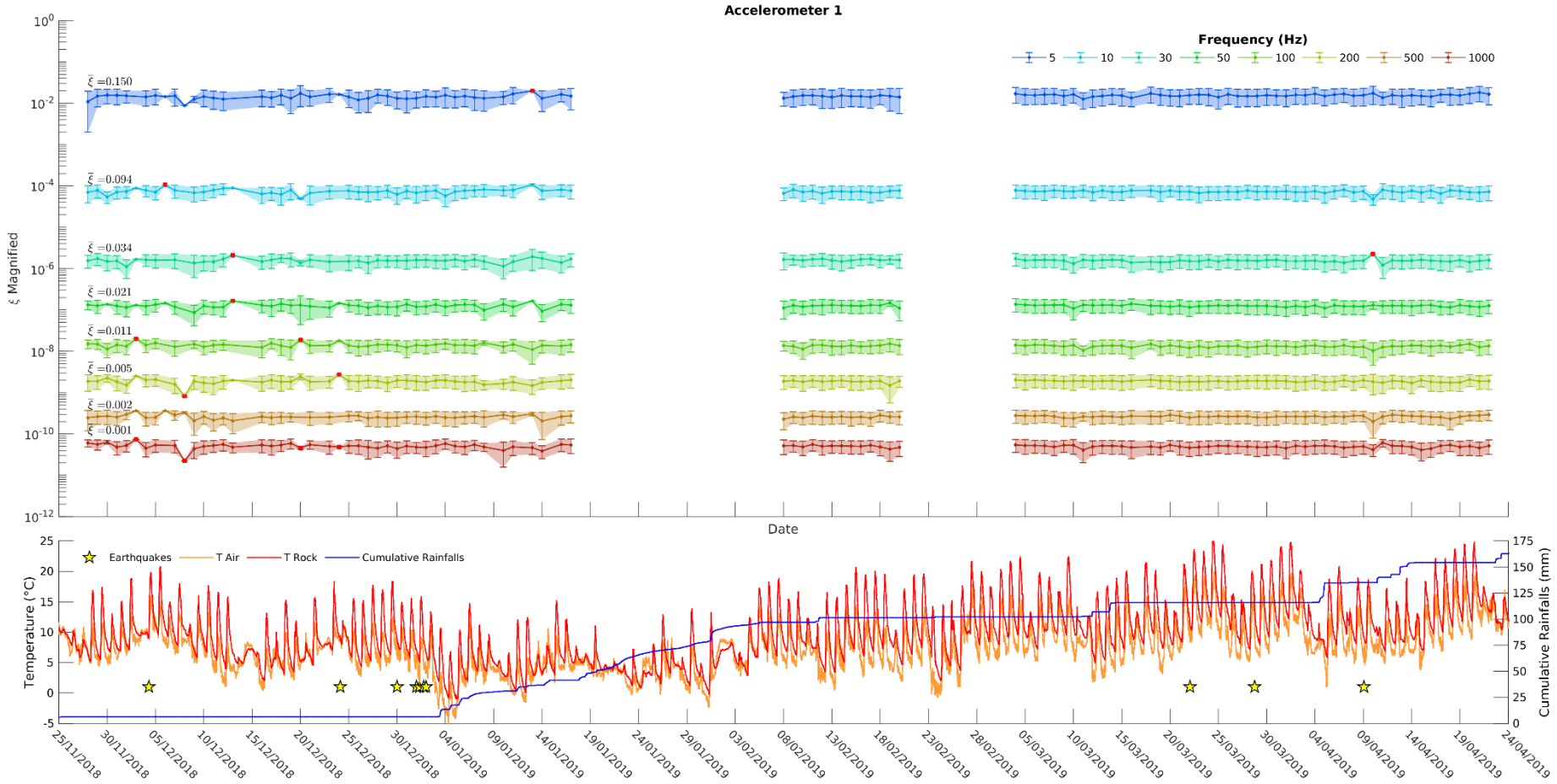

Figure 35: Damping analysis of the microseismic events detected for the second monitoring campaign conducted at the Acuto test site (Acuto 2019), relative to accelerometer 1 (Figure 12). The panel below shows the environmental parameters recorded on site and the earthquakes occurred within a radius of 50 km (details in the text).

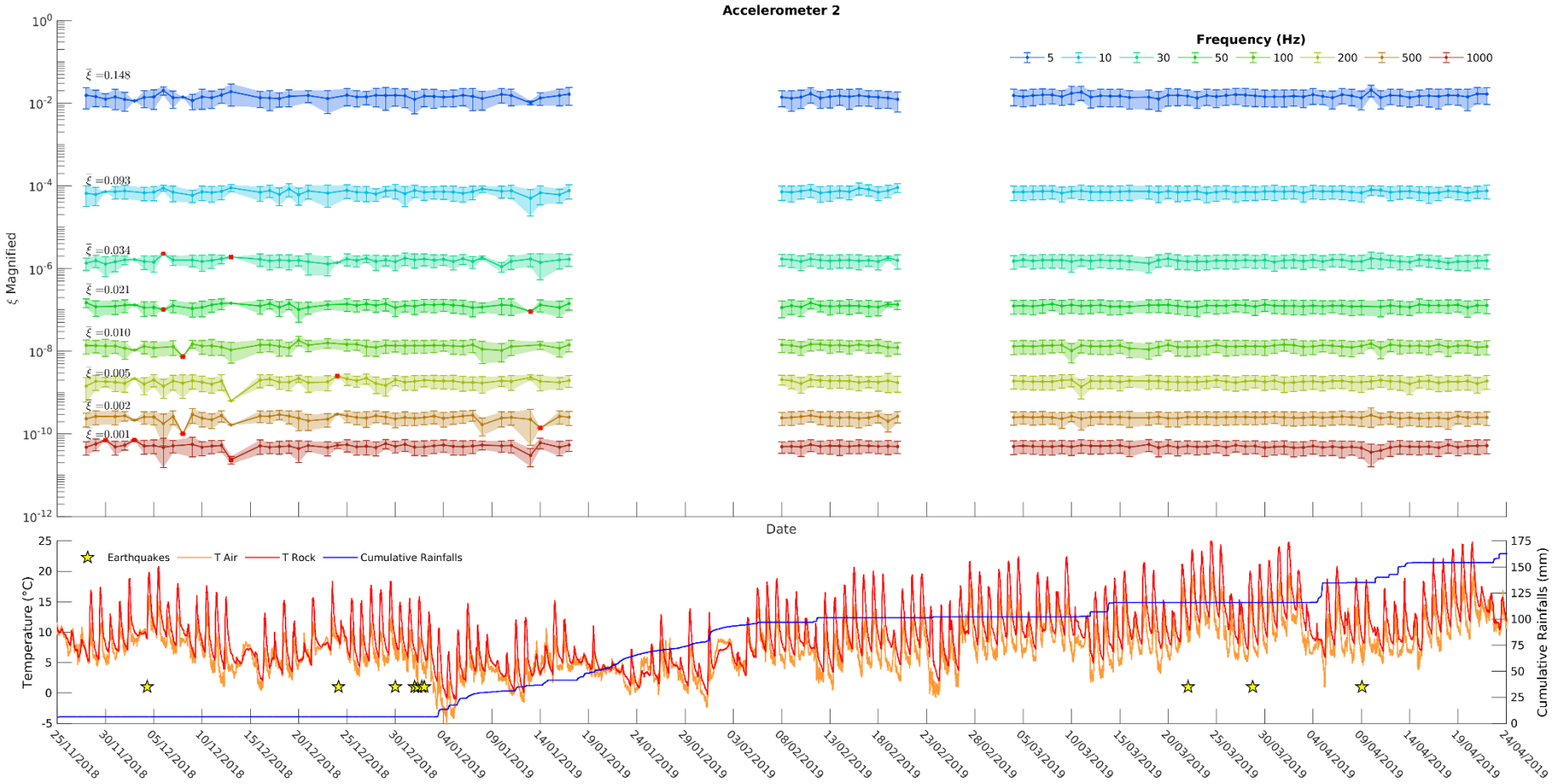

Figure 36: Damping analysis of the microseismic events detected for the second monitoring campaign conducted at the Acuto test site (Acuto 2019), relative to accelerometer 2 (Figure 12). The panel below shows the environmental parameters recorded on site and the earthquakes occurred within a radius of 50 km (details in the text).

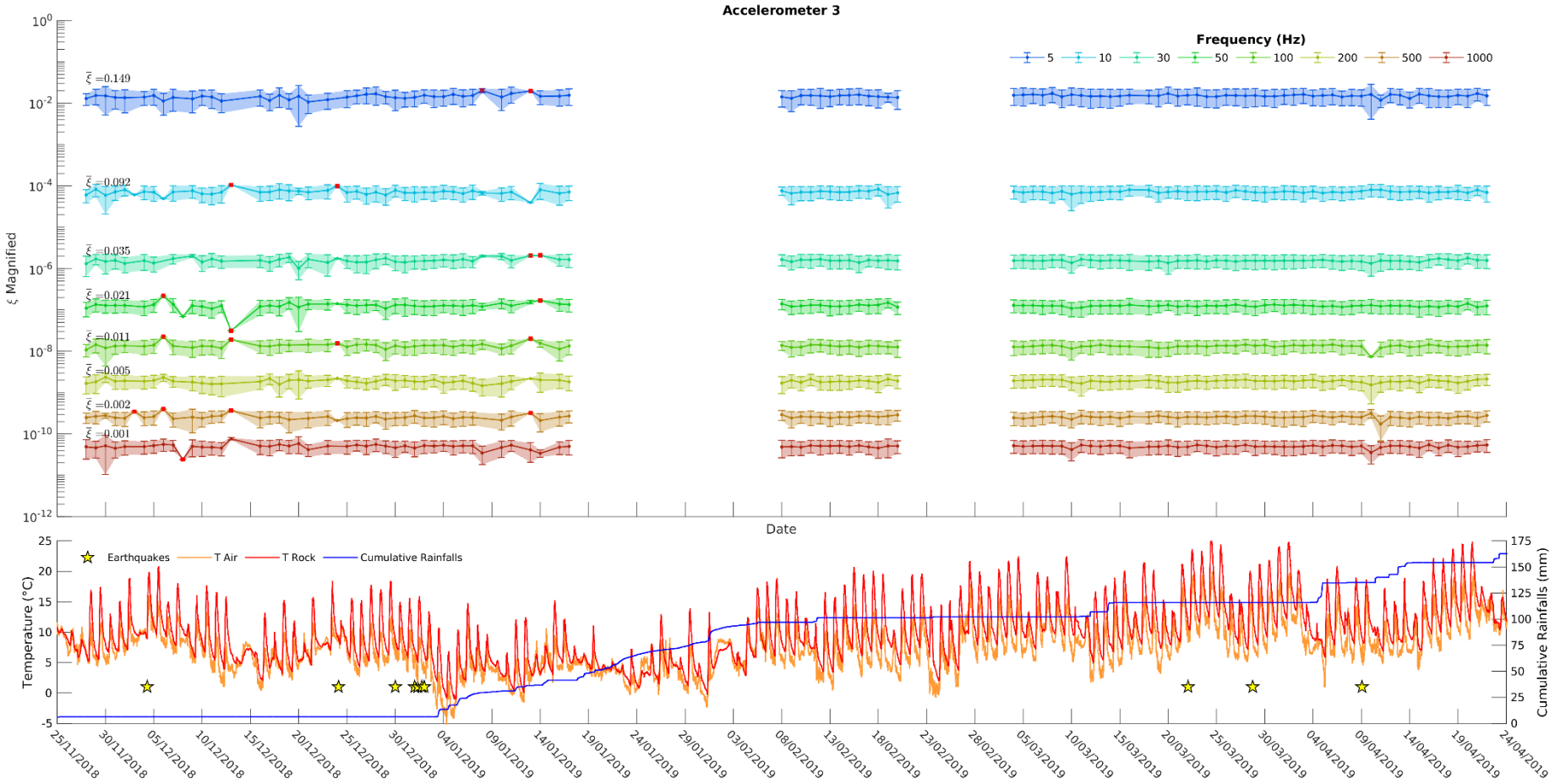

Figure 37: Damping analysis of the microseismic events detected for the second monitoring campaign conducted at the Acuto test site (Acuto 2019), relative to accelerometer 3 (Figure 12). The panel below shows the environmental parameters recorded on site and the earthquakes occurred within a radius of 50 km (details in the text).

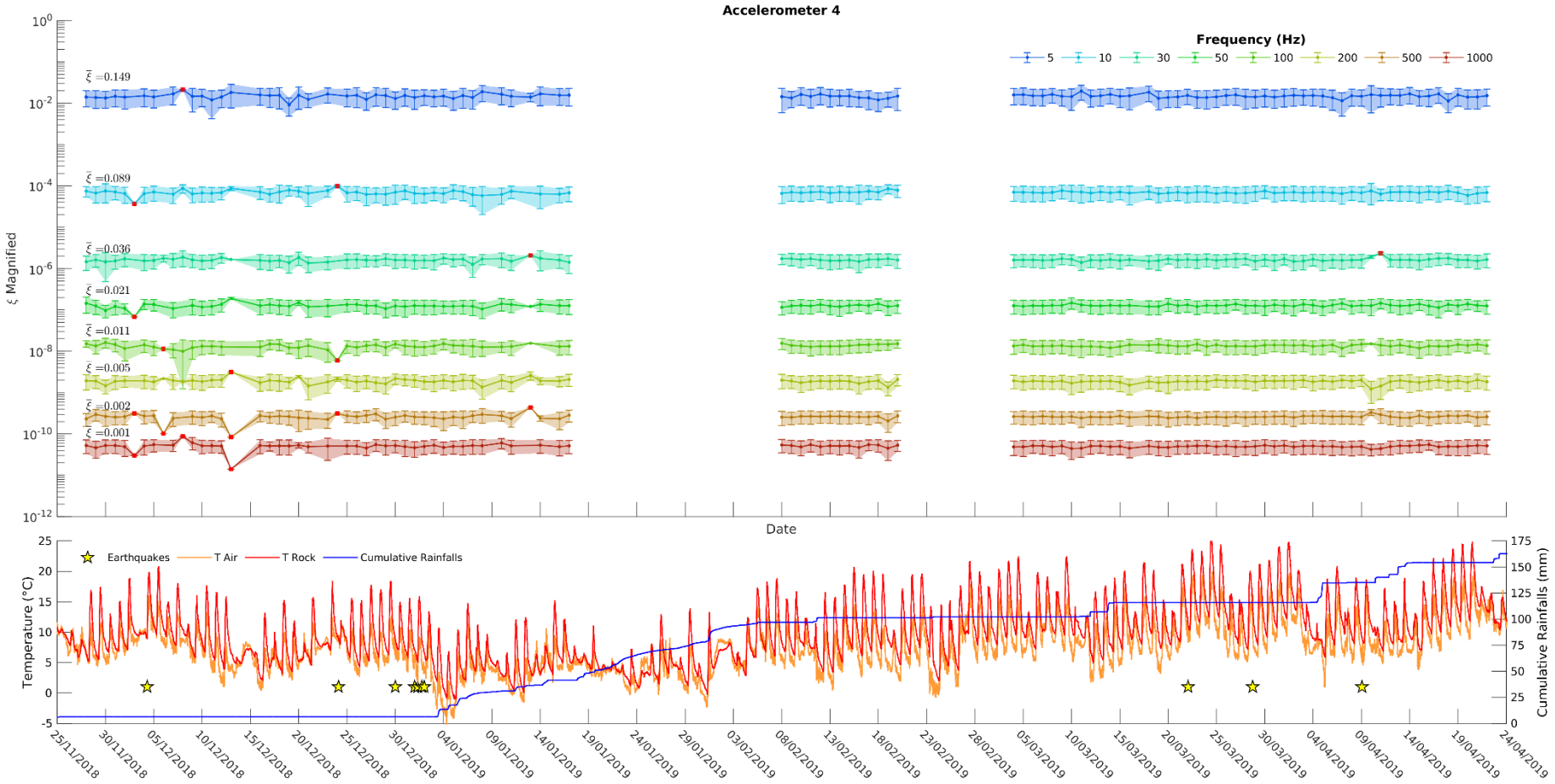

Figure 38: Damping analysis of the microseismic events detected for the second monitoring campaign conducted at the Acuto test site (Acuto 2019), relative to accelerometer 4 (Figure 12). The panel below shows the environmental parameters recorded on site and the earthquakes occurred within a radius of 50 km (details in the text).

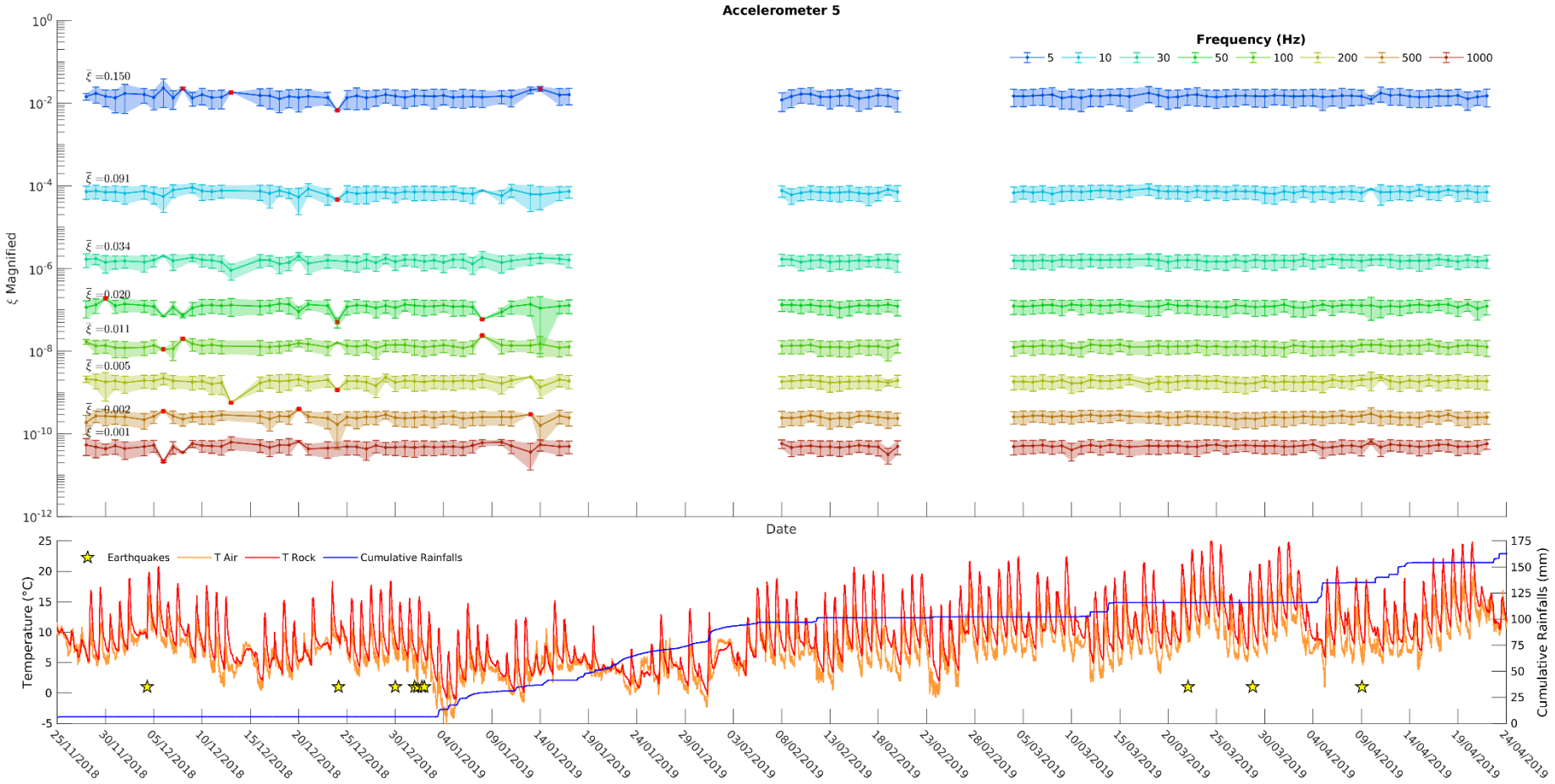

Figure 39: Damping analysis of the microseismic events detected for the second monitoring campaign conducted at the Acuto test site (Acuto 2019), relative to accelerometer 5 (Figure 12). The panel below shows the environmental parameters recorded on site and the earthquakes occurred within a radius of 50 km (details in the text).

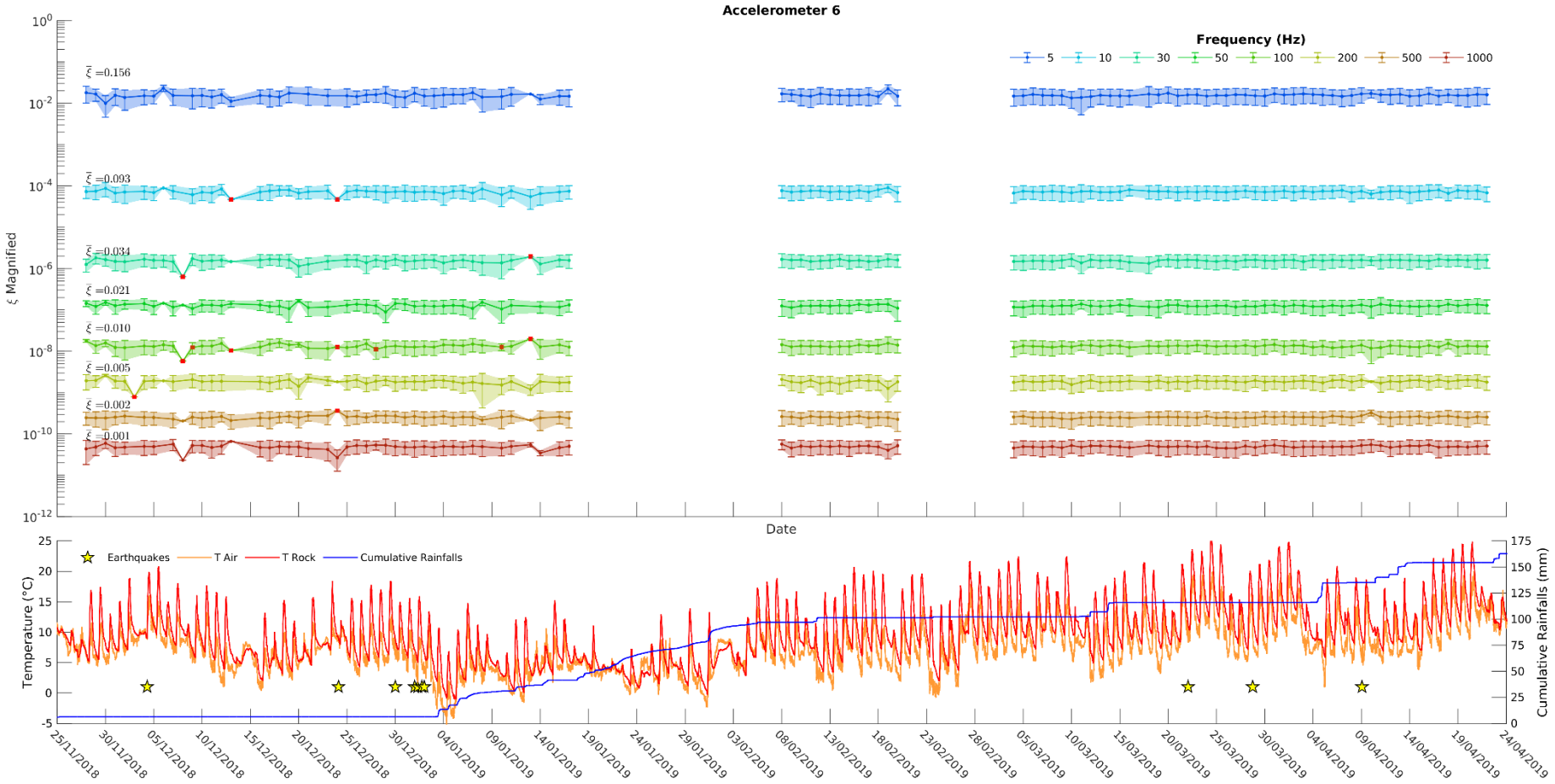

Figure 40: Damping analysis of the microseismic events detected for the second monitoring campaign conducted at the Acuto test site (Acuto 2019), relative to accelerometer 6 (Figure 12). The panel below shows the environmental parameters recorded on site and the earthquakes occurred within a radius of 50 km (details in the text).

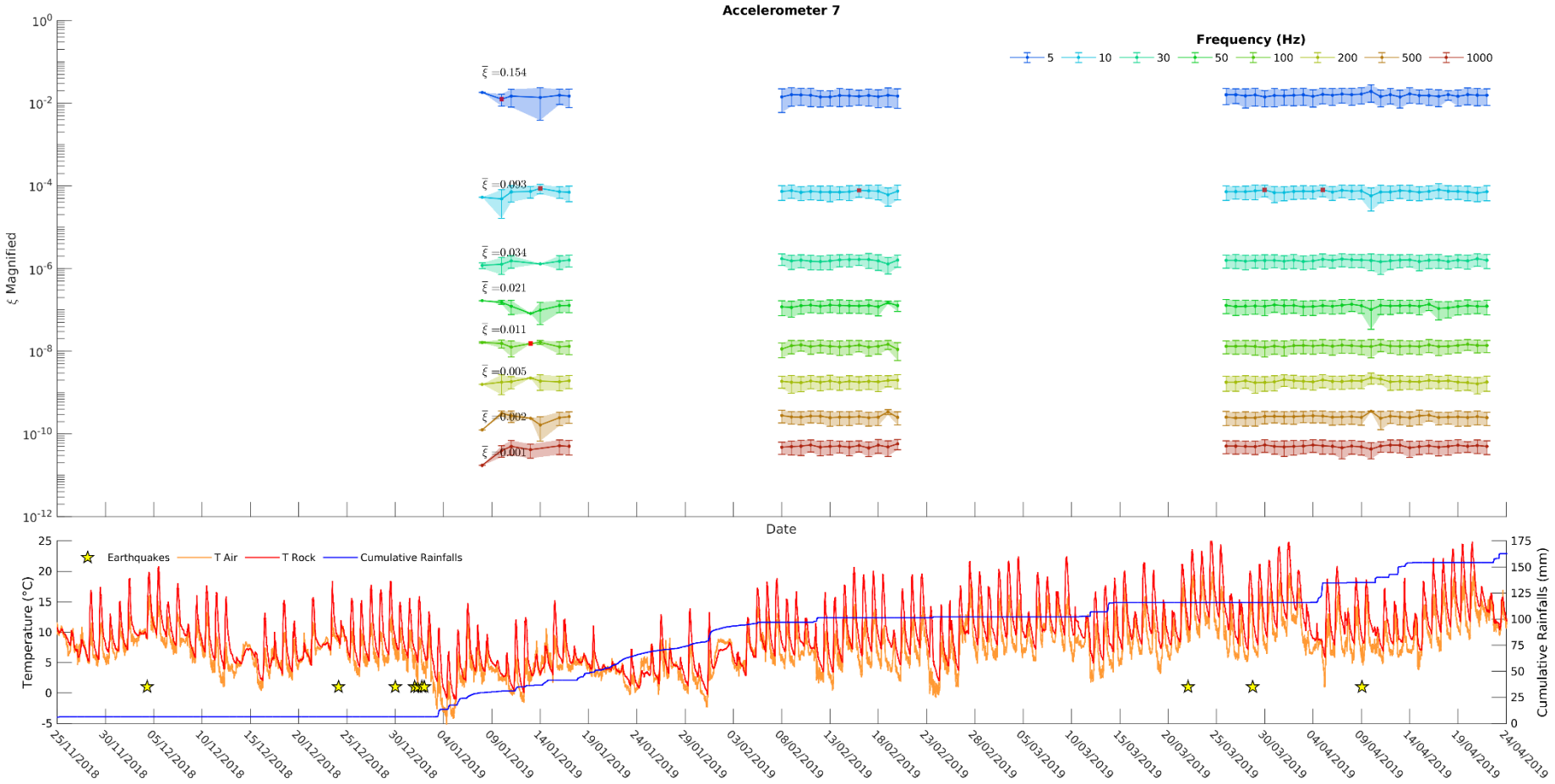

Figure 41: Damping analysis of the microseismic events detected for the second monitoring campaign conducted at the Acuto test site (Acuto 2019), relative to accelerometer 7 (Figure 12). The panel below shows the environmental parameters recorded on site and the earthquakes occurred within a radius of 50 km (details in the text).

Figure 43, Figure 44, Figure 45, Figure 46, Figure 47 and Figure 48 are referred to the damping analysis carried out for the microseismic events recorded at the Terni test site. In the panel related to the external actions (i.e. rainfalls, air temperature and earthquakes), the transited trains were also marked. In the last period of the monitoring, coincident with the end of October 2018 and the occurrence of rainfalls, the actual time of acquisition of the microseismic devices was very limited.

Even the damping time series derived for the Terni test site do not show a persistent variation over time, but it is possible to note the different distribution of the anomalies, which appears to be clustered in the second period of the monitoring, starting from September 18th 2018 to the end of the dataset. The distribution of the anomalies in the damping time series has been investigated with the same approach previously used for the Acuto 2019 datasets. The time series were divided into two periods: a first one, from the beginning of the monitoring to September 4th 2018; a second one with the remnant data. The percentage of the anomalies in the two periods are presented in Figure 42, which show that the anomalies are prevalently localised in the second monitored period. Although the repeated trains transit seems to not influence the general trend of the damping, it may have played a role in provoking the transient anomalous values found.

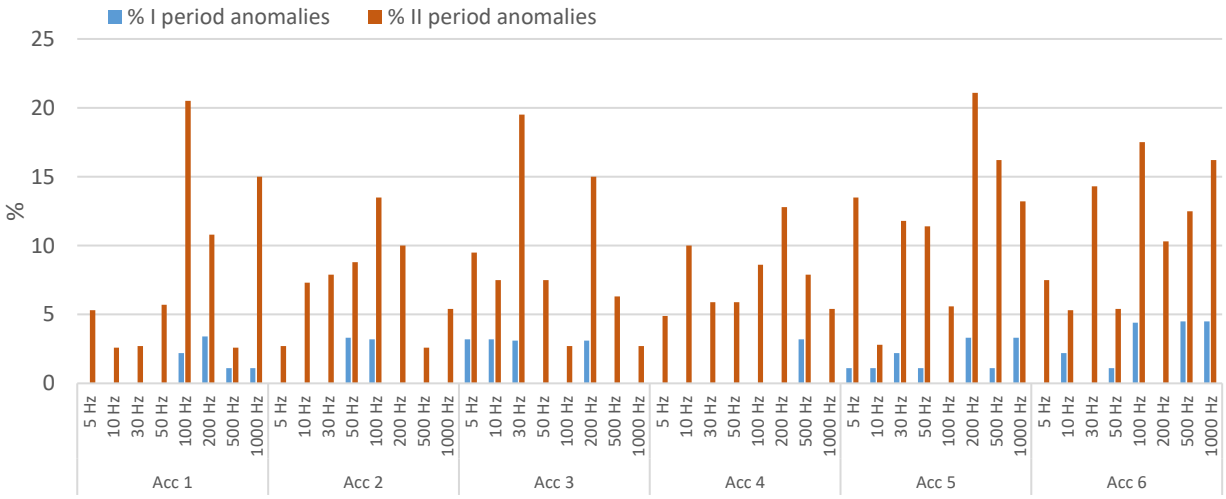

Figure 42: Percentage of anomalies in respect to the available data for the damping time series subdivided into two time intervals, before (I period) and after (II period) September 4th 2018.

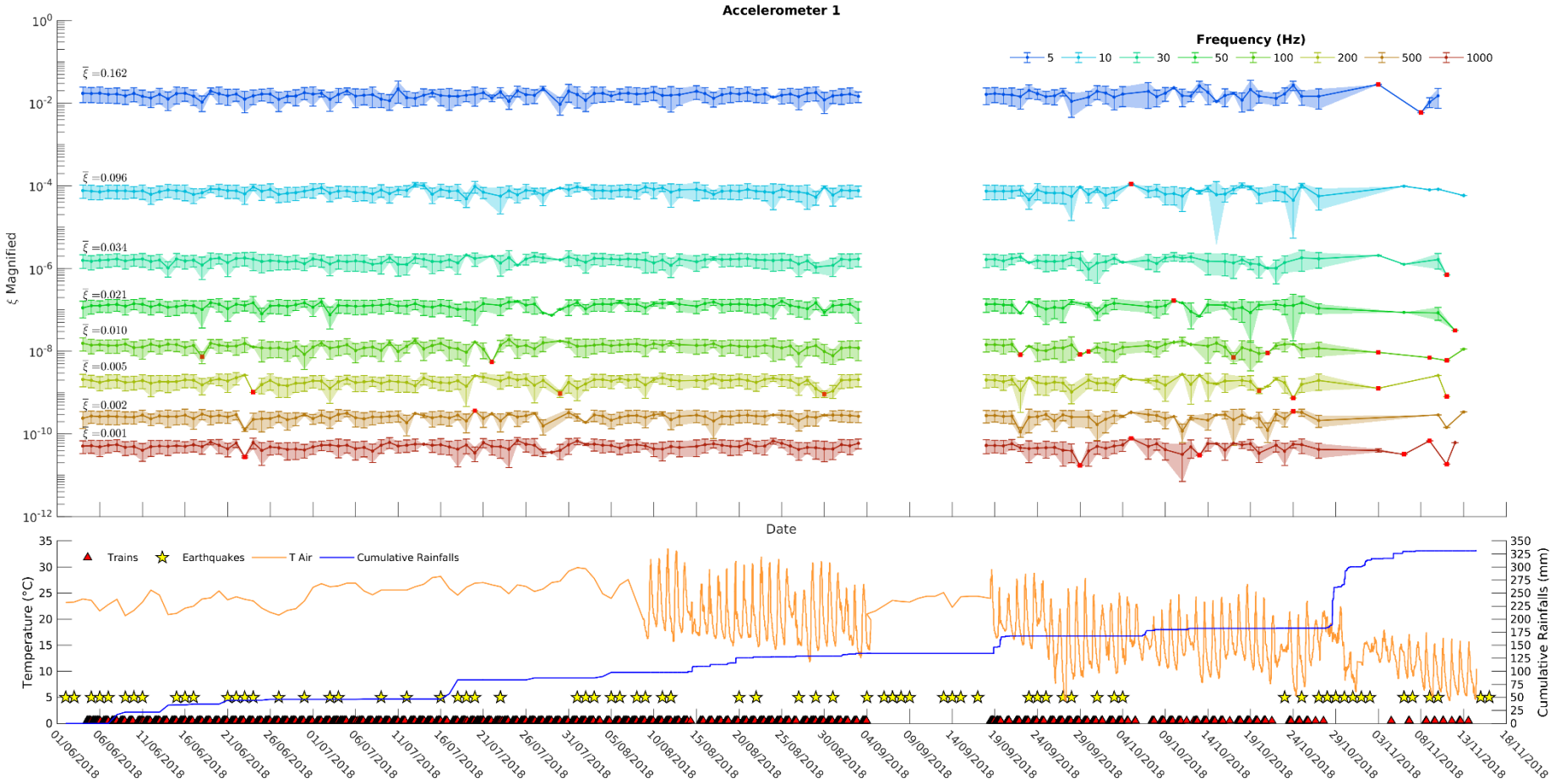

Figure 43: Damping analysis of the microseismic events detected for the monitoring campaign conducted at the Terni test site (Terni 2018), relative to accelerometer 1 (Figure 16). The panel below shows the environmental parameters recorded on site, the trains transited and the earthquakes occurred within a radius of 50 km (details in the text).

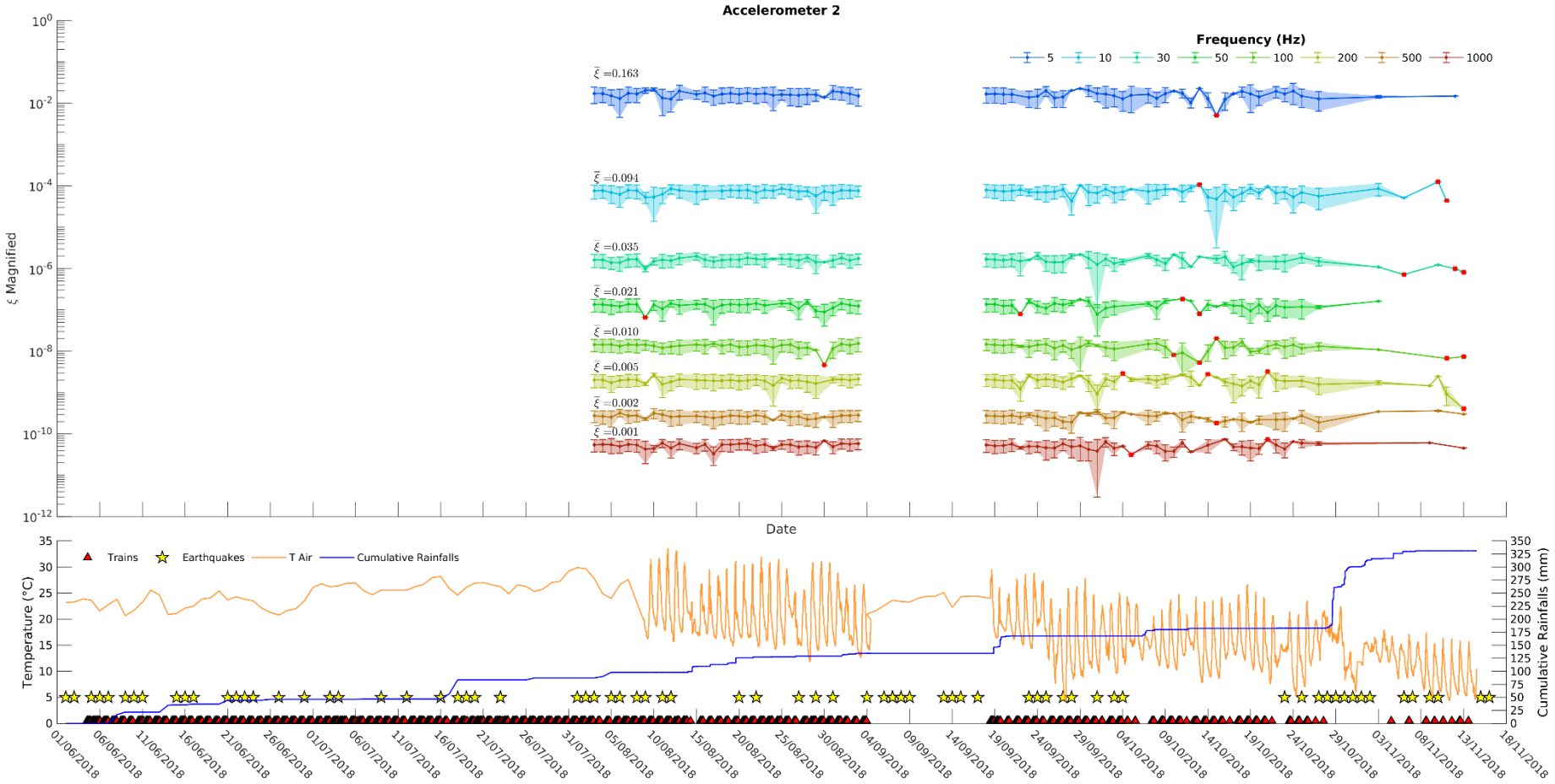

Figure 44: Damping analysis of the microseismic events detected for the monitoring campaign conducted at the Terni test site (Terni 2018), relative to accelerometer 2 (Figure 16). The panel below shows the environmental parameters recorded on site, the trains transited and the earthquakes occurred within a radius of 50 km (details in the text).

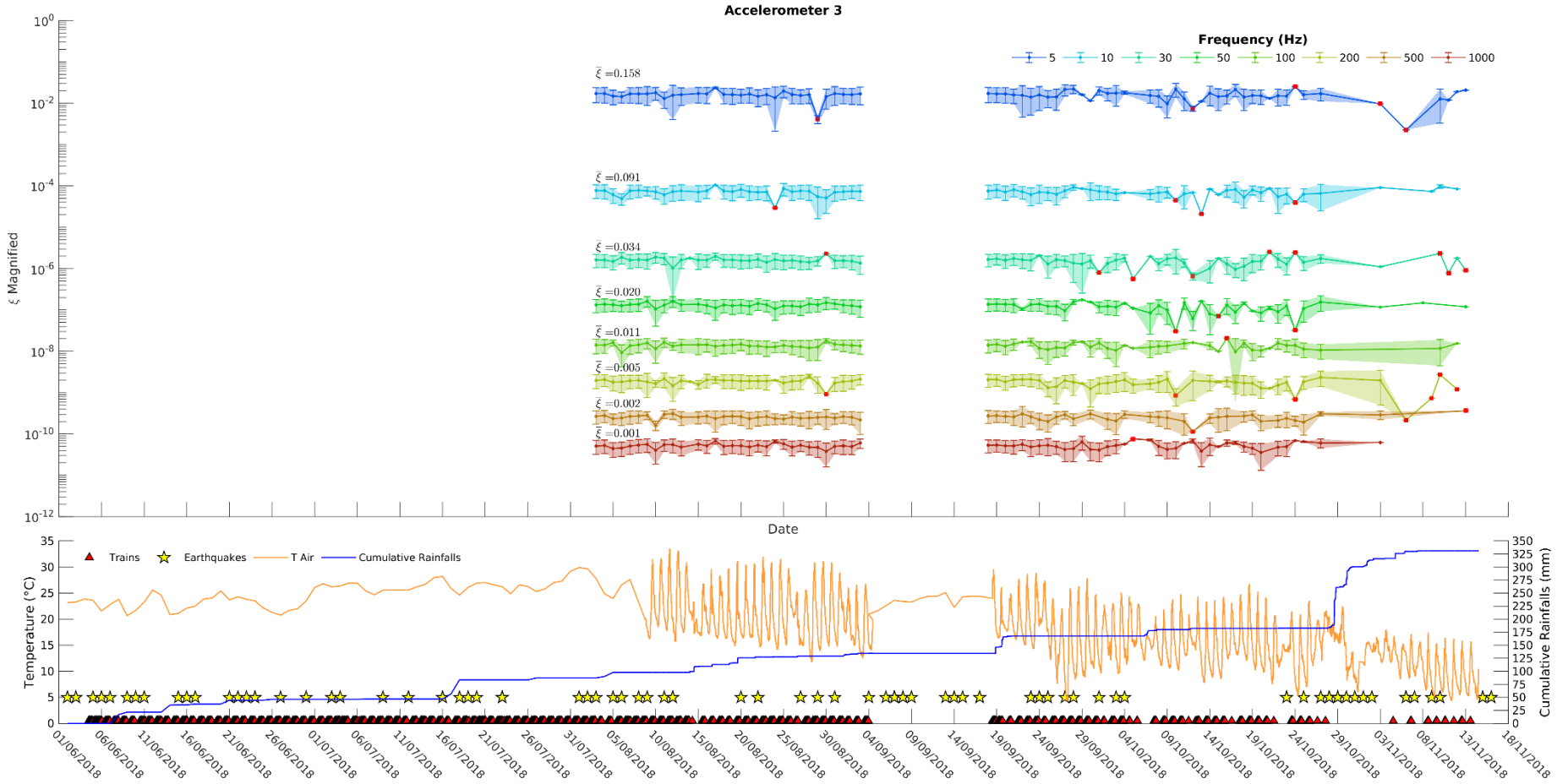

Figure 45: Damping analysis of the microseismic events detected for the monitoring campaign conducted at the Terni test site (Terni 2018), relative to accelerometer 3 (Figure 16). The panel below shows the environmental parameters recorded on site, the trains transited and the earthquakes occurred within a radius of 50 km (details in the text).

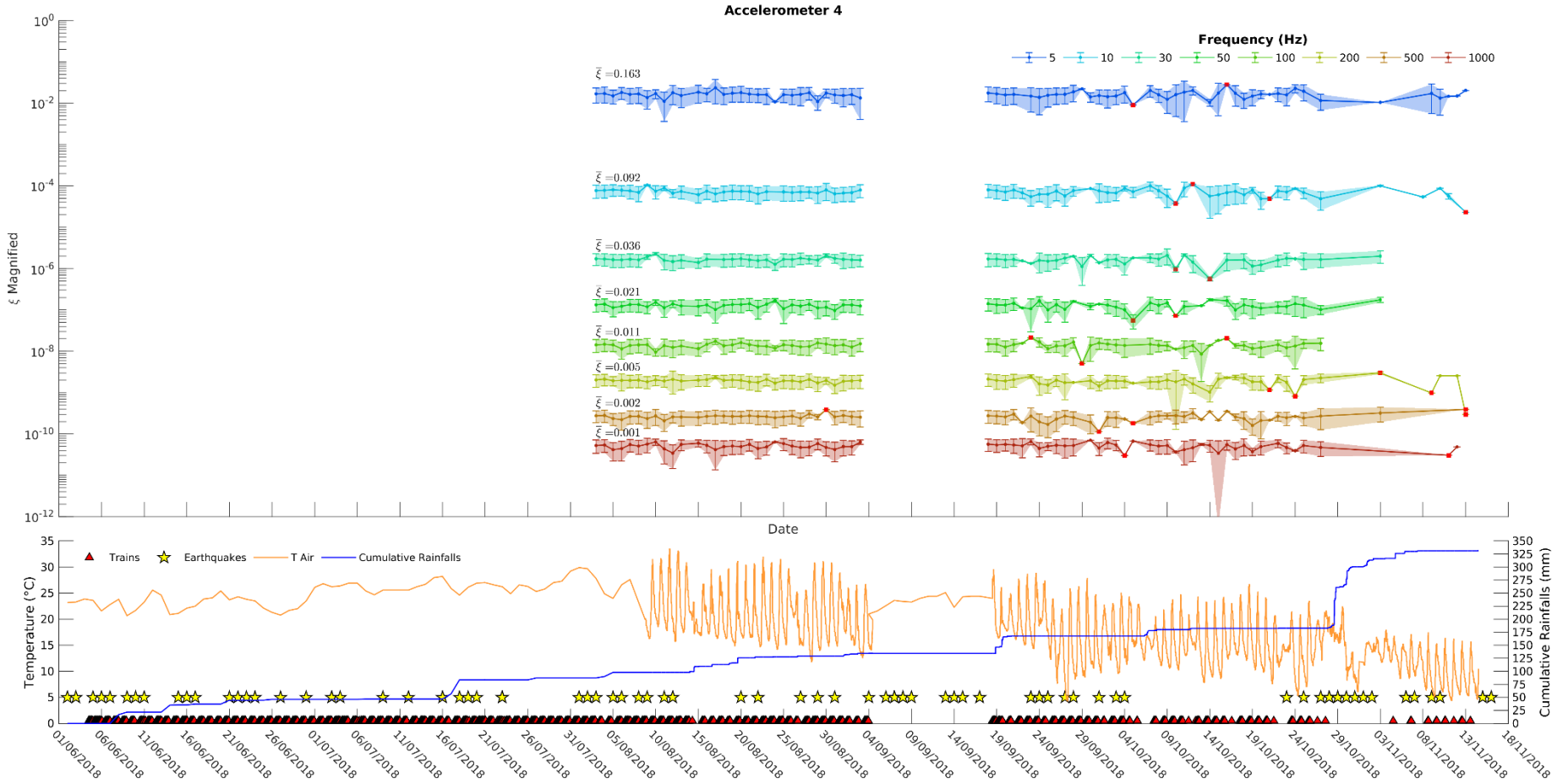

Figure 46: Damping analysis of the microseismic events detected for the monitoring campaign conducted at the Terni test site (Terni 2018), relative to accelerometer 4 (Figure 16). The panel below shows the environmental parameters recorded on site, the trains transited and the earthquakes occurred within a radius of 50 km (details in the text).

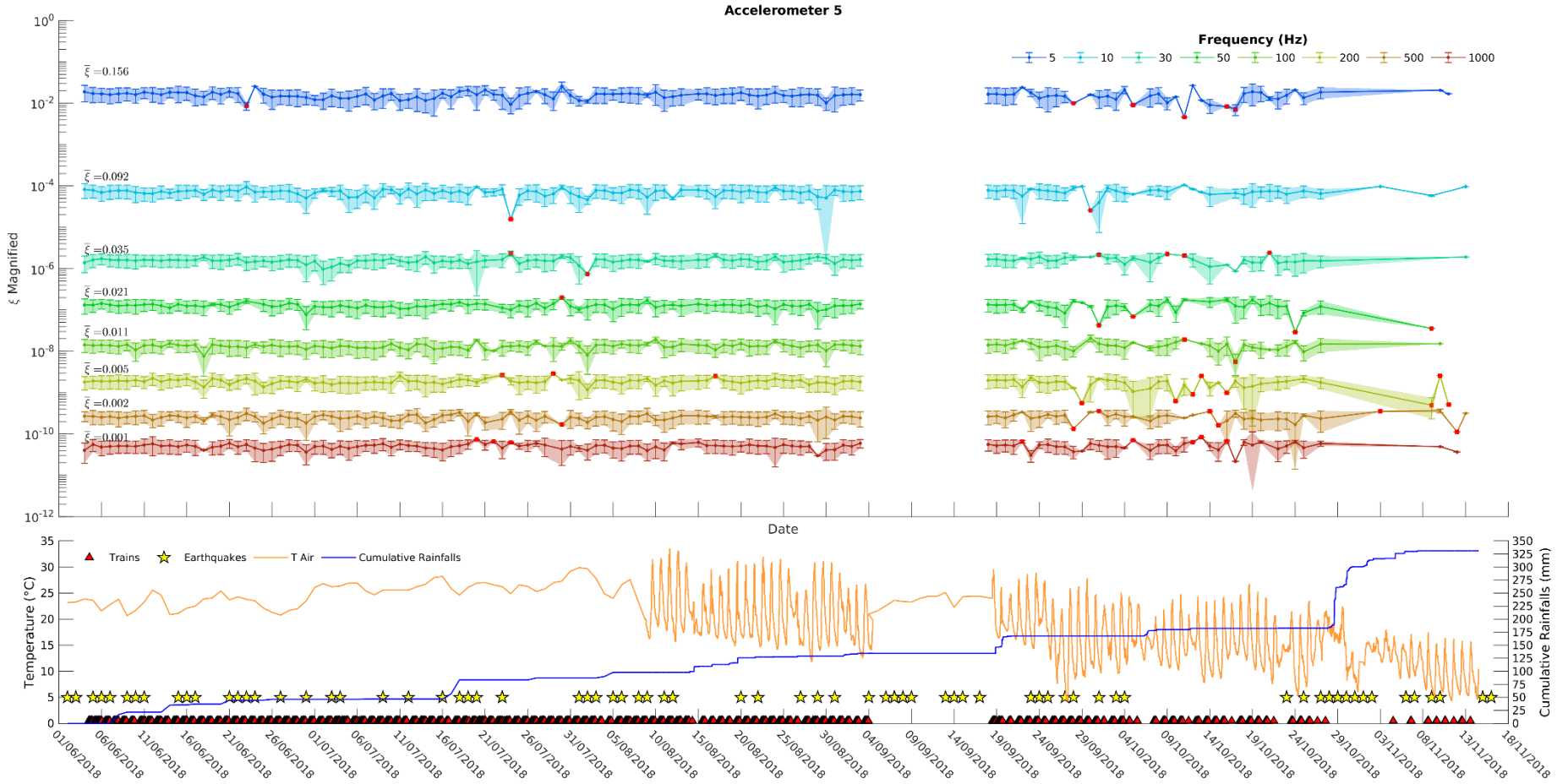

Figure 47: Damping analysis of the microseismic events detected for the monitoring campaign conducted at the Terni test site (Terni 2018), relative to accelerometer 5 (Figure 16). The panel below shows the environmental parameters recorded on site, the trains transited and the earthquakes occurred within a radius of 50 km (details in the text).

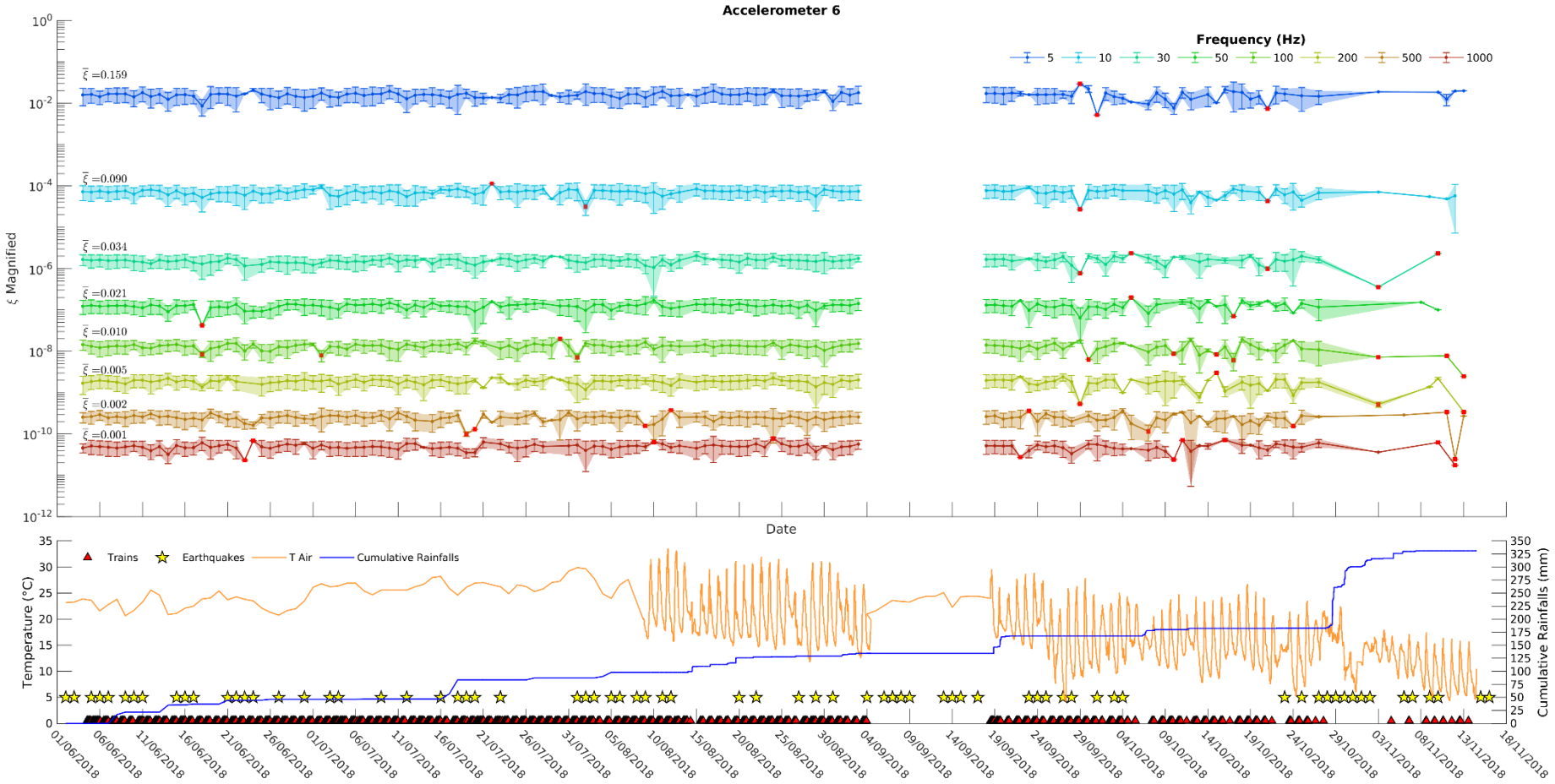

Figure 48: Damping analysis of the microseismic events detected for the monitoring campaign conducted at the Terni test site (Terni 2018), relative to accelerometer 6 (Figure 16). The panel below shows the environmental parameters recorded on site, the trains transited and the earthquakes occurred within a radius of 50 km (details in the text).

4.3 Results of cross-correlation and RMS analysis

In this section, the main results obtained for the RMS analysis and the cross-correlation of the recordings related to the train passages are shown. In particular, the results referred to two train types are presented: IC 541 (Figure 49) and REG 2324 (Figure 50). As the RMS was computed on the unfiltered time history and on specific waveforms (30, 50, 80, 100, 120, 200, 500, 1000 Hz), the results shown are referred to the unfiltered signal and to the 120 Hz waveform, which resulted to be the most energised one among those analysed. In fact, as it is possible to observe from the graphs, the RMS computed for the 120 Hz frequency follows the trend of the unfiltered signal with an order of magnitude less. Generally, the RMS appears to be stable over all the considered period, except for marked negative peaks that are likely due to a wrong train identification by the algorithm, as previously explained. Thus, those peaks are probably referred to several microseismic events or to a not balanced acquisition in that period.

The cross-correlation of the train transits evaluated for couple of sensors disposed at increasing distances, keeping sensor 1 as reference, is also shown in Figure 49 and Figure 50. As expected, the maximum lag of the cross-correlation resulted to increase from the closest couple considered (accelerometers 1 and 2) to the most spaced one (accelerometers 1 and 6). Furthermore, given the almost equal spacing among the sensors, the lags linearly increase with the distance, augmenting of one unity per each interspace crossed between sensors. Given the very reduced deviation among the values, the moving mean of the lag series referred to each train was computed, in order to better observe the evolution of the lag values over time. By looking at the lag series computed for the couple of sensors 1-5 and referred to the train IC 541 (Figure 49), the lag gradually increase over time, passing from 3 to 4, and therefore potentially representing a variation occurred in the portion of the rock mass comprised between these two sensors. On the other hand, this trend is not common to all the trains, for instance considering the same couple of sensors but for the REG 2324 (Figure 50), the lag remains fixed on a value (4) without showing particular variations.

Given the great variability of the lags derived from the cross-correlation, as well as the tiny variations in the RMS values for the several trains considered, the correlation with the environmental datasets remains hard to be established. However, more in general, it is possible

to assess that no irreversible variations capable of modifying these parameters, occurred within the rock mass in the monitored period, while transient fluctuations were observed.

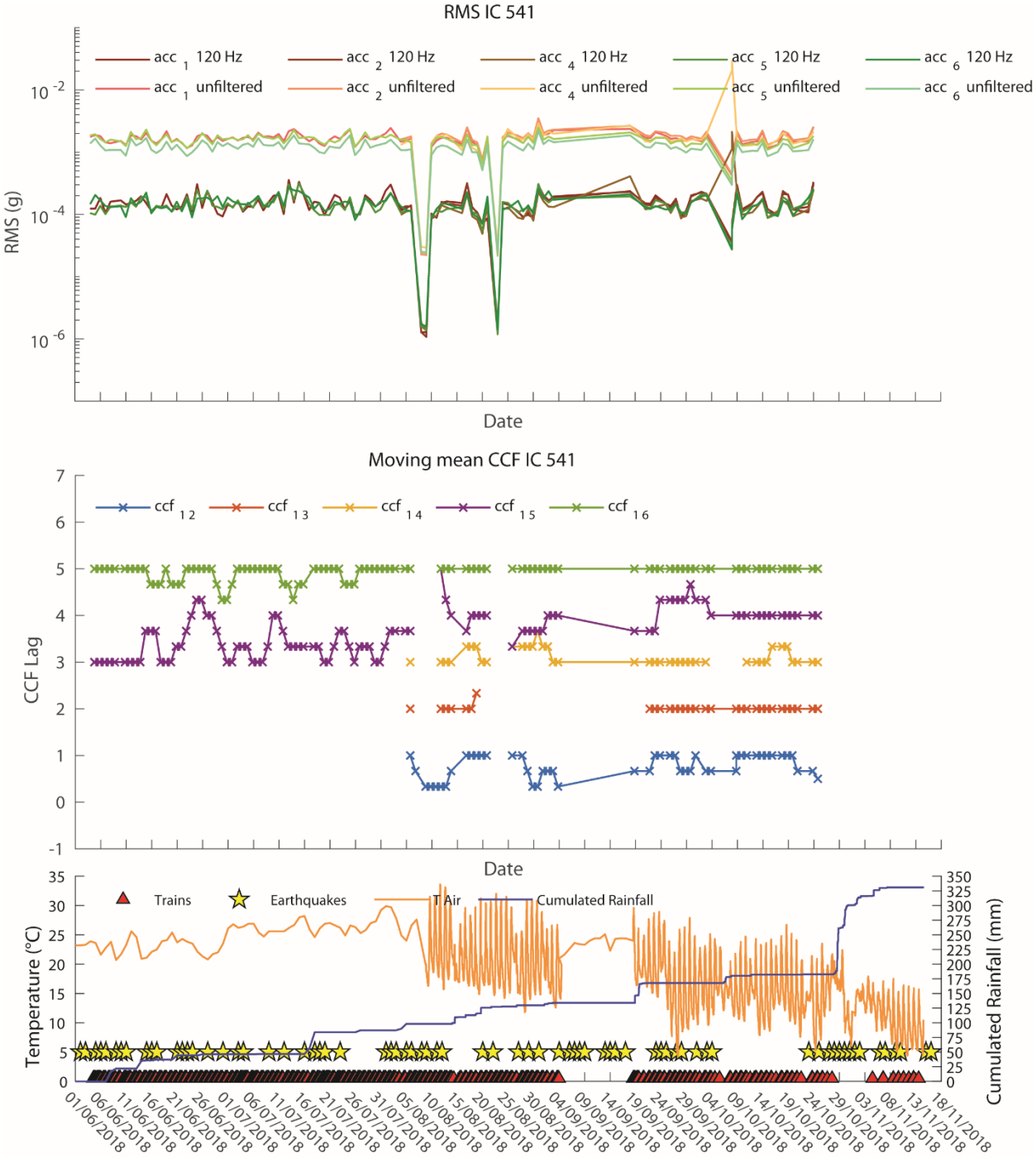

Figure 49: RMS and cross-correlation analysis relative to the passenger train IC 541.

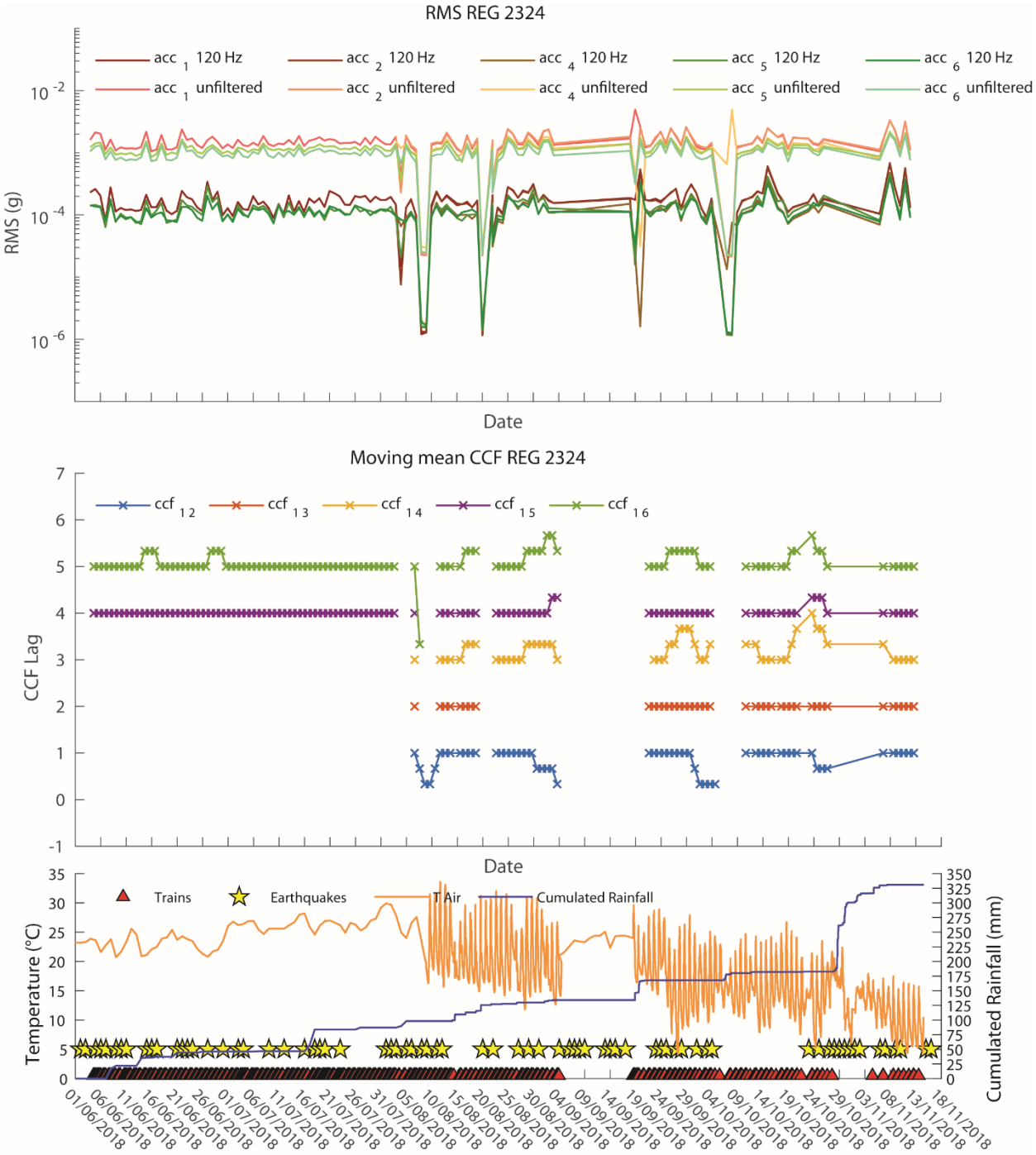

Figure 50: RMS and cross-correlation analysis relative to the passenger train REG 2324.

4.4 Results of Frequency Band Ambient Noise Disaggregation analysis

In this paragraph, the main results relative to the analysis of the ambient noise records are presented. In particular, the significant graphs relative to one accelerometer per each monitoring campaign are shown. The cumulative of the ambient noise filtered in six frequency bands (0.5 –

30, 30 – 50, 50 – 100, 100 – 250, 250 – 500, 500 – 1000 Hz) and averaged in time intervals of one minute, relative to one accelerometer per each monitoring campaign is shown in Figure 51. The graphs presented in Figure 51 are representative also for the other accelerometers deployed in the respective monitoring campaigns, as no relevant variations among the sensors were detected. The higher frequency band (500 – 1000 Hz) was the most energised one in all the monitoring campaigns, followed by the lower band (0.5 – 30 Hz) at the Acuto test site and by the 250 – 500 Hz band in the Terni test site. Even if the classes used were not equally spaced, and thus it is not possible to objectively comment the distribution of the bands, it is remarked the importance of the energisation relative to high-frequency intervals, which are linked to physical elements of about 4 to 8 meters. Moreover, the higher response of the 250 – 500 Hz frequency band at the Terni test site in respect to the Acuto quarry, may be related to the effect produced by the trains transit.

The derivative of the ambient noise, previously averaged in one-minute time intervals and filtered in the already introduced frequency bands, was compared with the external solicitations registered in both the test sites (Figure 52). In particular, the cross-correlation for each filtered band was performed in respect to rainfalls and the air and rock mass temperature for the Acuto test site and the rainfalls, air temperature and trains transit for the Terni test site (Figure 53).

Figure 52 shows the comparison of the derivative of the ambient noise filtered in the 0.5 – 30 Hz band with the rainfalls and the air and rock mass temperature for the Acuto test site and the rainfalls, air temperature and trains transit for the Terni test site. The cross-correlations relative to these comparisons are shown in Figure 53. From these figures, it is possible to note the close correlation of temperature data and of train passages with the ambient noise variations, while no significant correlation was found for the rainfalls.

From the cross-correlations performed for both the test sites on all the other frequency bands, resulted that by referring to temperature data, only the lower band (0.5 – 30 Hz) shows a simultaneous correlation (lag equal to 0), while no significant correlation exists for the other bands. No correlation was found with the rainfalls for any frequency bands, while the train passages are well correlated (lag equal to 1) for all the considered bands.

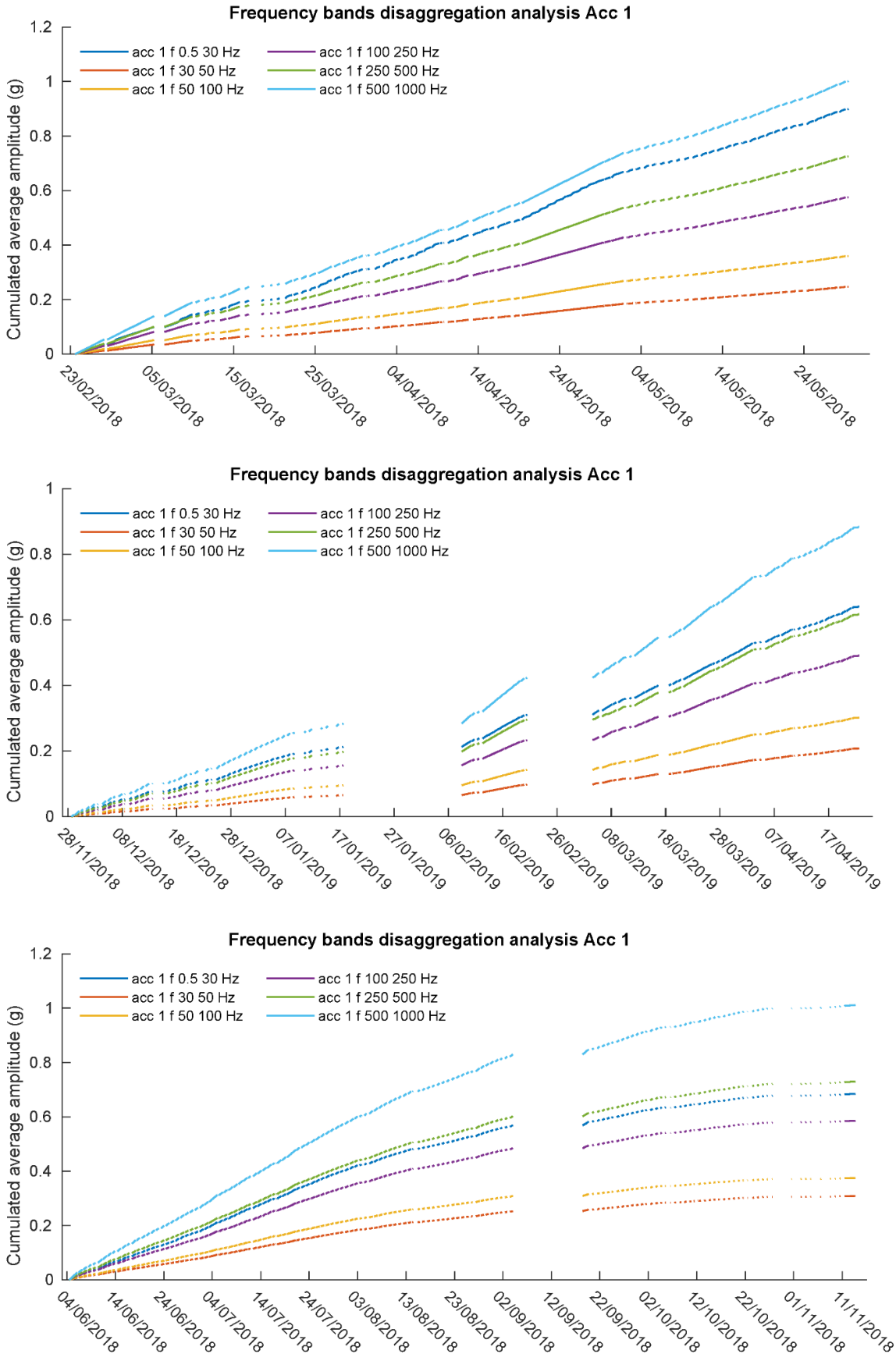

Figure 51: Cumulative of the ambient noise in six frequency bands relative to the accelerometer 1 for the monitoring campaigns of Acuto 2018 (top), Acuto 2019 (middle) and Terni 2018 (bottom).

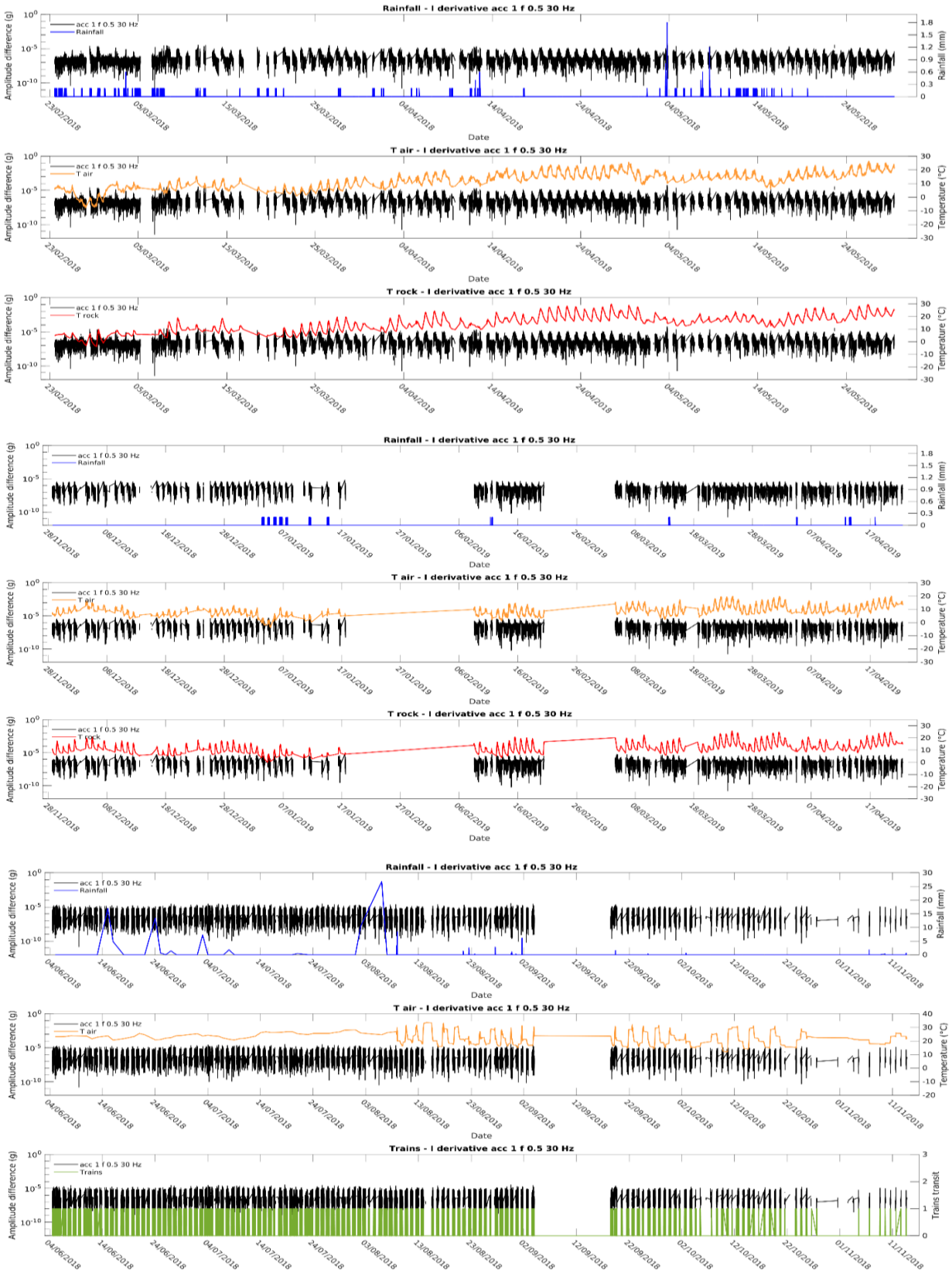

Figure 52: Derivative of the one-minute averaged ambient noise filtered between 0.5 and 30 Hz compared with rainfalls, air and rock mass temperature for the monitoring campaigns of Acuto 2018 (top) and Acuto 2019 (middle). For the Terni 2018 monitoring campaign (bottom) the correlation with train passages was computed replacing the unavailable rock mass temperature data. The ambient noise is relative to an accelerometer (ID 1) representative for each monitoring campaigns.

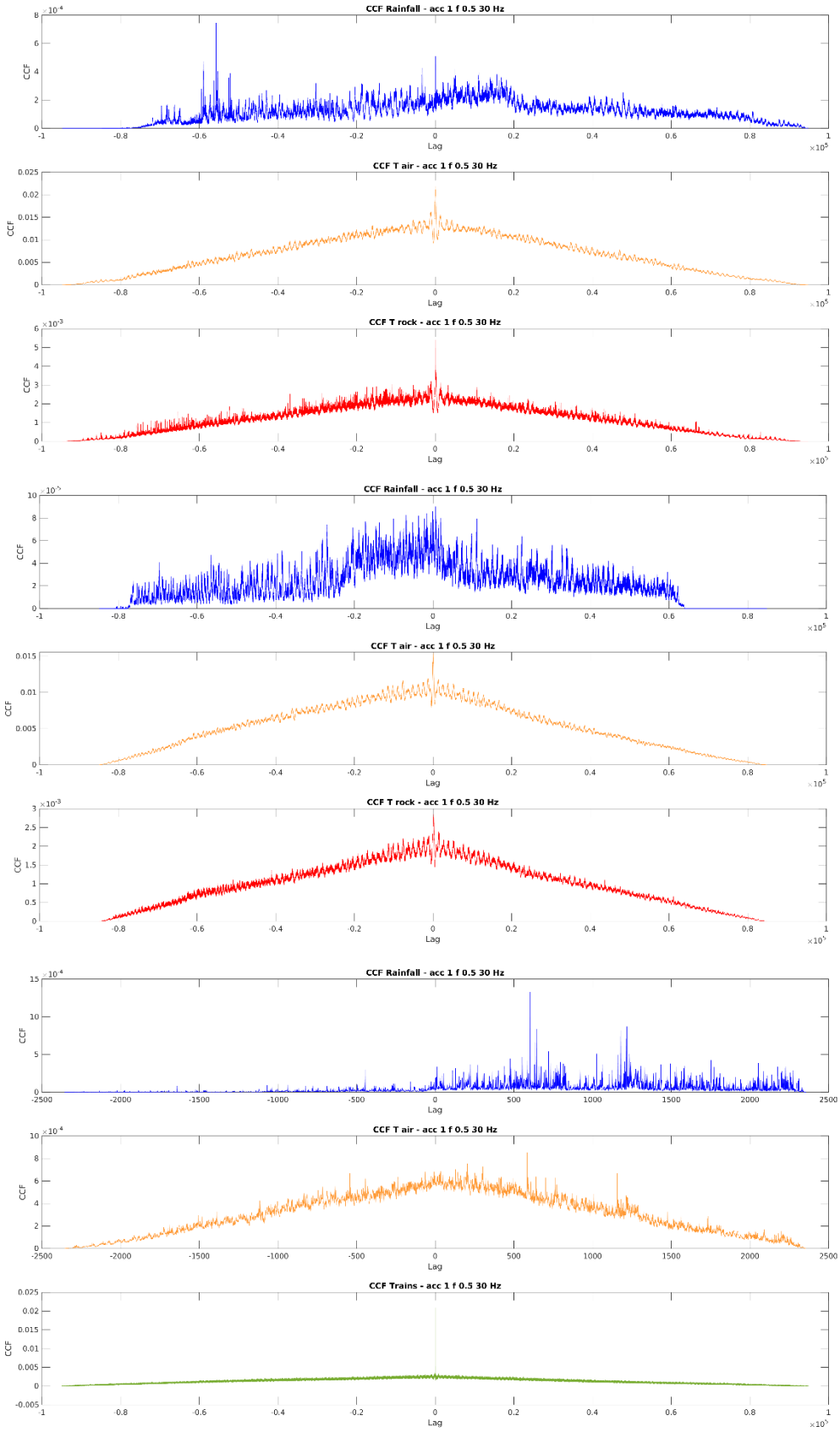

Figure 53: Cross-correlation between the derivative of the one-minute averaged ambient noise filtered between 0.5 and 30 Hz and the environmental parameters relative to the accelerometer 1 for the monitoring campaigns of Acuto 2018 (top), Acuto 2019 (middle) and Terni 2018 (bottom).

4.5 Synthesis of the results

In this section, the obtained results are briefly summarised and referred to the respective test site. In particular, Table 8 and Table 9 are referred to the analyses performed for the Acuto test site, while Table 10 and Table 11 reports the analyses carried out for the Terni-Giuncano railway test site.

Concerning both the test sites, the damping analysis did not show a permanent variation in the long-term trend of the damping, but significant variations related to transient processes have been detected. Moreover, considering that the anomalies are clustered in the coldest period, also cyclical variations related to temperature oscillations may have been observed, but only longer acquisition periods could confirm this hypothesis. Cyclical oscillations have been certainly observed in the ambient noise variations, which resulted closely correlated with temperature variations, especially in the lower frequency band considered (0.5 – 30 Hz).

Table 8: Synthesis of the analyses performed at the Acuto test site.

			Causes		**Observed effects**		
Technique	**Scope of the analysis**	**Aim of the analysis**	**Natural**	**Anthropic**	**Elastic**	**Inelastic**	**Type of cause/effect**
Damping analysis	Detection of rock mass damaging phenomena	Variation of the damping ratio of the microseismic emissions over time	✓ Rainfalls	✓ Impacts	✓	×	Transient
			✓ Temperature	×	(✓)	×	Cyclical
			✓ Creep	×	×	×	Continuous
F-BAND analysis	Correlation of ambient noise with environmental parameters	Variation of the energetic contribution at different frequency bands over time	✓ Rainfalls	✓ Impacts	✓	×	Transient
			✓ Temperature	×	✓	×	Cyclical
			✓ Creep	×	×	×	Continuous

Table 9: Synthesis of the correlations found between the ambient noise variations and the environmental parameters recorded at the Acuto test site.

	Frequency band (Hz)					
Parameter	0.5 - 30	30 - 50	50 - 100	100 - 250	250 - 500	500 - 1000
Rainfalls	×	×	×	×	×	×
Air temperature	✓	×	×	×	×	×
Rock mass temperature	✓	×	×	×	×	×

For the Terni-Giuncano railway test site, additional analyses were carried out on the train passages recordings, deriving the associated RMS and performing a cross-correlation between couples of sensors with the aim of inferring rock mass damage phenomena from the potential variations over time of these two parameters. Even in this case, although no long-term trend variations were observed, transient variations likely related to external factors were found. The identification of the causative factors was not possible and the discrimination of them is an open challenge for future studies.

Table 10: Synthesis of the analyses performed at the Terni-Giuncano railway test site.

			Causes		**Observed effects**		
Technique	**Scope of the analysis**	**Aim of the analysis**	**Natural**	**Anthropic**	**Elastic**	**Inelastic**	**Type of cause/effect**
Damping analysis	Detection of rock mass damaging phenomena	Variation of the damping ratio of the microseismic emissions over time	✓ Rainfalls	✓ Impacts	✓	×	Transient
			✓ Temperature	✓ Trains	(✓)	×	Cyclical
			✓ Creep	×	×	×	Continuous
F-BAND analysis	Correlation of ambient noise with environmental parameters	Variation of the energetic contribution at different frequency bands over time	✓ Rainfalls	✓ Impacts	✓	×	Transient
			✓ Temperature	✓ Trains	✓	×	Cyclical
			✓ Creep	×	×	×	Continuous
RMS analysis	Detection of rock mass damaging phenomena	Variation of the RMS parameter of the trains passages over time	✓ Rainfalls	✓ Impacts	✓	×	Transient
			✓ Temperature	✓ Trains	×	×	Cyclical
			✓ Creep	×	×	×	Continuous
Cross-correlation analysis	Detection of rock mass damaging phenomena	Variation of the CCF lag of the trains passages between couples of sensors over time	✓ Rainfalls	✓ Impacts	✓	×	Transient
			✓ Temperature	✓ Trains	×	×	Cyclical
			✓ Creep	×	×	×	Continuous

Table 11: Synthesis of the correlations found between the ambient noise variations the environmental parameters and the train passages recorded at the Terni-Giuncano railway test site.

	Frequency band (Hz)					
Parameter	0.5 - 30	30 - 50	50 - 100	100 - 250	250 - 500	500 - 1000
Rainfalls	×	×	×	×	×	×
Air temperature	✓	×	×	×	×	×
Train passages	✓	✓	✓	✓	✓	✓

5 Discussions

The novel damping analysis approach proposed in this PhD thesis aims at providing a further way for analysing the rock mass damaging phenomena occurring in jointed rock masses. The current state of art on the microseismic monitoring points out several information about the changes within the rock mass before instabilities events, as the shifting of the main resonance frequency and marked variations in the ambient seismic noise. Nevertheless, these effects are recordable only in the phases preceding the collapse event and are well visible when significant portions of the rock mass are involved. An analysis based on the amplitude/time domain may better reflect the development of damaging processes in the rock mass fracturation network.

In this sense, the here-presented approach was originally designed for the observation of long-time trend variations in the damping ratio associated with the microseismic events. These variations could be directly related to rock mass damaging phenomena, as the vibrations associated with microseismic emission might travel across a modified fractures network, which also influences the wave paths and their associated properties.

Although no long-term irreversible changes were observed, probably for the short time window considered, also the potentiality of this technique for the investigation of transient and cyclical modifications related to external solicitations was appraised. However, a direct correlation of the detected damping anomalies with the external causes, environmental (rainfalls, air and rock mass temperature, earthquakes) and anthropic ones (train passages) was not found. The identification of the causative factors of anomalous phenomena remains an open challenge for future applications and investigations.

The individuation of anomalies at specific frequencies can be also related to the characteristic dimensions of the solicited physical elements. In fact, the decomposition of the signal in monofrequential waveforms was needed to obtain simple sinusoids for the derivation of the damping; on the other hand, it is possible to relate the specific frequency investigated to the structural lineaments and three-dimensional energised masses.

It is clear that the type and the amount of signals inputted for the approach is crucial and might also have an influence on the final derivations. In fact, since the damping values were averaged in one-day intervals, a sufficient number of events should be accounted for the average, on the

contrary, the averaging window has to be enlarged. For each averaging interval, more than one sample should be taken into account, in order to evaluate the standard deviation associated with several measurements. It is worth to note that for some of the detected transient damping anomalies, no standard deviation is associated, which means that just one measurement is available for that interval. Although for many of the anomalies a marked difference in the damping is computed, the lack of further samples may negatively affect the assessment done.

A general outcome common to all the monitoring campaigns is the reduction of the damping ratio ξ with the increase of the monofrequential waveform considered, as shown in Figure 54. This not intuitive result seems to be in contrast with the typical behaviour of seismic waves, in which higher frequencies are commonly attenuated faster than the lower ones, which are able to travel on longer distances. However, the waves propagation through a medium is not only controlled by the damping but also by the geometrical spreading and the attenuation phenomena occurring along joints and high impedance interfaces within the studied medium.

A limitation of the method consists in the inapplicability on complex signals as those ones referred to train recordings. In fact, the coda waves generated after the passage of the last bogie of a train are characterised by many reflexions and refractions phenomena, resulting in a continuous rising and falling of the signal. Consequently, the identification of the last maximum peak associated with the vibration on which analyse the damping is a very complex task. Given the impossibility of deriving the damping associated with the trains recording, the RMS parameter was used for characterising the train induced vibration on the rock mass.

As the microseismic signals are typical of any natural and anthropic systems, being the simplest signals testifying the release of inelastic energy from a medium, the here-presented approach can be used for any other study devoted to the microseismic monitoring. Furthermore, investigations carried out on seismic datasets characterised by an higher resolution in frequency can provide information about the deformation of smaller elements within the rock mass, to which a more marked variation of the damping ratio might be associated.

Another possible application of this method consists in the analysis of yearly microseismic datasets collected on unstable rock slopes, which could show more visible variations in the damping ratio. A further conceivable usage of this method is the analysis of the monofrequential waveform that corresponds to the eigenfrequency for a rock column or a rock block: more

marked variations in the damping ratio associated with the microseismic emissions might be also found.

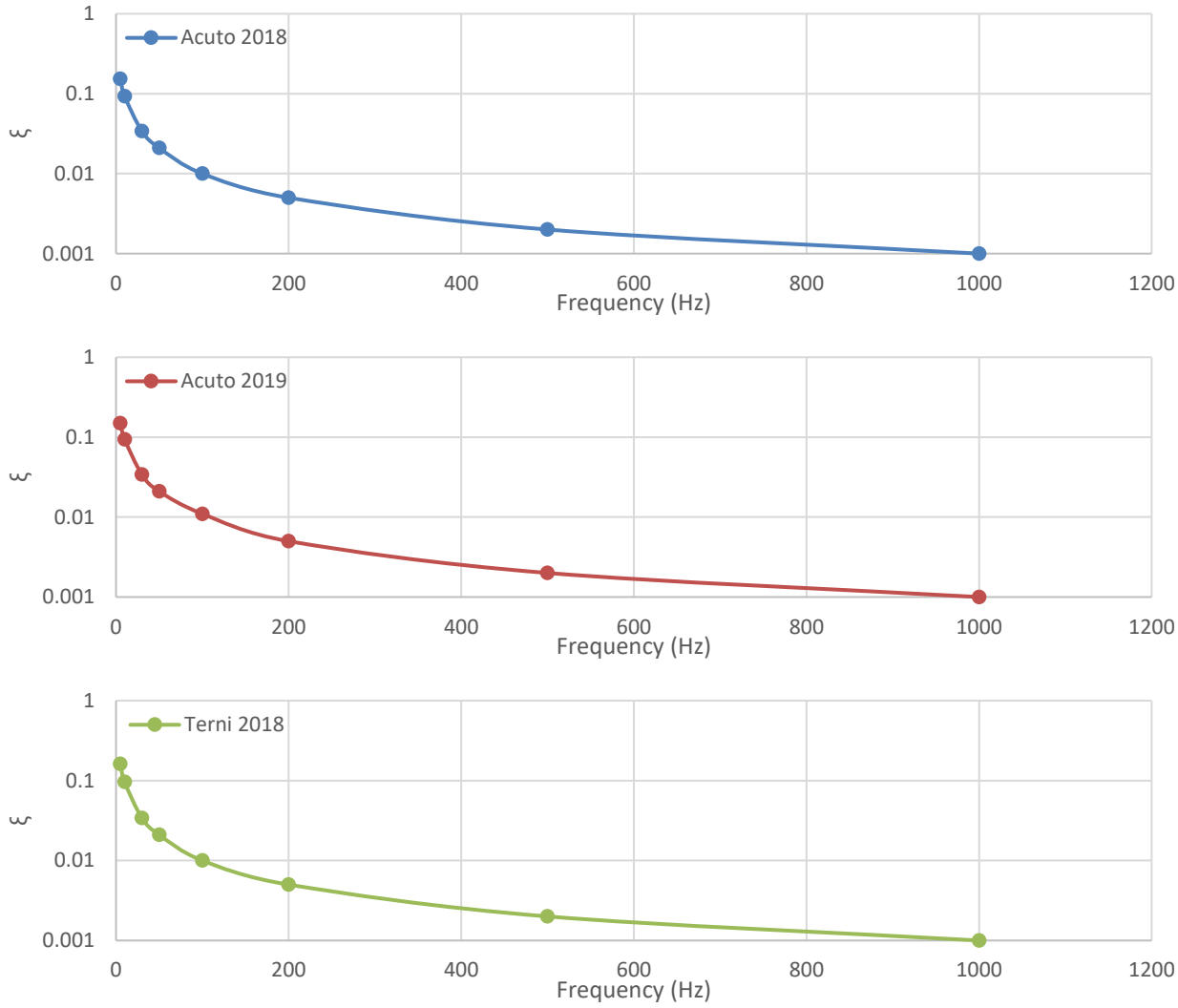

Figure 54: Average damping values as a function of the monofrequential waveforms analysed for the monitoring campaigns of Acuto 2018 (top), Acuto 2019 (middle) and Terni 2018 (bottom).

Some considerations are also made with respect to the additional analyses carried out for the transit of the trains, as well as the investigation on the seismic ambient noise.

The RMS and CCF analyses carried out on the trains transit recorded at the Terni-Giuncano railway test site were aimed at studying rock mass damaging phenomena through the observation of potential modification in the derived values of the two techniques. The flat trend of the RMS derived for each train typology testifies the unvaried long-term vibrational behaviour of the studied rock mass, thus confirming the same results obtained with the damping analysis

technique. Besides, the RMS series calculated on monofrequential waveforms show the same tendency of the unfiltered RMS but at lower energisation level.

The cross-correlation output strictly depends on the sampling frequency associated with the datasets used as inputs. In fact, the minimum lag detectable among the correlated time series corresponds to the reciprocal of the sampling frequency of the signals, which in this case correspond to 4.16×10^{-4} seconds. The results obtained from the cross-correlations executed on couples of sensors for the trains passages show an increment of a unity of lag for each interspace crossed, passing from a mean lag of 1 for the closest sensors (1 and 2) to a mean lag of 5 for the most distant accelerometers (1 and 6). Given the minimum spacing among the sensors and considering the high velocity of propagation of the seismic waves, an error in the accuracy of the obtained CCF lag has to be taken into account. In fact, with a higher sampling frequency would be possible to observe finer lag differences suitable for the detection of variations in the wave paths. However, the results obtained up to now, confirm an unvaried long term trend, with transient modification whose causes were not well identified, but that may lie in the accuracy error hypothesised, as the observed transient variations mostly oscillate between sequent lag values.

Considering the analysis of the ambient noise variations, the correlation with the environmental datasets showed a marked correlation only for the lower frequency interval considered (0.5 – 30 Hz). The reason for absence of correlation in other frequency bands is not very clear, but may be related to the growing width of the classes (i.e. more frequencies included in the bandpass filter): the superimposition of many different wavelengths may have produced a total response too much complex, very dissimilar from a sinusoidal signal and thus hard to relate to the temperature series by using the cross-correlation function. To verify this hypothesis, the frequency classes will be equally spaced, in order to attempt a novel cross-correlation with the thermal dataset and assess if a real difference in the response to temperature variations exist among the different frequencies intervals of the spectrum. By taking into account the rainfalls, it seems that they have a certain influence in provoking an increase of the microseismic emissions; on the other hand, they do not affect the ambient noise level, as the cross-correlation performed do not show a clear peak. Therefore, the temperature variations remain the main factor controlling the cyclical ambient noise variations, while impulsive modifications are connected to transient solicitations like the train transits.

In conclusion, since the damping analysis has been applied on monthly-long microseismic datasets, that might be not sufficiently extended to allow the occurrence of permanent variation in the rock mass structure, and thus observe modification also in the damping ratio, a future perspective consists in applying this approach to yearly-long microseismic datasets.

6 Conclusions

Rockfall hazard assessment is a main research theme in geosciences, given the high impact of these instabilities phenomena on the anthropic society, especially for the safeness of inhabited mountainous areas and transportation routes. Nowadays, the microseismic monitoring of rock masses is an affirmed tool suitable for providing quantitative information on the rock mass damaging processes (i.e. formation of new fractures and extension of the pre-existing ones) acting within the rock mass and associated with microseismic emissions.

In this PhD thesis, a novel approach for the analysis of the microseismic signals registered on rock masses is presented and discussed. With the aim of evaluating the rock mass damaging processes, the damping ratios associated with the microseismic emissions were derived. Three microseismic monitoring campaigns were conducted in two test sites located in central Italy: a) the Acuto quarry test site, where the vibrational behaviour of a 12 m^3 rock block partially detached from the back rock wall has been investigated; b) the Terni-Giuncano railway test site, where a rock mass close to a railway was studied to analyse the effects produced by the repeated trains transit. The microseismic datasets, acquired by means of 6 one-component accelerometers, have been acquired in continuous mode with a sampling frequency of 2400 Hz. A STA/LTA event detection algorithm has been implemented for the recognition of the microseismic events occurred and a procedure for the analysis of the characteristic damping of the signals filtered in monofrequential waveforms has been coded. The daily mean damping values for each frequency were compared with respect to the environmental parameters monitored on site. Even if no irreversible trend variations were noted, several anomalies referable to transient or cyclic forcing were remarked. Limitations and potentialities of the approach are discussed.

Furthermore, the train transits at the Terni test site were analysed by means of two techniques conceived as suitable for showing potential variations in the vibrational behaviour of the rock mass monitored linkable to fracturation phenomena. Each train transit was analysed in terms of: a) RMS value of the recording; b) cross-correlation between couples of sensors. The observation of the RMS and cross-correlation series over time confirmed the unvaried long-term vibrational behaviour of the rock mass, in agreement with the results of the damping analysis.

In addition to the studies carried out on the microseismic signals, also the seismic noise was investigated. The seismic recordings were filtered in specific frequency bands in order to observe the most energised part of the frequency spectrum and then averaged in time intervals of one minute. The cumulative of these values allowed to determine the main energised frequency band, which resulted to be the one comprised between 500 and 1000 Hz. The derivative of the averaged noise was compared with the environmental parameters recorded in the two test sites. A marked correlation between the variation of air and rock mass temperature and the derivative of the noise in the frequency band comprised between 0.5 and 30 Hz was noted, while the correlation is feeble or lost for the other frequency bands considered. The correlation observed between thermal cycles and ambient noise variations is in agreement with previous bibliographical studies; moreover, a differentiation in the vibrational response for the different frequency bands has been detected.

References

Abellán, A., Calvet, J., Vilaplana, J.M. & Blanchard, J. (2010) Detection and spatial prediction of rockfalls by means of terrestrial laser scanner monitoring. *Geomorphology*, **119**, 162–171, Elsevier B.V. doi:10.1016/j.geomorph.2010.03.016

Abellán, A., Oppikofer, T., Jaboyedoff, M., Rosser, N.J., Lim, M. & Lato, M.J. (2014) Terrestrial laser scanning of rock slope instabilities. *Earth Surf. Process. Landforms*, **39**, 80–97. doi:10.1002/esp.3493

Accordi, G., Carbone, F., Civitelli, G., Corda, L., Rita, D. De, Esu, D., Funiciello, R., *et al.* (1986) Lithofacies map of Latium-Abruzzi and neighbouring areas, scale 1: 250000. *Progett. Final. Geodin. Cons. Naz. Riverche Italy, Roma*.

Akdag, S., Karakus, M., Taheri, A., Nguyen, G. & Manchao, H. (2018) Effects of Thermal Damage on Strain Burst Mechanism for Brittle Rocks Under True-Triaxial Loading Conditions. *Rock Mech. Rock Eng.*, **51**, 1657–1682, Springer Vienna. doi:10.1007/s00603-018-1415-3

Amitrano, D. (2003) Brittle-ductile transition and associated seismicity: Experimental and numerical studies and relationship with the b value. *J. Geophys. Res. Solid Earth*, **108**, 1–15. doi:10.1029/2001jb000680

Amitrano, D. & Helmstetter, A. (2006) Brittle creep , damage , and time to failure in rocks. *J. Geophys. Res.*, **111**, 1–17. doi:10.1029/2005JB004252

Arosio, D., Longoni, L., Papini, M., Boccolari, M. & Zanzi, L. (2018) Analysis of microseismic signals collected on an unstable rock face in the Italian Prealps. *Geophys. J. Int.*, **213**, 475–488. doi:10.1093/gji/ggy010

ASTM. (2005) Standard Test Method for Laboratory Determination of Pulse Velocities and Ultrasonic Elastic Constants of Rock. *Astm*, **i**, 5–11. doi:10.1520/D2845-08.2

ASTM. (2006) Standard test methods for specific gravity of soil solids by water pycnometer. *ASTM*, **4**.

ASTM. (2008) Standard test method for determination of the Point Load Strength Index of rock and application to rock strength classifications. *ASTM*, **4**.

Azarov, A. & Serdyukov, A. (2019) Locating harmonic microseismic sources using phases of signals and spectral transformations. *IOP Conf. Ser. Earth Environ. Sci.*, **262**, 012004. doi:10.1088/1755-1315/262/1/012004

Bakun-Mazor, D., Hatzor, Y.H., Glaser, S.D. & Carlos Santamarina, J. (2013) Thermally vs. seismically induced block displacements in Masada rock slopes. *Int. J. Rock Mech. Min. Sci.*, **61**, 196–211, Elsevier. doi:10.1016/j.ijrmms.2013.03.005

Bard, P.Y., Cadet, H., Endrun, B., Hobiger, M., Renalier, F., Theodulidis, N., Ohrnberger, M., *et al.* (2010) From Non-invasive Site Characterization to Site Amplification: Recent Advances in the Use of Ambient Vibration Measurements. *Geotech. Geol. Earthq. Eng.*, **17**, 105–123. doi:10.1007/978-90-481-9544-2_5

Barla, G., Antolini, F., Barla, M., Mensi, E. & Piovano, G. (2010) Monitoring of the Beauregard landslide (Aosta Valley, Italy) using advanced and conventional techniques. *Eng. Geol.*, **116**, 218–235, Elsevier B.V. doi:10.1016/j.enggeo.2010.09.004

Barton, N. & Choubey, V. (1977) The shear strength of rock joints in theory and practice. *Rock Mech.*, **10**, 1–54. doi:10.1007/BF01261801

Bonnefoy-Claudet, S., Cotton, F. & Bard, P.Y. (2006) The nature of noise wavefield and its applications for site effects studies. A literature review. *Earth-Science Rev.*, **79**, 205–227. doi:10.1016/j.earscirev.2006.07.004

Bottelin, P., Jongmans, D., Baillet, L., Lebourg, T., Hantz, D., Levy, C., Roux, O. Le, *et al.* (2013) Spectral Analysis of Prone-to-fall Rock Compartments using Ambient Vibrations. *J. Environ. Eng. Geophys.*, **18**, 205–217. doi:10.2113/jeeg18.4.205

Bottelin, P., Lévy, C., Baillet, L., Jongmans, D. & Guéguen, P. (2013) Modal and thermal analysis of les arches unstable rock column (vercors massif, french alps). *Geophys. J. Int.*, **194**, 849–858. doi:10.1093/gji/ggt046

Bozzano, F., Cipriani, I., Esposito, C., Martino, S., Mazzanti, P., Prestininzi, A., Rocca, A.P., *et al.* (2013) Landslide risk reduction by coupling monitoring and numerical modeling. *Ital. J. Eng. Geol. Environ.*, **2013**, 315–322. doi:10.4408/IJEGE.2013-06.B-29

Brantut, N., Heap, M.J., Meredith, P.G. & Baud, P. (2013) Time-dependent cracking and brittle creep in crustal rocks: A review. *J. Struct. Geol.*, **52**, 17–43, Elsevier Ltd. doi:10.1016/j.jsg.2013.03.007

Bretschneider, A., Genevois, R., Martino, S., Prestininzi, A. & Verbena, G. (2013) A physically-based scale approach to the analysis of the creep process involving Mt. Granieri (Southern Italy). *Ital. J. Eng. Geol. Environ.*, 123–132. doi:10.4408/IJEGE.2013-06.B-09

Brückl, E. & Parotidis, M. (2005) Prediction of slope instabilities due to deep-seated gravitational creep. *Nat. Hazards Earth Syst. Sci.*, **5**, 155–172. doi:10.5194/nhess-5-155-2005

Bruni, F., Calamita, F., Maranci, M. & Pierantoni, P.P. (1995) Il controllo della tettonica giurassica sulla strutturazione neogenica dei Monti Martani meridionali (Preappennino umbro). *Stud. Geol. Camerti*, **Volume Spe**, 121–135, Università di Camerino.

Budetta, P. (2004) Assessment of rockfall risk along roads. *Nat. Hazards Earth Syst. Sci.*, **4**, 71–81.

Burjánek, J., Gassner-Stamm, G., Poggi, V., Moore, J.R. & Fäh, D. (2010) Ambient vibration analysis of an unstable mountain slope. *Geophys. J. Int.*, **180**, 820–828. doi:10.1111/j.1365-246X.2009.04451.x

Cai, M., Kaiser, P.K., Morioka, H., Minami, M., Maejima, T., Tasaka, Y. & Kurose, H. (2007) FLAC/PFC coupled numerical simulation of AE in large-scale underground excavations. *Int. J. Rock Mech. Min. Sci.*, **44**, 550–564. doi:10.1016/j.ijrmms.2006.09.013

Cai, M., Kaiser, P.K., Tasaka, Y., Maejima, T., Morioka, H. & Minami, M. (2004) Generalized crack initiation and crack

damage stress thresholds of brittle rock masses near underground excavations. *Int. J. Rock Mech. Min. Sci.*, **41**, 833–847. doi:10.1016/j.ijrmms.2004.02.001

Calamita, F. & Pierantoni, P.P. (1994) Structural setting of the southern Martani Mountains (Umbrian Apennines: Central Italy). *Mem. della Soc. Geol. Ital.*, **48**, 549–557.

Cao, P., Liu, T., Pu, C. & Lin, H. (2015) Crack propagation and coalescence of brittle rock-like specimens with pre-existing cracks in compression. *Eng. Geol.*, **187**, 113–121, Elsevier B.V. doi:10.1016/j.enggeo.2014.12.010

Cardinali, M., Reichenbach, P., Guzzetti, F., Ardizzone, F., Antonini, G., Cacciano, M., Castellani, M., *et al.* (2002) A geomorphological approach to the estimation of landslide hazards and risks in Umbria , Central Italy To cite this version : System Sciences A geomorphological approach to the estimation of landslide hazards and risks in Umbria , Central Italy. *Nat. Hazards Earth Syst. Sci.*, 57–72.

Carlà, T., Farina, P., Intrieri, E., Botsialas, K. & Casagli, N. (2017) On the monitoring and early-warning of brittle slope failures in hard rock masses: Examples from an open-pit mine. *Eng. Geol.*, **228**, 71–81, Elsevier. doi:10.1016/j.enggeo.2017.08.007

Che, A., Yang, H., Wang, B. & Ge, X. (2016) Wave propagations through jointed rock masses and their effects on the stability of slopes. *Eng. Geol.*, **201**, 45–56, Elsevier B.V. doi:10.1016/j.enggeo.2015.12.018

Chen, Y. (2018) Automatic microseismic event picking via unsupervised machine learning. *Geophys. J. Int.*, **212**, 88–102. doi:10.1093/gji/ggx420

Collins, B.D. & Stock, G.M. (2016) Rockfall triggering by cyclic thermal stressing of exfoliation fractures. *Nat. Geosci.*, **9**, 395–400. doi:10.1038/ngeo2686

Colombero, C., Baillet, L., Comina, C., Jongmans, D., Larose, E., Valentin, J. & Vinciguerra, S. (2018) Integration of ambient seismic noise monitoring, displacement and meteorological measurements to infer the temperature-controlled long-term evolution of a complex prone-to-fall cliff. *Geophys. J. Int.*, **213**, 1876–1897. doi:10.1093/gji/ggy090

Colombero, C., Comina, C., Vinciguerra, S. & Benson, P.M. (2018) Microseismicity of an Unstable Rock Mass: From Field Monitoring to Laboratory Testing. *J. Geophys. Res. Solid Earth*, **123**, 1673–1693. doi:10.1002/2017JB014612

Dai, F., Li, B., Xu, N., Fan, Y. & Zhang, C. (2016) Deformation forecasting and stability analysis of large-scale underground powerhouse caverns from microseismic monitoring. *Int. J. Rock Mech. Min. Sci.*, **86**, 269–281, Elsevier. doi:10.1016/j.ijrmms.2016.05.001

Dietze, M., Turowski, J.M., Cook, K.L. & Hovius, N. (2017) Spatiotemporal patterns, triggers and anatomies of seismically detected rockfalls. *Earth Surf. Dyn.*, **5**, 757–779. doi:10.5194/esurf-5-757-2017

Dong, L., Zou, W., Li, X., Shu, W. & Wang, Z. (2019) Collaborative localization method using analytical and iterative solutions for microseismic/acoustic emission sources in the rockmass structure for underground mining. *Eng.*

Fract. Mech., **210**, 95–112, Elsevier. doi:10.1016/j.engfracmech.2018.01.032

Eberhardt, E., Stead, D. & Coggan, J.S. (2004) Numerical analysis of initiation and progressive failure in natural rock slopes-the 1991 Randa rockslide. *Int. J. Rock Mech. Min. Sci.*, **41**, 69–87. doi:10.1016/S1365-1609(03)00076-5

Fanti, R., Gigli, G., Lombardi, L., Tapete, D. & Canuti, P. (2013) Terrestrial laser scanning for rockfall stability analysis in the cultural heritage site of Pitigliano (Italy). *Landslides*, **10**, 409–420. doi:10.1007/s10346-012-0329-5

Fantini, A., Fiorucci, M. & Martino, S. (2017) Rock Falls Impacting Railway Tracks: Detection Analysis through an Artificial Intelligence Camera Prototype. *Wirel. Commun. Mob. Comput.*, **2017**, 1–11. doi:10.1155/2017/9386928

Fantini, A., Fiorucci, M., Martino, S., Marino, L., Napoli, G., Prestininzi, A., Salvetti, O., *et al.* (2016) Multi-sensor system designed for monitoring rock falls: the experimental test-site of Acuto (Italy). *Rend. Online Soc. Geol. Ital.*, **41**, 147–150, SOC GEOLOGICA ITALIANA UNIV DEGLI STUDI LA SAPIENZA, DIPART SCI DELLA TERRA ….

Fantini, A., Fiorucci, M., Martino, S. & Paciello, A. (2017) Investigating Rock Mass Failure Precursors Using a Multi-sensor Monitoring System: Preliminary Results from a Test-Site (Acuto, Italy). *Procedia Eng.*, **191**, 188–195, The Author(s). doi:10.1016/j.proeng.2017.05.171

Ferlisi, S., Cascini, L., Corominas, J. & Matano, F. (2012) Rockfall risk assessment to persons travelling in vehicles along a road: The case study of the Amalfi coastal road (southern Italy). *Nat. Hazards*, **62**, 691–721. doi:10.1007/s11069-012-0102-z

Fiorucci, M. (2018) *Approaches of data analysis from multi-parametric monitoring system for landslide risk management.*, Sapienza University of Rome (Italy).

Fiorucci, M., Marmoni, G.M., Martino, S. & Mazzanti, P. (2018) Thermal response of jointed rock masses inferred from infrared thermographic surveying (Acuto test-site, italy). *Sensors (Switzerland)*, **18**. doi:10.3390/s18072221

Fourmaintraux, D. (1975) Quantification des discontinuités des roches et des massifs rocheux. *Rock Mech. Felsmechanik Mec. des Roches*, **7**, 83–100. doi:10.1007/BF01351903

Froude, M.J. & Petley, D.N. (2018) Global fatal landslides 2004 to 2016. *Nat. Hazards Earth Syst. Sci.*, **18**, 2161–2181.

Galea, P., D'Amico, S. & Farrugia, D. (2014) Dynamic characteristics of an active coastal spreading area using ambient noise measurements-Anchor Bay, Malta. *Geophys. J. Int.*, **199**, 1166–1175. doi:10.1093/gji/ggu318

Galli, M. & Guzzetti, F. (2007) Landslide vulnerability criteria: A case study from Umbria, central Italy. *Environ. Manage.*, **40**, 649–664. doi:10.1007/s00267-006-0325-4

Gigli, G., Morelli, S., Fornera, S. & Casagli, N. (2014) Terrestrial laser scanner and geomechanical surveys for the rapid evaluation of rock fall susceptibility scenarios. *Landslides*, **11**, 1–14. doi:10.1007/s10346-012-0374-0

Gischig, V., Moore, J.R., Gischig, V., Amann, F. & Hunziker, M. (2012) Earthquake-triggered rock slope failures:

Damage and site effects.

Godio, A., Strobbia, C. & Bacco, G. De. (2006) Geophysical characterisation of a rockslide in an alpine region. *Eng. Geol.*, **83**, 273–286. doi:10.1016/j.enggeo.2005.06.034

Goldstein, P., Dodge, D., Firpo, M. & Minner, L. (2003) SAC2000: Signal processing and analysis tools for seismologists and engineers. *IASPEI Int. Handb. Earthq. Eng. Seismol.* eds. WHK Lee, Kanamori, H., Jennings, P.C. & Kisslinger, C., Academic Press, London.

Goldstein, P. & Snoke, A. (2005) SAC Availability for the IRIS Community. *Inc. Institutions Seismol. Data Manag. Cent. Electron. Newsl.*

Got, J.L., Mourot, P. & Grangeon, J. (2010) Pre-failure behaviour of an unstable limestone cliff from displacement and seismic data. *Nat. Hazards Earth Syst. Sci.*, **10**, 819–829. doi:10.5194/nhess-10-819-2010

Gottardi, G., Govoni, L., Mentani, A. & Ranalli, M. (2011) The effectiveness of protection systems toward rockfall risk mitigation, 157–164.

Grøneng, G., Lu, M., Nilsen, B. & Jenssen, A.K. (2010) Modelling of time-dependent behavior of the basal sliding surface of the Åknes rockslide area in western Norway. *Eng. Geol.*, **114**, 414–422, Elsevier B.V. doi:10.1016/j.enggeo.2010.05.017

Gunzburger, Y., Merrien-Soukatchoff, V. & Guglielmi, Y. (2005) Influence of daily surface temperature fluctuations on rock slope stability: Case study of the Rochers de Valabres slope (France). *Int. J. Rock Mech. Min. Sci.*, **42**, 331–349. doi:10.1016/j.ijrmms.2004.11.003

Guzzetti, F., Reichenbach, P., Cardinali, M., Ardizzone, F. & Galli, M. (2003) The impact of landslides in the Umbria region, central Italy. *Nat. Hazards Earth Syst. Sci.*, **3**, 469–486. doi:10.5194/nhess-3-469-2003

Guzzetti, F, Cardinali, M., Reichenbach, P., Galli, M., Ardizzone, F. & Salvati, P. (2004) Geomorphological mapping to assess landslide risk: examples from the Umbria Region, Central Italy. *Proc. 2004 Int. Conf. Slopel. Disaster Mitig.*

Guzzetti, Fausto. (2000) Landslide fatalities and the evaluation of landslide risk in Italy. *Eng. Geol.*, **58**, 89–107. doi:10.1016/S0013-7952(00)00047-8

Guzzetti, Fausto, Reichenbach, P. & Ghigi, S. (2004) Rockfall hazard and risk assessment along a transportation corridor in the Nera valley, central Italy. *Environ. Manage.*, **34**, 191–208. doi:10.1007/s00267-003-0021-6

Hakes, C., Fiorucci, M., Iannucci, R., Martino, S. & Paciello, A. (2018) Nanoseismic Monitoring for Detection of Rockfalls: Experiments in Quarry Areas Extended Abstract. *Ital. J. Eng. Geol. Environ.*, 1. doi:10.4408/IJEGE.2018-01.O-03

Hao, H., Wu, Y., Ma, G. & Zhou, Y. (2001) Characteristics of surface ground motions induced by blast in jointed rock mass. *Soil Dyn. Earthq. Eng.*, **21**, 85–98. doi:10.1016/S0267-7261(00)00104-4

Heap, M.J., Vinciguerra, S. & Meredith, P.G. (2009) The evolution of elastic moduli with increasing crack damage during cyclic stressing of a basalt from Mt. Etna volcano. *Tectonophysics*, **471**, 153–160, Elsevier B.V. doi:10.1016/j.tecto.2008.10.004

Helmstetter, A. & Garambois, S. (2010) Seismic monitoring of Schilienne rockslide (French Alps): Analysis of seismic signals and their correlation with rainfalls. *J. Geophys. Res. Earth Surf.*, **115**, 1–15. doi:10.1029/2009JF001532

Hoek, E. & Martin, C.D. (2014) Fracture initiation and propagation in intact rock - A review. *J. Rock Mech. Geotech. Eng.*, Elsevier Ltd. doi:10.1016/j.jrmge.2014.06.001

Hussain, Y., Martinez-Carvajal, H., Condori, C., Uagoda, R., Cárdenas-Soto, M., Cavalcante, A.L.B., Cunha, L.S. da, *et al.* (2019) Ambient Seismic Noise: A Continuous Source for the Dynamic Monitoring of Landslides. *Terrae Didat.*, **15**, 1–5. doi:10.20396/td.v15i1.8652455

ISRM. (1978) Suggested methods for the quantitative description of discontinuities in rock masses. *ISRM, Int. J. Rock Mech. Min. Sci. Geomech. Abstr.*, **15**, 319–368.

ISRM. (1979) Suggested methods for determining water content, porosity, density absorption and related properties and swelling and slake- durability index properties. *Int. J. Rock Mech. Min. Sci.*, **16**, 141–156.

Jongmans, D. & Garambois, S. (2007) Geophysical investigation of landslides: A review. *Bull. la Soc. Geol. Fr.*, **178**, 101–112. doi:10.2113/gssgfbull.178.2.101

Joswig, M. (2008) Nanoseismic monitoring fills the gap between microseismic networks and passive seismic. *First Break*, **26**, 121–128.

Kinali, M., Pytharouli, S., Lunn, R.J., Shipton, Z.K., Stillings, M., Lord, R. & Thompson, S. (2018) Detection of weak seismic signals in noisy environments from unfiltered, continuous passive seismic recordings. *Bull. Seismol. Soc. Am.*, **108**, 2993–3004. doi:10.1785/0120170358

Kirschbaum, D., Stanley, T. & Zhou, Y. (2015) Spatial and temporal analysis of a global landslide catalog. *Geomorphology*, **249**, 4–15, Elsevier B.V. doi:10.1016/j.geomorph.2015.03.016

Kirschbaum, D.B., Adler, R., Hong, Y., Hill, S. & Lerner-Lam, A. (2010) A global landslide catalog for hazard applications: Method, results, and limitations. *Nat. Hazards*, **52**, 561–575. doi:10.1007/s11069-009-9401-4

Klein, E., Nadim, C., Bigarré, P. & Dünner, C. (2008) Global monitoring strategy applied to ground failure hazards. *10th Int. Symp. Landslides Eng. Slopes*, Xi'an - Chine.

Kleinbrod, U., Burjánek, J. & Fäh, D. (2019) Ambient vibration classification of unstable rock slopes: A systematic approach. *Eng. Geol.*, **249**, 198–217. doi:10.1016/j.enggeo.2018.12.012

Koukouvelas, I., Litoseliti, A., Nikolakopoulos, K. & Zygouri, V. (2015) Earthquake triggered rock falls and their role in the development of a rock slope: The case of Skolis Mountain, Greece. *Eng. Geol.*, **191**, 71–85, Elsevier B.V. doi:10.1016/j.enggeo.2015.03.011

Kranz, R.L. (1983) Microcracks in rocks: A review. *Tectonophysics*. doi:10.1016/0040-1951(83)90198-1

Lacerda, W., Ehrlich, M., Fontoura, S., Sayão, A., Willenberg, H., Evans, K., Eberhardt, E., *et al.* (2004) Geological, geophysical and geotechnical investigations into the internal structure and kinematics of an unstable, complex sliding mass in crystalline rock. *Landslides Eval. Stab. Terrain Eval. Stabilisation, Set 2 Vol.*, 489–494. doi:10.1201/b16816-69

Lacroix, P. & Amitrano, D. (2013) Long-term dynamics of rockslides and damage propagation inferred from mechanical modeling. *J. Geophys. Res. Earth Surf.*, **118**, 2292–2307. doi:10.1002/2013JF002766

Lan, H., Martin, C.D. & Andersson, J.C. (2013) Evolution of in situ rock mass damage induced by mechanical-thermal loading. *Rock Mech. Rock Eng.*, **46**, 153–168. doi:10.1007/s00603-012-0248-8

Larose, E., Carrière, S., Voisin, C., Bottelin, P., Baillet, L., Guéguen, P., Walter, F., *et al.* (2015) Environmental seismology: What can we learn on earth surface processes with ambient noise? *J. Appl. Geophys.*, **116**, 62–74. doi:10.1016/j.jappgeo.2015.02.001

Lee, M., Byun, J., Kim, D., Choi, J. & Kim, M. (2017) Improved modified energy ratio method using a multi-window approach for accurate arrival picking. *J. Appl. Geophys.*, **139**, 117–130, Elsevier B.V. doi:10.1016/j.jappgeo.2017.02.019

Lévy, C., Baillet, L., Jongmans, D., Mourot, P. & Hantz, D. (2010) Dynamic response of the Chamousset rock column (Western Alps, France). *J. Geophys. Res. Earth Surf.*, **115**, 1–13. doi:10.1029/2009JF001606

Levy, C., Jongmans, D. & Baillet, L. (2011) Analysis of seismic signals recorded on a prone-to-fall rock column (Vercors massif, French Alps). *Geophys. J. Int.*, **186**, 296–310. doi:10.1111/j.1365-246X.2011.05046.x

Li, J., Ma, G. & Huang, X. (2010) Analysis of wave propagation through a filled rock joint. *Rock Mech. Rock Eng.*, **43**, 789–798. doi:10.1007/s00603-009-0033-5

Li, X., Shang, X., Wang, Z., Dong, L. & Weng, L. (2016) Identifying P-phase arrivals with noise: An improved Kurtosis method based on DWT and STA/LTA. *J. Appl. Geophys.*, **133**, 50–61, Elsevier B.V. doi:10.1016/j.jappgeo.2016.07.022

Lin, B., Wei, X. & Junjie, Z. (2019) Automatic recognition and classification of multi-channel microseismic waveform based on DCNN and SVM. *Comput. Geosci.*, **123**, 111–120, Elsevier Ltd. doi:10.1016/j.cageo.2018.10.008

Lisjak, A. & Grasselli, G. (2014) A review of discrete modeling techniques for fracturing processes in discontinuous rock masses. *J. Rock Mech. Geotech. Eng.*, Elsevier Ltd. doi:10.1016/j.jrmge.2013.12.007

Liu, F., Ma, T., Tang, C. & Chen, F. (2018) Prediction of rockburst in tunnels at the Jinping II hydropower station using microseismic monitoring technique. *Tunn. Undergr. Sp. Technol.*, **81**, 480–493, Elsevier. doi:10.1016/j.tust.2018.08.010

Liu, X., Tang, C., Li, L., Lv, P. & Sun, R. (2018) Microseismic monitoring and stability analysis of the right bank slope at

Dagangshan hydropower station after the initial impoundment. *Int. J. Rock Mech. Min. Sci.*, **108**, 128–141, Elsevier Ltd. doi:10.1016/j.ijrmms.2018.06.012

Loew, S., Gschwind, S., Gischig, V., Keller-Signer, A. & Valenti, G. (2017) Monitoring and early warning of the 2012 Preonzo catastrophic rockslope failure. *Landslides*, **14**, 141–154, Landslides. doi:10.1007/s10346-016-0701-y

Lu, C.P., Dou, L.M., Zhang, N., Xue, J.H., Wang, X.N., Liu, H. & Zhang, J.W. (2013) Microseismic frequency-spectrum evolutionary rule of rockburst triggered by roof fall. *Int. J. Rock Mech. Min. Sci.*, **64**, 6–16, Elsevier. doi:10.1016/j.ijrmms.2013.08.022

Ma, K., Tang, C.A., Liang, Z.Z., Zhuang, D.Y. & Zhang, Q.B. (2017) Stability analysis and reinforcement evaluation of high-steep rock slope by microseismic monitoring. *Eng. Geol.*, **218**, 22–38. doi:10.1016/j.enggeo.2016.12.020

Macciotta, R., Martin, C.D., Cruden, D.M., Hendry, M. & Edwards, T. (2017) Rock fall hazard control along a section of railway based on quantified risk. *Georisk*, **11**, 272–284, Taylor & Francis. doi:10.1080/17499518.2017.1293273

Mainsant, G., Larose, E., Brnnimann, C., Jongmans, D., Michoud, C. & Jaboyedoff, M. (2012) Ambient seismic noise monitoring of a clay landslide: Toward failure prediction. *J. Geophys. Res. Earth Surf.*, **117**. doi:10.1029/2011JF002159

Martino, S., Bozzano, F., Caporossi, P., D'Angiò, D., Seta, M. Della, Esposito, C., Fantini, A., *et al.* (2019) Impact of landslides on transportation routes during the 2016–2017 Central Italy seismic sequence. *Landslides*, **16**, 1221–1241. doi:10.1007/s10346-019-01162-2

Martino, Salvatore, Bozzano, F., Caporossi, P., D'Angio, D., Seta, M. Della, Esposito, C., Fantini, A., *et al.* (2017) Ground effects triggered by the 24th August 2016, Mw 6.0 Amatrice (Italy) earthquake: surveys and inventorying to update the CEDIT catalogue. *Geogr. Fis. e Din. Quat.*, **40**, 77–95.

Mateos, R.M., García-Moreno, I. & Azañón, J.M. (2012) Freeze-thaw cycles and rainfall as triggering factors of mass movements in a warm Mediterranean region: The case of the Tramuntana Range (Majorca, Spain). *Landslides*, **9**, 417–432. doi:10.1007/s10346-011-0290-8

Matsuoka, N. & Sakai, H. (1999) Rockfall activity from an alpine cliff during thawing periods. *Geomorphology*, **28**, 309–328. doi:10.1016/S0169-555X(98)00116-0

Meric, O., Garambois, S., Jongmans, D., Wathelet, M., Chatelain, J.L. & Vengeon, J.M. (2005) Application of geophysical methods for the investigation of the large gravitational mass movement of Séchilienne, France. *Can. Geotech. J.*, **42**, 1105–1115. doi:10.1139/t05-034

Messenzehl, K., Meyer, H., Otto, J.C., Hoffmann, T. & Dikau, R. (2017) Regional-scale controls on the spatial activity of rockfalls (Turtmann Valley, Swiss Alps) — A multivariate modeling approach. *Geomorphology*, **287**, 29–45, Elsevier B.V. doi:10.1016/j.geomorph.2016.01.008

Michoud, C., Derron, M.H., Horton, P., Jaboyedoff, M., Baillifard, F.J., Loye, A., Nicolet, P., *et al.* (2012) Rockfall hazard

and risk assessments along roads at a regional scale: Example in Swiss Alps. *Nat. Hazards Earth Syst. Sci.*, **12**, 615–629. doi:10.5194/nhess-12-615-2012

Miranda, S. de, Gentilini, C., Gottardi, G., Govoni, L., Mentani, A. & Ubertini, F. (2015) Virtual testing of existing semi-rigid rockfall protection barriers. *Eng. Struct.* doi:10.1016/j.engstruct.2014.12.022

Moore, J.R., Gischig, V., Burjanek, J., Loew, S. & Fäh, D. (2011) Site effects in unstable rock slopes: Dynamic behavior of the Randa instability (Switzerland). *Bull. Seismol. Soc. Am.*, **101**, 3110–3116. doi:10.1785/0120110127

Nadim, F., Kjekstad, O., Peduzzi, P., Herold, C. & Jaedicke, C. (2006) Global landslide and avalanche hotspots. *Landslides*, **3**, 159–173. doi:10.1007/s10346-006-0036-1

Nakamura, Y. (1989) Method for dynamic characteristics estimation of subsurface using microtremor on the ground surface. *Q. Rep. RTRI (railw. Tech. Res. Institute)*, **30**, 25–33.

Occhiena, C., Pirulli, M. & Scavia, C. (2014) A microseismic-based procedure for the detection of rock slope instabilities. *Int. J. Rock Mech. Min. Sci.*, **69**, 67–79, Elsevier. doi:10.1016/j.ijrmms.2014.02.020

Panzera, F., D'Amico, S., Lotteri, A., Galea, P. & Lombardo, G. (2012) Seismic site response of unstable steep slope using noise measurements: The case study of Xemxija Bay area, Malta. *Nat. Hazards Earth Syst. Sci.*, **12**, 3421–3431. doi:10.5194/nhess-12-3421-2012

Papini, M., Alba, M., Longoni, L., Arosio, D., Zanzi, L. & Scaioni, M. (2009) Towards rockfall forecasting through observing deformations and listening to microseismic emissions. *Nat. Hazards Earth Syst. Sci.*, **9**, 1119–1131. doi:10.5194/nhess-9-1119-2009

Pazzi, V., Morelli, S. & Fanti, R. (2019) A Review of the Advantages and Limitations of Geophysical Investigations in Landslide Studies. *Int. J. Geophys.*, **2019**, 1–27. doi:10.1155/2019/2983087

Pecker, A. (2010) *Dynamique des structures et des ouvrages*.

Peng, P., He, Z. & Wang, L. (2019) Automatic Classification of Microseismic Signals Based on MFCC and GMM-HMM in Underground Mines. *Shock Vib.*, **2019**, 1–9. doi:10.1155/2019/5803184

Perino, A., Zhu, J.B., Li, J.C., Barla, G. & Zhao, J. (2010) Theoretical methods for wave propagation across jointed rock masses. *Rock Mech. Rock Eng.*, **43**, 799–809. doi:10.1007/s00603-010-0114-5

Pilz, M., Parolai, S., Bindi, D., Saponaro, A. & Abdybachaev, U. (2014) Combining Seismic Noise Techniques for Landslide Characterization. *Pure Appl. Geophys.*, **171**, 1729–1745. doi:10.1007/s00024-013-0733-3

Prick, A. (2003) Frost weathering and rock fall in an arctic environment, Longyearbyen, Svalbard. *8th Int. Conf. Permafr.*, **2**, 907–912.

Provost, F., Malet, J.P., Hibert, C., Helmstetter, A., Radiguet, M., Amitrano, D., Langet, N., *et al.* (2018) Towards a standard typology of endogenous landslide seismic sources. *Earth Surf. Dyn.*, **6**, 1059–1088. doi:10.5194/esurf-6-1059-2018

Riva, F., Agliardi, F., Crosta, G.B. & Amitrano, D. (2016) Damage-based long term modelling of a large alpine rock slope. *Landslides Eng. Slopes. Exp. Theory Pract.*, Vol. 3, pp. 1723–1730.

Romeo, S., Matteo, L. Di, Melelli, L., Cencetti, C., Dragoni, W. & Fredduzzi, A. (2017) Seismic-induced rockfalls and landslide dam following the October 30, 2016 earthquake in Central Italy. *Landslides*, **14**, 1457–1465, Landslides. doi:10.1007/s10346-017-0841-8

Salvini, R., Francioni, M., Riccucci, S., Bonciani, F. & Callegari, I. (2013) Photogrammetry and laser scanning for analyzing slope stability and rock fall runout along the Domodossola-Iselle railway, the Italian Alps. *Geomorphology*, **185**, 110–122, Elsevier B.V. doi:10.1016/j.geomorph.2012.12.020

Sättele, M., Krautblatter, M., Bründl, M. & Straub, D. (2016) Forecasting rock slope failure: how reliable and effective are warning systems? *Landslides*, **13**. doi:10.1007/s10346-015-0605-2

Scholtès, L. & Donzé, F.V. (2012) Modelling progressive failure in fractured rock masses using a 3D discrete element method. *Int. J. Rock Mech. Min. Sci.*, **52**, 18–30. doi:10.1016/j.ijrmms.2012.02.009

Shang, X., Li, X., Morales-Esteban, A. & Chen, G. (2017) Improving microseismic event and quarry blast classification using Artificial Neural Networks based on Principal Component Analysis. *Soil Dyn. Earthq. Eng.*, **99**, 142–149, Elsevier Ltd. doi:10.1016/j.soildyn.2017.05.008

Spillmann, T., Maurer, H., Green, A.G., Heincke, B., Willenberg, H. & Husen, S. (2007) Microseismic investigation of an unstable mountain slope in the Swiss Alps. *J. Geophys. Res. Solid Earth*, **112**, 1–25. doi:10.1029/2006JB004723

Strozzi, T., Delaloye, R., Kääb, A., Ambrosi, C., Perruchoud, E. & Wegmüller, U. (2010) Combined observations of rock mass movements using satellite SAR interferometry, differential GPS, airborne digital photogrammetry, and airborne photography interpretation. *J. Geophys. Res. Earth Surf.*, **115**, 1–11. doi:10.1029/2009JF001311

Sun, J., Wang, L. & Hou, H. (2012) Application of micro-seismic monitoring technology in mining engineering. *Int. J. Min. Sci. Technol.*, **22**, 79–83, China University of Mining & Technology. doi:10.1016/j.ijmst.2011.06.007

Tang, Chun'an, Li, L., Xu, N. & Ma, K. (2015) Microseismic monitoring and numerical simulation on the stability of high-steep rock slopes in hydropower engineering. *J. Rock Mech. Geotech. Eng.*, **7**, 493–508. doi:10.1016/j.jrmge.2015.06.010

Tang, Chun'an, Wang, J. & Zhang, J. (2010) Preliminary engineering application of microseismic monitoring technique to rockburst prediction in tunneling of Jinping II project. *J. Rock Mech. Geotech. Eng.*, **2**, 193–208, Elsevier Masson SAS. doi:10.3724/sp.j.1235.2010.00193

Travelletti, J., Malet, J.P., Samyn, K., Grandjean, G. & Jaboyedoff, M. (2013) Control of landslide retrogression by discontinuities: Evidence by the integration of airborne- and ground-based geophysical information. *Landslides*, **10**, 37–54. doi:10.1007/s10346-011-0310-8

Vaezi, Y. & Baan, M. Van Der. (2015) Comparison of STA/LTA and power spectral density methods for microseismic

event detection. *Geophys. J. Int.*, 1896–1908.

Valentin, J., Capron, A., Jongmans, D., Baillet, L., Bottelin, P., Donze, F., Larose, E., *et al.* (2017) The dynamic response of prone-to-fall columns to ambient vibrations: Comparison between measurements and numerical modelling. *Geophys. J. Int.*, **208**, 1058–1076. doi:10.1093/gji/ggw440

Varnes, D.J. (1978) Slope movement types and processes. in *Landslides Analysis and Control, Special Report 176* eds. Schuster, R.L. & Krizek, R.J., pp. 11–33, National Academy of Science.

Walter, M., Schwaderer, U. & Joswig, M. (2012) Seismic monitoring of precursory fracture signals from a destructive rockfall in the Vorarlberg Alps, Austria. *Nat. Hazards Earth Syst. Sci.*, **12**, 3545–3555. doi:10.5194/nhess-12-3545-2012

Wang, H., Jiang, Y., Xue, S., Shen, B., Wang, C., Lv, J. & Yang, T. (2015) Assessment of excavation damaged zone around roadways under dynamic pressure induced by an active mining process. *Int. J. Rock Mech. Min. Sci.*, **77**, 265–277, Elsevier. doi:10.1016/j.ijrmms.2015.03.032

Wang, Y., Wang, S., Zhao, Y., Guo, P., Liu, Y. & Cao, P. (2018) Blast Induced Crack Propagation and Damage Accumulation in Rock Mass Containing Initial Damage. *Shock Vib.*, **2018**.

Wei, X.Y., Zhao, Z.Y. & Gu, J. (2009) Numerical simulations of rock mass damage induced by underground explosion. *Int. J. Rock Mech. Min. Sci.*, **46**, 1206–1213, Elsevier. doi:10.1016/j.ijrmms.2009.02.007

Wesseloo, J. & Sweby, G.J. (2008) Microseismic Monitoring of Hard Rock Mine Slopes. *South. Hemisph. Int. Rock Mech. Symp.*, 18.

Willenberg, H., Loew, S., Eberhardt, E., Evans, K.F., Spillmann, T., Heincke, B., Maurer, H., *et al.* (2008) Internal structure and deformation of an unstable crystalline rock mass above Randa (Switzerland): Part I - Internal structure from integrated geological and geophysical investigations. *Eng. Geol.*, **101**, 1–14. doi:10.1016/j.enggeo.2008.01.015

Withers, M., Aster, R., Young, C., Beiriger, J., Harris, M., Moore, S. & Trujillo, J. (1998) A comparison of select trigger algorithms for automated global seismic phase and event detection. *Bull. Seismol. Soc. Am.*, **88**, 95–106.

Wu, Y.K., Hao, H., Zhou, Y.X. & Chong, K. (1998) Propagation characteristics of blast-induced shock waves in a jointed rock mass. *Soil Dyn. Earthq. Eng.*, **17**, 407–412. doi:10.1016/S0267-7261(98)00030-X

Xu, J., Yan, C., Zhao, X., Du, K., Li, H. & Xie, Y. (2017) Monitoring of train-induced vibrations on rock slopes. *Int. J. Distrib. Sens. Networks*, **13**. doi:10.1177/1550147716687557

Xu, N.W., Dai, F., Liang, Z.Z., Zhou, Z., Sha, C. & Tang, C.A. (2014) The dynamic evaluation of rock slope stability considering the effects of microseismic damage. *Rock Mech. Rock Eng.*, **47**, 621–642. doi:10.1007/s00603-013-0432-5

Xu, N.W., Li, T.B., Dai, F., Li, B., Zhu, Y.G. & Yang, D.S. (2015) Microseismic monitoring and stability evaluation for the

large scale underground caverns at the Houziyan hydropower station in Southwest China. *Eng. Geol.*, **188**, 48–67. doi:10.1016/j.enggeo.2015.01.020

Xu, T., Xu, Q., Deng, M., Ma, T., Yang, T. & Tang, C. an. (2014) A numerical analysis of rock creep-induced slide: A case study from Jiweishan Mountain, China. *Environ. Earth Sci.*, **72**, 2111–2128. doi:10.1007/s12665-014-3119-7

Yan, Y., Li, T., Liu, J., Wang, W. & Su, Q. (2019) Monitoring and early warning method for a rockfall along railways based on vibration signal characteristics. *Sci. Rep.*, **9**, 1–10, Springer US. doi:10.1038/s41598-019-43146-1

Yang, J., Lu, W., Hu, Y., Chen, M. & Yan, P. (2015) Numerical Simulation of Rock Mass Damage Evolution During Deep-Buried Tunnel Excavation by Drill and Blast. *Rock Mech. Rock Eng.*, **48**, 2045–2059, Springer Vienna. doi:10.1007/s00603-014-0663-0

Yavuz, H., Demirdag, S. & Caran, S. (2010) Thermal effect on the physical properties of carbonate rocks. *Int. J. Rock Mech. Min. Sci.*, **47**, 94–103, Elsevier. doi:10.1016/j.ijrmms.2009.09.014

Yuan-hui, L., Gang, L., Shi-da, X. & Da-wei, W. (2018) The spatial-temporal evolution law of microseismic activities in the failure process of deep rock masses. *J. Appl. Geophys.*, **154**, 1–10, Elsevier B.V. doi:10.1016/j.jappgeo.2018.04.024

Zare, M.A., Haghshenas, E. & Jafari, M.K. (2017) Interpretation of dynamic response of a very complex landslide (Latian-Tehran) based on ambient noise investigation. *Soil Dyn. Earthq. Eng.*, **100**, 559–572, Elsevier Ltd. doi:10.1016/j.soildyn.2017.07.006

Zhao, Y., Yang, T., Bohnhoff, M., Zhang, P., Yu, Q., Zhou, J. & Liu, F. (2018) Study of the Rock Mass Failure Process and Mechanisms During the Transformation from Open-Pit to Underground Mining Based on Microseismic Monitoring. *Rock Mech. Rock Eng.*, **51**, 1473–1493, Springer Vienna. doi:10.1007/s00603-018-1413-5

Zhao, Y., Yang, T., Yu, Q. & Zhang, P. (2019) Dynamic reduction of rock mass mechanical parameters based on numerical simulation and microseismic data – A case study. *Tunn. Undergr. Sp. Technol.*, **83**, 437–451, Elsevier. doi:10.1016/j.tust.2018.09.018

Zhao, Y., Yang, T., Zhang, P., Zhou, J., Yu, Q. & Deng, W. (2017) The analysis of rock damage process based on the microseismic monitoring and numerical simulations. *Tunn. Undergr. Sp. Technol.*, **69**, 1–17, Elsevier. doi:10.1016/j.tust.2017.06.002

Zhuang, D., Ma, K., Tang, C., Cui, X. & Yang, G. (2019) Study on crack formation and propagation in the galleries of the Dagangshan high arch dam in Southwest China based on microseismic monitoring and numerical simulation. *Int. J. Rock Mech. Min. Sci.*, **115**, 157–172. doi:10.1016/j.ijrmms.2018.11.016